POLISH MARITIME RESEARCH

No 2(73)   2012   Vol 19

CONTENTS

Editorial

POLISH MARITIME RESEARCH is a scientific journal of worldwide circulation. The journal appears as a quarterly four times a year. The first issue of it was published in September 1994. Its main aim is to present original, innovative scientific ideas and Research & Development achievements in the field of :

Engineering, **Computing & Technology**, **Mechanical Engineering**,

which could find applications in the broad domain of maritime economy. Hence there are published papers which concern methods of the designing, manufacturing and operating processes of such technical objects and devices as : ships, port equipment, ocean engineering units, underwater vehicles and equipment as well as harbour facilities, with accounting for marine environment protection.

The Editors of POLISH MARITIME RESEARCH make also efforts to present problems dealing with education of engineers and scientific and teaching personnel. As a rule, the basic papers are supplemented by information on conferences , important scientific events as well as cooperation in carrying out international scientific research projects.

Scientific Board

Effect of the working liquid compressibility on the picture of volumetric and mechanical losses in a high pressure displacement pump used in a hydrostatic drive

Part I

Energy losses in a drive system, volumetric losses in a pump

Zygmunt Paszota, Prof.
Gdansk University of Technology, POLAND

ABSTRACT

Working liquid compressibility may considerably change the values and proportions of coefficients of volumetric and mechanical energy losses in the displacement pump used in a hydrostatic drive system. This effect can be particularly seen in the operation under high pressure and also in the system, where aeration of the working liquid can occur. In the Part I a diagram is presented, proposed by the author, of power increase in a hydrostatic drive system (hydraulic motor, pump) opposite to the direction of power flow, replacing the Sankey diagram of power decrease in the direction of power flow. Mathematical model is presented of volumetric losses in the pump and its laboratory verification.

Keywords: hydrostatic drive system; pressure displacement pump; energy losses;
energy efficiency; energy saving; liquid compressibility; Sankey diagram;

1. INTRODUCTION

The evaluation of energy efficiency of hydrostatic drive system elements (pump, hydraulic motor, throttling control assembly, conduits) is only justified when performed during their operation in the system. The hydraulic motor speed control structure determines in an essential way the level of power of energy losses in the system elements, losses related to the instantaneous values of the hydraulic motor speed $\overline{\omega}_M$ and load $\overline{M}_M$ coefficients as well as to the working liquid viscosity ratio ν/ν_n [1÷19].

Evaluation of the energy efficiency of a displacement machine (pump, hydraulic motor), performed independently of the drive system cannot be used for evaluation of energy efficiency of the system where the machine is operating.

It is necessary to evaluate the energy (mechanical, volumetric and pressure) losses in the pump and hydraulic motor as a function of the machine parameters which directly effect the losses. It is also necessary to determine the k_i coefficients of those losses. The knowledge of k_i coefficients allows to develop the mathematical models of losses taking into account also the system structure. The mathematical models should also allow to evaluate losses and energy efficiency of the elements and the system as a whole as a function of the hydraulic motor speed $\overline{\omega}_M$ and load $\overline{M}_M$ coefficients as well as a function of the working liquid viscosity ratio ν/ν_n.

The knowledge of k_i coefficients of losses in the elements allows also to determine the necessary mathematical models describing the maximum values $\overline{\omega}_{Mmax} = f(\overline{M}_M)$ and $\overline{M}_{Mmax} = f(\overline{\omega}_M)$ of the hydraulic motor operating field $(0 \leq \overline{\omega}_M \langle \overline{\omega}_{Mmax}, 0 \leq \overline{M}_M \langle \overline{M}_{Mmax})$ in a system with a given structure, the field that changes also with the change of the working liquid viscosity ratio ν/ν_n.

Compressibility of the working liquid (hydraulic oil) in the working chambers of the investigated pump decreases the volumetric intensity Q_P of flow in the discharge conduit compared with the intensity of low pressure flow in the pump inlet conduit. Therefore it reduces the theoretical volume q_{Pt} (V_P) and the geometrical volume q_{Pgv} (V_{Pgv}) of the pump operating under high pressure. The liquid compressibility increases at the same time the value of coefficient k1 of the volumetric losses in the pump.

Simultaneously, the liquid compressibility, reducing the theoretical volume q_{Pt} (V_P) and the geometrical volume q_{Pgv} (V_{Pgv}) of the pump working chambers, decreases the value, determined in the investigation, of the coefficient $k_{4.2}$ of the increase $\Delta M_{Pm|\Delta pPi}$, b_P, ν_n of torque of mechanical losses in the „working chambers - shaft" assembly. The increase of torque is a function of the torque MPi indicated in the working chambers.

The coefficient $k_{lc|p_n}$ of working liquid compressibility has been introduced in the analysis.

The $k_{lc|p_n}$ coefficient is defined at the increase Δp_{Pi} of pressure in the pump working chambers equal to the system nominal pressure $p_n - \Delta p_{Pi} = p_n$.

The working liquid compressibility coefficient $k_{lc|p_n}$ determines the degree of decrease, as an effect of compressibility (without taking leakage into account), of the active volume of the working liquid displaced by the pump in one shaft revolution, compared with the active volume equal to the theoretical capacity $q_{Pt}(V_{Pt})$ or geometrical capacity $q_{Pgv}(V_{Pgv})$ per one shaft revolution determined at the increase Δp_{Pi} of pressure in the working chambers equal to zero – $\Delta p_{Pi} = 0$:

$$k_{lc|p_n} = \frac{q_{Pt} - q_{Pt}|_{\Delta p_{Pi} = p_n}}{q_{Pt}}$$

$$k_{lc|p_n} = \frac{q_{Pgv} - q_{Pgv}|_{\Delta p_{Pi} = p_n}}{q_{Pgv}} = \frac{b_P q_{Pt} - b_P q_{Pt}|_{\Delta p_{Pi} = p_n}}{b_P q_{Pt}} \quad (1.1)$$

It is possible to evaluate the effect of coefficient $k_{lc|p_n}$ of liquid compressibility on the value of the coefficient $k_{4.2}$ of the increase of torque of mechanical losses in the pump „working chambers - shaft" assembly and then to evaluate the effect of that coefficient on the value of coefficient k_1 of volumetric losses in the pump working chambers. This is possible during investigation of the pump with variable capacity q_{Pgv} (b_P q_{Pt}) per one shaft revolution.

The working liquid compressibility has no effect on the evaluation of coefficient k_8 of volumetric losses in the working chambers of the hydraulic rotational motor and also on the evaluation of coefficient $k_{7.2}$ of the increase of torque of mechanical losses in the motor „shaft - working chambers" assembly.

The hydraulic motor working chambers are fed with compressed working liquid (with the pressure resulting, among others, from the torque M_M on the motor shaft). The calculated value of the torque M_{Mi} indicated in the motor working chambers is not influenced by the change of the theoretical volume q_{Mt} (V_M) or geometrical volume q_{Mgv} (V_{Mgv}) of the motor working chambers.

2. DIRECTION OF POWER INCREASE IN THE DRIVE SYSTEM

The Sankey diagram is the fundamental cause of incorrect evaluation of losses in a drive system.

The Sankey diagram connected with a drive system suggests an evaluation defining the output power of the system as a difference between the system input power and sum of the powers of losses occurring in the system. Therefore the energy losses in the system are evaluated as a function of parameters describing the input power.

In accordance with the proposed by the author (Fig. 2.1) diagram of power increase in a power transmission system opposite to the direction of power flow, **the system input power is a sum of the system output power and powers of losses occurring in the system. The energy losses in the system are evaluated as a function of parameters describing the system output power**.

Full picture of the energy losses in a hydrostatic drive system is a picture of power of energy losses in the system elements. Shaft power of the system feeding pump is equal to the sum of hydraulic motor shaft (or piston rod) power and powers of individual losses in the power flowing from the pump shaft to the hydraulic motor shaft (or piston rod).

<u>**The quantity of power increases, in order to overcome the power of energy losses, in the opposite direction to the direction of power flow**</u>. Therefore, the image of power of energy losses in the system should be constructed in the direction

from the hydraulic rotational motor shaft or from linear motor piston rod towards the system feeding pump shaft.

Power of the hydraulic motor, pump and other system element losses (mechanical, volumetric, pressure losses) should be determined as functions of the parameters independent of those losses and influencing directly those losses.

Power of energy losses in the system elements and also power of those elements must be precisely defined.

Fig. 2.1 presents (as an example of the system with the hydraulic motor speed series throttling control assembly fed by a constant capacity pump cooperating with an overflow valve) the diagram, proposed by the author, of the direction of power increase from the shaft or piston rod of a hydraulic motor to the pump shaft, power increasing as an effect of the imposed powers of energy losses in the hydrostatic drive and control elements.

The useful power $P_{Mu} = M_M \omega_M$ determined on the rotational hydraulic motor shaft or $P_{Mu} = F_M v_M$ determined on the linear hydraulic motor piston rod, changing in the work field ($0 \leq M_M < M_{Mmax}$ and $0 \leq \omega_M < \omega_{Mmax}$) or ($0 \leq F_M < F_{Mmax}$ and $0 \leq v_M < v_{Mmax}$) of the motor driven device, is a result of instantaneous requirements of the device toward motor both as regards load M_M (F_M) and speed ω_M(v_M). Therefore, the instantaneous useful power P_{Mu} is independent of the structure of hydraulic system (used for changing the motor speed ω_M(v_M)) and of the power ΔP of losses in the system elements. However, this does not apply to the upper limits of the device parameter ranges, i.e. maximum load M_{Mmax} (F_{Mmax}) and maximum speed ω_{Mmax} (v_{Mmax}).

The upper limits of work field, determined by the $M_{Mmax} = f(\omega_M)$ and $\omega_{Mmax} = f(M_M)$ or $F_{Mmax} = f(v_M)$ and $v_{Mmax} = f(F_M)$ lines, of the hydraulic motor driving the device, depend on the theoretical capacity Q_{Pt} of the pump in the system, on the nominal pressure p_n level of the system operation (the product $Q_{Pt} p_n$ is the reference power), on the motor speed control structure used, and also on the sum ΔP of powers of losses in the system elements. The upper limits of the motor work field differ in systems with different motor speed control structures.

On the other hand, the instantaneous power $P_{Pc} = M_P \omega_P$ required (consumed) by the pump from the drive (electric or internal combustion) motor, determined on the pump shaft, is a sum of the instantaneous useful power P_{Mu} of the hydraulic motor and instantaneous sum ΔP of powers of losses in the hydraulic system elements:

$$P_{Pc} = P_{Mu} + \Delta P \quad (2.1)$$

Power P_{Pc} on the pump shaft is equal to the sum ΔP of power of energy losses in the system elements ($P_{Pc} = \Delta P$) during operation with the unloaded motor (when $M_M = 0$ or $F_M = 0$) or with the stopped motor (when $\omega_M = 0$ or $v_M = 0$). The useful power P_{Mu} of the motor and energy efficiency η of the system are then equal to zero ($P_{Mu} = 0$, $\eta = 0$). The information on the level of power P_{Pc} absorbed then by the pump and entirely lost in the system is particularly important at the system operation with unloaded motor (when $M_M = 0$ or $F_M = 0$). Power P_{Pc} of the pump operating with hydraulic motor stopped (when $\omega_M = 0$ or $v_M = 0$) may be minimized by simultaneous cutting of the pump discharge conduit from the hydraulic motor and connecting this conduit with the tank, i.e. unloading the pump. However, this is only possible in an individual system, when the pump feeds only one hydraulic motor.

3. DIAGRAM OF POWER INCREASE IN A HYDRAULIC MOTOR

Fig. 3.1 illustrates the diagram, proposed by the author, of power increase in a rotational hydraulic motor opposite to the direction of power flow, replacing the Sankey diagram of power decrease in the direction of power flow.

Sankey diagram of power decrease in a power transmission system
in the direction of power flow
(example of hydrostatic drive)

$$P_{Mu} = P_{Pc} - \Delta P = P_{Pc} - \Delta P_{Pm} - \Delta P_{Pv} - \Delta P_{Pp} - \Delta P_{stv} - \Delta P_{stp} - \Delta P_C - \Delta P_{Mp} - \Delta P_{Mv} - \Delta P_{Mm}$$

diagram, according to Z.Paszota, of power increase in a power transmission system
opposite to the direction of power flow
(example of hydrostatic drive)

$$P_{Pc} = P_{Mu} + \Delta P = P_{Mu} + \Delta P_{Mm} + \Delta P_{Mv} + \Delta P_{Mp} + \Delta P_C + \Delta P_{stp} + \Delta P_{stv} + \Delta P_{Pp} + \Delta P_{Pv} + \Delta P_{Pm}$$
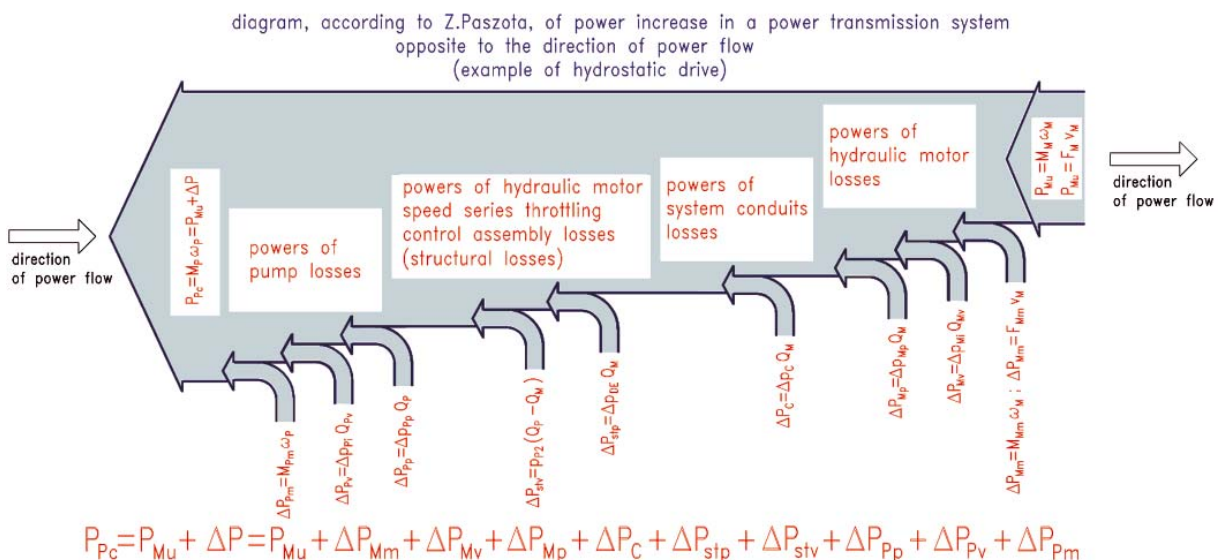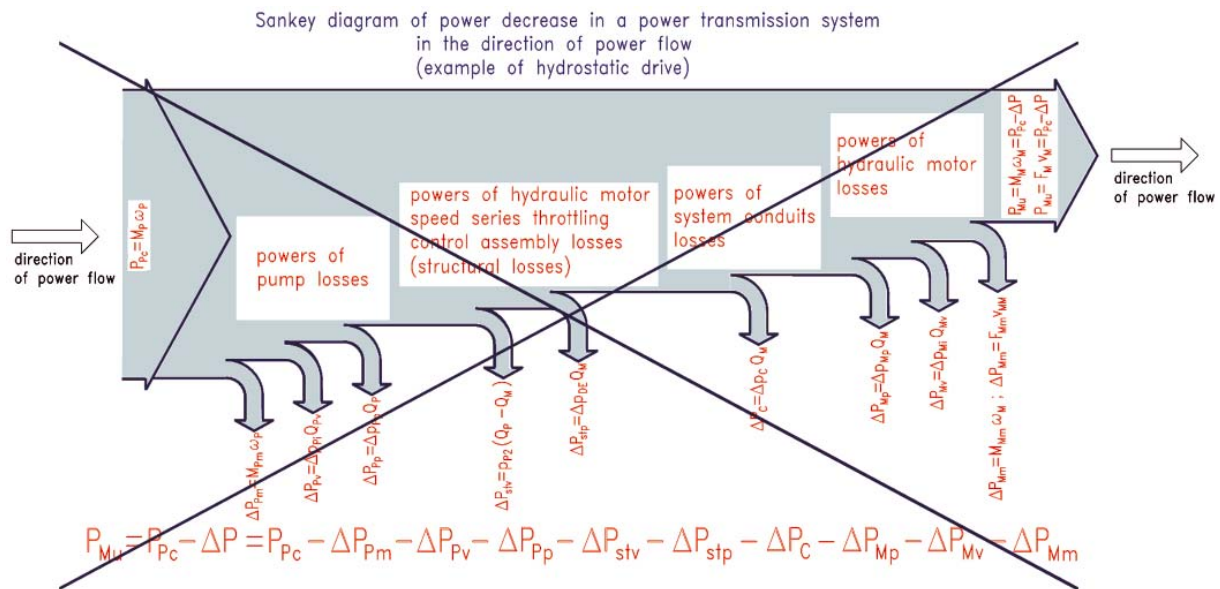
Fig. 2.1. *Diagram, proposed by the author, of power increase in a hydrostatic drive system opposite to the direction of power flow, replacing the Sankey diagram of power decrease in the direction of power flow.*
Power increases from the motor useful power P_{Mu}, required by the driven machine (device) on the rotational motor shaft or on the linear motor piston rod, to the power P_{Pc} consumed and required by the pump shaft from the motor (electric or internal combustion) driving the pump. The increase of power is a sum ΔP of powers of losses in the system elements (example of a system with the hydraulic motor speed series throttling control fed by a constant capacity pump cooperating with an overflow valve).
Powers of the losses are functions of the output parameters: M_M, ω_M of the rotational hydraulic motor shaft or F_M, v_M of the linear hydraulic motor piston rod and diversified functions of the working fluid viscosity v.
$P_{Mu} = M_M \omega_M$ – motor useful power on the rotational motor shaft required by the driven machine (device); $P_{Mu} = F_M v_M$ – motor useful power on the linear motor piston rod, $\Delta P_{Mm} = M_{Mm} \omega_M$ – power of mechanical losses in the rotational motor, $\Delta P_{Mm} = F_{Mm} v_M$ – power of mechanical losses in the linear motor, $\Delta P_{Mv} = \Delta p_{Mi} Q_{Mv}$ – power of volumetric losses in the motor, $\Delta P_{Mp} = \Delta p_{Mp} Q_M$ – power of pressure losses in the motor, $\Delta P_C = \Delta p_C Q_M$ – power of pressure losses in the system conduits, $\Delta P_{stp} = \Delta p_{DE} Q_M$ – power of structural pressure losses in the throttling control assembly (in servo-valve, directional proportional valve, set throttling valve or set two-way flow regulator), $\Delta P_{stv} = p_{SP} (Q_P - Q_M)$ – power of structural volumetric losses in the throttling control assembly (in the overflow valve), $\Delta P_{Pp} = \Delta p_{Pp} Q_P$ – power of pressure losses in the pump, $\Delta P_{Pv} = \Delta p_{Pi} Q_{Pv}$ – power of volumetric losses in the pump, $\Delta P_{Pm} = M_{Pm} \omega_P$ – power of mechanical losses in the pump, $P_{Pc} = M_P \omega_P$ – power consumed on the pump shaft, required by the pump shaft from the motor driving the pump

The power P_{Mc} consumed by the hydraulic motor is a sum of motor shaft useful power P_{Mu} and powers of three different energy losses in the motor. The losses occur in series (one after another), increasing the power in the opposite direction to the direction of power flow. In effect, the power in the motor increases from the shaft useful power P_{Mu} to the working fluid power P_{Mc} consumed by the motor:

$$P_{Mc} = P_{Mu} + \Delta P_{Mm} + \Delta P_{Mv} + \Delta P_{Mp} \qquad (3.1)$$

Mechanical losses (and power ΔP_{Mm} of mechanical losses) occur in the „shaft – working chambers" assembly.

Volumetric losses (and power ΔP_{Mv} of volumetric losses) occur in the working chambers.

Pressure losses (and power ΔP_{Mp} of pressure losses) occur in the motor channels.

4. DIAGRAM OF POWER INCREASE IN A PUMP

Fig. 4.1 presents the diagram, proposed by the author, of power increase in a pump opposite to the direction of power flow, replacing the Sankey diagram of power decrease in the direction of power flow.
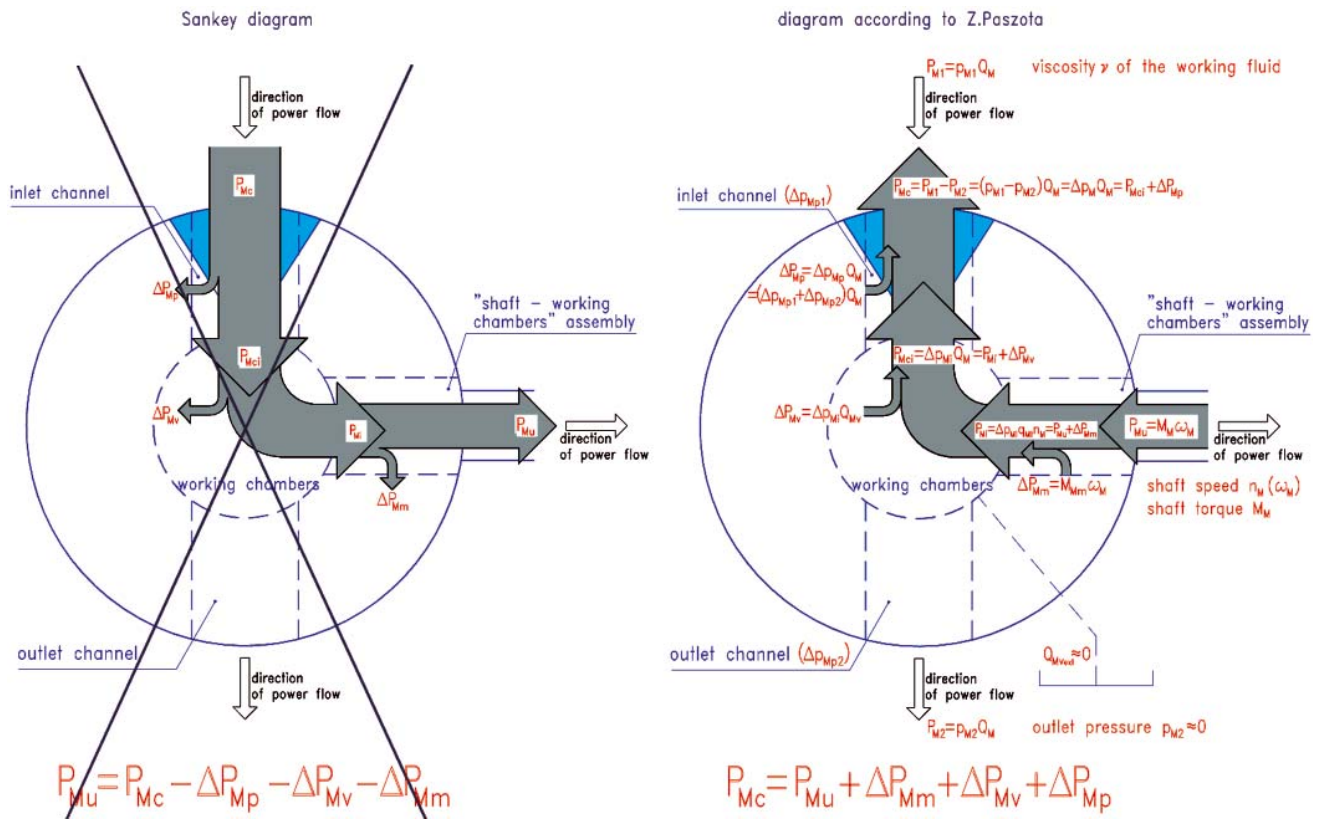
Fig. 3.1. *Diagram of power increase in a rotational displacement hydraulic motor opposite to the direction of power flow, replacing the Sankey diagram of power decrease in the direction of power flow Power increases from the motor useful power P_{Mu} required on the motor shaft by the driven machine (device) to power P_{Mc} consumed and required by the motor from the working fluid.*
The increase of power is an effect of the powers of losses in the motor: power ΔP_{Mm} of mechanical losses in the „shaft- working chambers" assembly, power ΔP_{Mv} of volumetric losses in the working chambers and power ΔP_{Mp} of pressure losses in the motor channels.
Powers ΔP_{Mm}, ΔP_{Mv} and ΔP_{Mp} of the losses are functions of the output parameters of the motor assembly where the losses occur and diversified functions of the working fluid viscosity v: power ΔP_{Mm} of mechanical losses is a function of torque M_M and shaft speed n_M (Δ_M) required from the motor by the driven machine (device) and a function of the working fluid viscosity Δ, power ΔP_{Mv} of volumetric losses is a function of the decrease Δp_{Mi} of pressure indicated in working chambers (torque M_{Mi} indicated in the chambers) and of the shaft rotational speed n_M as well as a function of the working fluid viscosity v, power ΔP_{Mp} of pressure losses is a function of motor capacity Q_M and of the working fluid viscosity v.
Power P_{Mi} indicated in the working chambers: $P_{Mi} = P_{Mu} + \Delta P_{Mm}$, power P_{Mci} of the working fluid consumed in the working chambers:
$P_{Mci} = P_{Mu} + \Delta P_{Mm} + \Delta P_{Mv}$, power P_{Mc} of the working fluid consumed by the motor: $P_{Mc} = P_{Mu} + \Delta P_{Mm} + \Delta P_{Mv} + \Delta P_{Mp}$.
The diagram replaces the Sankey diagram of distribution of power in a hydraulic motor causing incorrect loss evaluation during the hydraulic motor energy investigations

The power P_{Pc} consumed by the pump shaft is a sum of pump useful power P_{Pu} and powers of three different losses in the pump. The losses occur in series (one after another), increasing the power in the opposite direction to the direction of power flow. In effect, the power in the pump increases from the working fluid useful power P_{Pu} to the pump shaft consumed power P_{Pc}:

$$P_{Pc} = P_{Pu} + \Delta P_{Pp} + \Delta P_{Pv} + \Delta P_{Pm} \qquad (4.1)$$

Pressure losses (and power ΔP_{Pp} of pressure losses) occur in the pump channels.

Volumetric losses (and power ΔP_{Pv} of volumetric losses) occur in the working chambers.

Mechanical losses (and power ΔP_{Pm} of mechanical losses) occur in the „working chambers - shaft" assembly.

5. MATHEMATICAL MODELS OF THE DISPLACEMENT MACHINE LOSSES

Assessment of the capability of energy savings in the hydrostatic drive system operation requires the system losses to be defined.

The simulation determination of the system energy efficiency may be used for the purpose in the system design and operation process [24]. The following factors in the simulation model should be taken into account:

– the hydraulic motor speed control system structure,
– energy losses in the system elements,
– the pump driving motor speed decrease,
– the system control element characteristics,
– load and speed of the controlled hydraulic motor,
– hydraulic oil viscosity, changing in the system operation process due to change of the oil temperature.

In order to make the transmission system efficiency determination method easily applicable, it is necessary to:
1) use the computer programs for the mathematical models, allowing to analyse the hydraulic system efficiency as a function of the decisive parameters (hydraulic motor speed coefficient $\overline{\omega}_M$ and load coefficient $\overline{M}_M$, ratio v/v_n of the hydraulic oil viscosity v to the reference viscosity v_n),
2) determine the values of energy loss coefficients k_i for the pump, rotational hydraulic motor or hydraulic cylinder. Those coefficients should be clearly defined and precisely determined for a given displacement machine.

The mathematical model of the displacement machine losses allowing to fulfil the conditions given in points 1 and 2 above should take into account:
a) the form and simplicity of the description, deciding of the possible use of that description in the system efficiency model, with maintaining the system efficiency precise assessment,
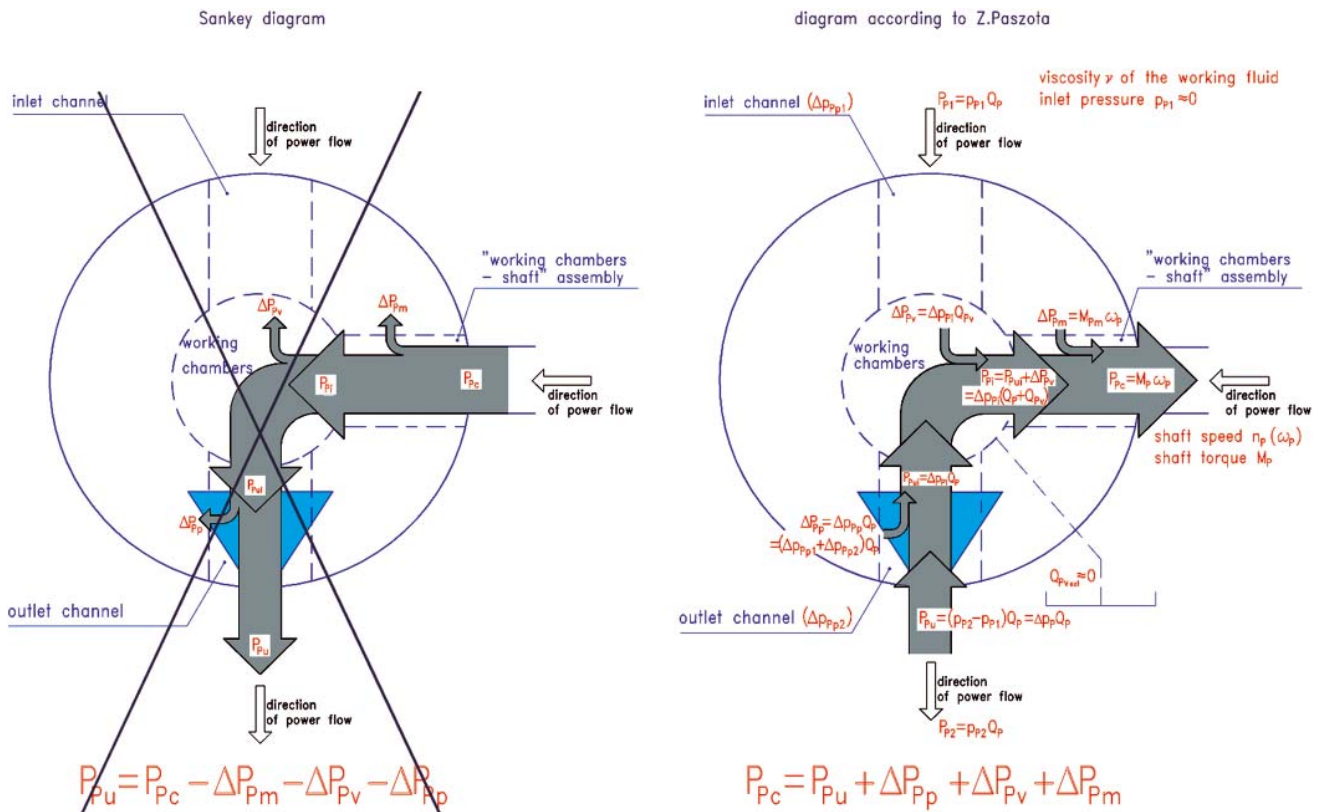
Fig. 4.1. *Diagram of power increase in a displacement pump opposite to the direction of power flow replacing the Sankey diagram of power decrease in the direction of power flow Power increases from the motor useful power P_{Pu}, required by the working fluid in the discharge conduit of the pump, to power P_{Pc} consumed and required by the pump shaft from (electric or internal combustion) motor driving the pump.*
The increase of power is an effect of the powers of losses in the pump: power ΔP_{Pp} of pressure losses in the pump channels, power Δp_{Pv} of volumetric losses in the working chambers and power ΔP_{Pm} of mechanical losses in the „working chambers - shaft" assembly.
Powers ΔP_{Pp}, ΔP_{Pv} and ΔP_{Pm} of the losses are functions of the output parameters of the pump assembly where the losses occur and diversified functions of the working fluid viscosity v: power ΔP_{Pp} of pressure losses is a function of pump capacity Q_P and of the working fluid viscosity v, power ΔP_{Pv} of volumetric losses is a function of the increase Δp_{Pi} of pressure indicated in working chambers and of the shaft rotational speed n_P as well as a function of the working fluid viscosity v, power ΔP_{Pm} of mechanical losses is a function of the torque M_{Pi} indicated in the chambers, of the pump shaft speed n_P (ω_P) and a function of the working fluid viscosity v.
Useful power P_{Pui} of the working fluid in the working chambers: $P_{Pui} = P_{Pu} + \Delta P_{Pp}$, power P_{Pi} indicated in the working chambers: $P_{Pi} = P_{Pu} + \Delta P_{Pp} + \Delta P_{Pv}$, power P_{Pc} consumed on the pump shaft: $P_{Pc} = P_{Pu} + \Delta P_{Pp} + \Delta P_{Pv} + \Delta P_{Pm}$.
The diagram replaces the Sankey diagram of distribution of power in a pump, causing incorrect loss evaluation during the pump energy investigations

b) description of the displacement machine mechanical, volumetric and pressure losses, allowing to evaluate the impact of hydraulic oil kinematic viscosity changing with oil temperature,

c) separate treatment of the mechanical, volumetric and pressure losses in the machine.

It is necessary to perform the laboratory and simulation investigations in the displacement machine real operating conditions. The investigations should allow to verify the proposed models of:
– machine mechanical losses,
– machine volumetric losses,
– machine pressure losses,

in the full range of working pressure up to nominal pressure p_n, in the wide range of pump capacity up to theoretical capacity Q_{Pt} and in wide range of the hydraulic oil kinematic viscosity v, and also to **determine the k_i coefficients of specific losses**.

6. MODEL OF VOLUMETRIC LOSSES IN THE PUMP WORKING CHAMBERS

Volumetric losses in the pump are connected first of all with the working liquid leaks through slots between displacement elements and the working chamber walls, distributor (if it exists) elements and **are also effect of the**

liquid compressibility, change of the pump working chambers volume and change of the slot height due to changes of pressure and temperature.

The model of volumetric losses presented in [24, 25 and 26] meets the requirements given in chapter 5. The author assumes the conditions and simplifications of the impact of certain factors on those losses and that impact is reflected in the coefficient k_1 of volumetric losses in the pump (equation (6.3)) and in power exponents describing the dependence of volumetric losses on Δp_{Pi} and v (equation (6.4)).

The theoretical working volume q_{Pt} (V_P) of constant or variable capacity pump (theoretical capacity q_{Pt} for one pump shaft revolution – at the pump capacity coefficient $b_P = 1$) – the geometrical difference between the maximum and minimum volume of working chambers – is a characteristic value of a pump. **It is determined at the pressure value $p_{P1i} = 0$ in the pump working chambers during their filling and at the increase $\Delta p_{Pi} = 0$ of the indicated pressure in the working chambers**.

Under the pressure and temperature, the geometric working volume q_{Pg} of the pump changes slightly compared with q_{Pt}. **It is assumed** (in order to simplify the description of volumetric and mechanical losses in the pump) **that the theoretical pump working volume q_{Pt} is constant and equal to the geometrical working volume q_{Pg}** determined at the working liquid

temperature corresponding to the recommended kinematic viscosity $v_n = 35 mm^2 s^{-1}$:

$$q_{Pt} = q_{Pg}\left|\begin{array}{l} p_{P1i}=0 \\ \Delta p_{Pi}=0 \\ v_n \end{array}\right. \qquad (6.1)$$

and the change of geometric working volume q_{Pg} during the system operation will be taken into account in the values of loss coefficients k_i in the pump.

The theoretical capacity Q_{Pt} of a constant capacity pump is given by the formula:

$$Q_{Pt} = q_{Pt}n_{P0} \qquad (6.2)$$

where:

n_{P0} – the rotational shaft speed of an unloaded pump ($\Delta p_{Pi} = 0$).

Coefficient k_1 of the volumetric losses Q_{Pv}, determined during one shaft revolution of a constant or variable capacity pump, at the pressure increase Δp_{Pi} equal to the hydraulic system nominal pressure $\Delta p_{Pi} = p_n$ and at the viscosity v_n, the losses related to the pump theoretical working volume $q_{Pt}(V_P)$, is described by the formula:

$$k_1 = \frac{Q_{Pv}\left|\begin{array}{l} q_{Pt} \\ \Delta p_{Pi}=p_n \\ v_n \end{array}\right.}{n_P\left|\begin{array}{l} q_{Pt} \\ \Delta p_{Pi}=p_n \\ v_n \end{array}\right.}\frac{1}{q_{Pt}} \qquad (6.3)$$

Using the volumetric loss coefficient k_1, the following mathematical model for the intensity Q_{Pv} of volumetric losses in the pump is proposed:

$$Q_{Pv} = k_1 q_{Pt}n_P\left|\begin{array}{l} q_{Pt} \\ \Delta p_{Pi}=p_n \\ v_n \end{array}\right.\left(\frac{\Delta p_{Pi}}{p_n}\right)^1\left(\frac{v}{v_n}\right)^{-0.8} \qquad (6.4)$$

The use of coefficient k_1 of volumetric losses for description of the relation of intensity Q_{Pv} to the indicated increase Δp_{Pi} of pressure in the pump working chambers allows to describe that relation by an exponential function **with the exponent not necessarily equal to 1**.

The expression describing the variable capacity pump capacity takes the form:

$$Q_P = b_P q_{Pt}n_P - k_1 q_{Pt}n_P\left|\begin{array}{l} q_{Pt} \\ \Delta p_{Pi}=p_n \\ v_n \end{array}\right.\left(\frac{\Delta p_{Pi}}{p_n}\right)^1\left(\frac{v}{v_n}\right)^{-0.8} \qquad (6.5)$$

The expressions (6.4) and (6.5) assume, that **change of the capacity coefficient b_P in the variable capacity pump (change of the pump capacity) does not influence the intensity of pump volumetric losses Q_{Pv}**.

In expressions (6.4) and (6.5), the value 1 of exponent describing the impact of the $\Delta p_{Pi}/p_n$ ratio and also the value -0.8 of exponent describing the impact of the v/v_n ratio on the intensity Q_{Pv} of pump volumetric losses should take into account all the factors influencing the volumetric losses (character of the flow in slots, change of the slots cross-section with pressure and temperature, **liquid compressibility**, change of the liquid viscosity in slots etc.).

The value 1 of exponent describing the impact of the $\Delta p_{Pi}/p_n$ ratio and also the value -0.8 of exponent describing the impact of the v/v_n ratio on the intensity Q_{Pv} of pump volumetric losses must be verified experimentally for each pump type.

Compressibility of the working liquid has an essential effect on the evaluation of the intensity Q_{Pv} of volumetric losses in the pump (equation (6.4)) and on the evaluation of coefficient k_1 of volumetric losses in the pump (equation (6.5)). The greater the liquid compressibility (mainly due to its aeration with the air not dissolved in the liquid) the greater the value of coefficient k_1 determined in the pump investigation. Therefore, **the liquid compressibility effects the evaluation of tightness of the pump structural solution**. It may be particularly evident in the displacement pump operating at high values ($32 \div 40$ MPa) of indicated pressure increase Δp_{Pi} in the pump working chambers.

VERIFICATION OF THE MATHEMATICAL MODEL OF VOLUMETRIC LOSSES IN THE PUMP WORKING CHAMBERS

Laboratory investigations of an axial piston variable displacement pump of bent axis design (HYDROMATIK A7V.58.DR.1.R.P.F.00 type – Fig. 7.1) were carried out by Jan Koralewski [20, 22] on a test stand (Fig. 7.2) in the Chair of Hydraulics and Pneumatics of the Gdansk University of Technology, Mechanical Engineering Faculty.
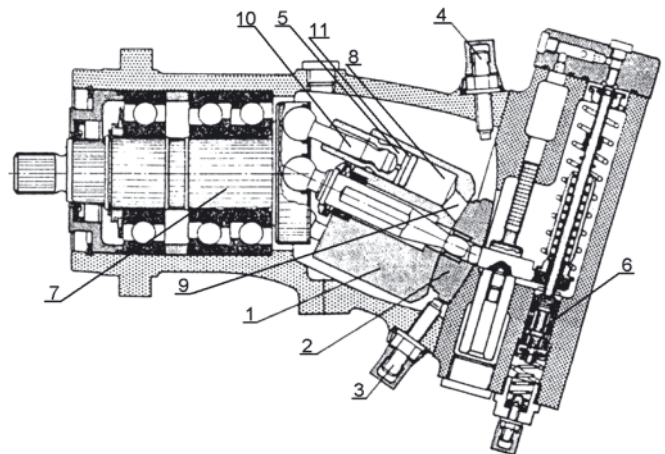
Fig. 7.1. Axial piston variable displacement pump of bent axis design (HYDROMATIK 7V.58.DR.1.R.P.F.00 type) [23]. 1) cylinder block, 2) collector (distributor), 3, 4) blockage of pump setting, 5) piston, 6) assembly of capacity zeroing at maximum set pressure, 7) shaft, 8) working chamber, 9) hole in the cylinder block connecting working chamber (8) with collector (distributor) (2), 10) connector with ball-and-socket joints-element of the „working chamber - shaft" assembly, 11) circumferential groove in the piston

In order to verify the mathematical model described by formula (6.4), it was replaced by a mathematical expression taking into account the relations, obtained during the investigations, of the intensity Q_{Pv} of pump volumetric losses to the indicated increase Δp_{Pi} of pressure in the pump working chambers (to the $\Delta p_{Pi}/p_n$ ratio) and also to the oil viscosity ratio v/v_n [20, 22]:

$$Q_{Pv} = k_1 q_{Pt}n_P\left|\begin{array}{l} q_{Pt} \\ v_n \\ \Delta p_{Pi}=p_n \end{array}\right.\left(\frac{\Delta p_{Pi}}{p_n}\right)^{a_{pv}}\left(\frac{v}{v_n}\right)^{a_{vv}} \qquad (7.1)$$

The obtained values (Fig. 7.3) of **the coefficient $k_1 = 0.065$** of intensity Q_{Pv} of volumetric losses, exponent $a_{pv} = 0.97$ of the relation of intensity Q_{Pv} of the volumetric losses to the ratio $\Delta p_{Pi}/p_n$ of the pressure increase in the working chambers, exponent $a_{vv} = -0.30$ of the relation of intensity Q_{Pv} of the volumetric losses to the v/v_n ratio of oil viscosity, have made it possible to present the mathematical model of the intensity Q_{Pv} of pump volumetric losses in the form:
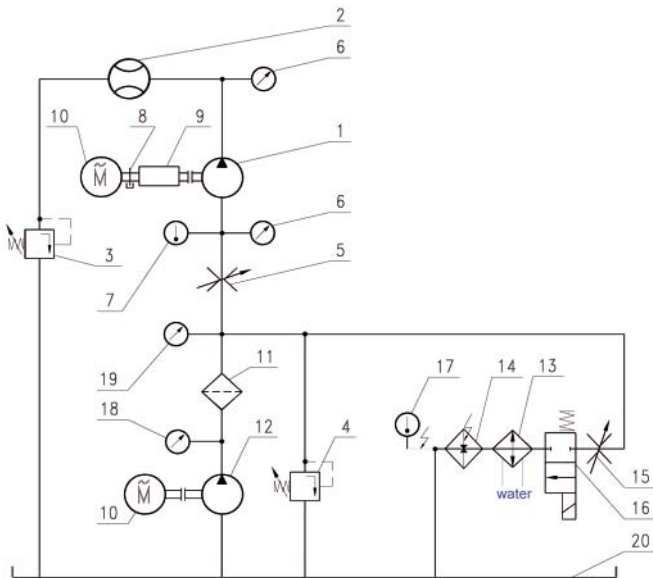
Fig. 7.2. *Test stand for investigating of the volumetric and mechanical losses in the pump (HYDROMATIK A7V.58.DR.1.R.P.F.00 type) [23].*
1) investigated pump, 2) piston flow- meter, 3,4) overflow valve,
5,15) throttling valve, 6) pressure sensor, 7) temperature sensor,
8) rotational speed sensor, 9) torque sensor, 10) asynchronic motor,
11) filter, 12) feeding screw pump, 13) cooler, 14) electric heater,
16) distributor, 17) thermostat, 18) manometer,
19) vacuum meter, 20) tank

$$Q_{Pv} = 0.065 q_{Pt} n_P \left|_{\substack{q_{Pt} \\ v_n \\ \Delta p_{Pi}=p_n}} \left(\frac{\Delta p_{Pi}}{p_n}\right)^{0.97} \left(\frac{v}{v_n}\right)^{-0.30} \quad (7)\right.$$

Model (7.2) describes precisely the intensity Q_{Pv} of volumetric losses in the nominal conditions of the pump operation, i.e. at the pump capacity coefficient $b_P = 1$, the pressure increase ratio $\Delta p_{Pi}/p_n = 1$ ($p_n = 32$MPa) and the oil viscosity ratio $v/v_n = 1$ ($v_n = 35$mm²s⁻¹). At the same time, this mathematical model is a simulation formula describing the change of intensity Q_{Pv} of volumetric losses with the change of the pressure increase ratio $\Delta p_{Pi}/p_n$ and the oil viscosity ratio v/v_n (the change of pump capacity coefficient b_P has practically no impact on the change of intensity Q_{Pv} of volumetric losses).

However, **the value of coefficient $k_1 = 0.065$** (equations (6.3), (7.1), (7.2)) of the intensity Q_{Pv} of volumetric losses, determined during one shaft revolution of the pump, at the pressure increase Δp_{Pi} equal to the system nominal pressure p_n – $\Delta p_{Pi} = p_n$ and at the viscosity v_n (the losses related to the pump theoretical working volume q_{Pt}) **is influenced by the working liquid compressibility coefficient k_{lc}**.

The liquid compressibility coefficient k_{lc} increases the value of coefficient k_1 of volumetric losses in the pump, „loading" the pump structure with non-existent excessive leakage mainly from the working chambers under the high discharge channel pressure to the working chambers connected with the low pressure inlet channel.

In the conditions of aerated hydraulic oil and high working pressure in the pump discharge channel, the value of liquid compressibility coefficient k_{lc} can significantly increase the value of volumetric loss coefficient k_1 and at the same time significantly decrease the value of coefficient $k_{4.2}$ of the increase $\Delta M_{Pm|\Delta p_{Pi}}$, b_P, v_n of the torque of mechanical losses in the pump.

Part II of the paper (titled: „Effect of the working liquid compressibility on the picture of volumetric losses in a high pressure displacement pump used in a hydrostatic drive, Part II
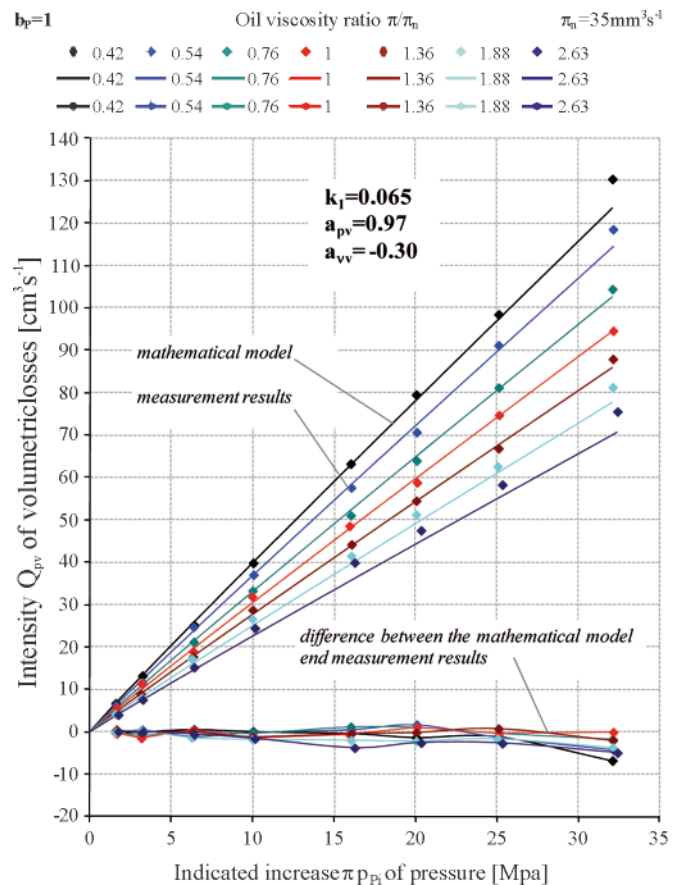
Fig. 7.3. *Comparison of the intensity Q_{Pv} of volumetric losses described by the mathematical model (6) with the laboratory investigation results and the absolute difference between the mathematical model values and the laboratory investigation values; assumed were: the coefficient $k_1 = 0.065$ of volumetric losses, exponent $a_{pv} = 0.97$, exponent $a_{vv} = -0,30$; example for the pump capacity coefficient $b_P = 1$ (pump HYDROMATIK A7V.58. DR.1.R.P.F.00 type) [20, 22]*

– Mechanical losses in a pump) to be published in the next issue of this journal will present a possibility of determining a value of the $k_{lc|p_n}$ coefficient and its effect on the $k_{4.2}$ and k_1 coefficient.

BIBLIOGRAPHY

1. Paszota Z.: *Graphical presentation of the power of energy losses and power developed in the elements of hydrostatic drive and control system. Part I – Rotational hydraulic motor speed series throttling control systems*. Chapter in the monograph: „*Research, design, production and operation of hydraulic systems*" (in Polish), Adam Klich, Edward Palczak and Andrzej Meder editors. „Cylinder" Library. Komag Mining Mechanisation Centre, Gliwice 2008

2. Paszota Z.: *Graphical presentation of the power of energy losses and power developed in the elements of hydrostatic drive and control system. Part II – Rotational hydraulic motor speed parallel throttling control and volumetric control systems*. Chapter in the monograph: „*Research, design, production and operation of hydraulic systems*" (in Polish), Adam Klich, Edward Palczak and Andrzej Meder editors. „Cylinder" Library. Komag Mining Mechanisation Centre, Gliwice 2008

3. Paszota Z.: *Direction of increase of power stream in the hydrostatic drive and control system. Graphical presentation of the power of energy losses and power developed in the elements of hydrostatic drive and control system. Part I – Rotational hydraulic motor speed series throttling control systems* (in Polish), Napędy i sterowanie, scientific monthly, No 10 (114), October 2008

4. Paszota Z.: *Direction of increase of power stream in the hydrostatic drive and control system. Graphical presentation of*

the power of energy losses and power developed in the elements of hydrostatic drive and control system. Part II – Rotational hydraulic motor speed parallel throttling control and volumetric control systems (in Polish), Napędy i sterowanie, scientific monthly, No 11 (115), November 2008

5. Paszota Z.: *Graphical presentation of the power of energy losses and power developed in the elements of hydrostatic drive and control system. Part I – Rotational hydraulic motor speed series throttling control systems.* Polish Maritime Research 3 (57) 2008, Vol. 15

6. Paszota Z.: *Graphical presentation of the power of energy losses and power developed in the elements of hydrostatic drive and control system. Part II – Rotational hydraulic motor speed parallel throttling control and volumetric control systems.* Polish Maritime Research 4 (58) 2008,Vol. 15

7. Paszota Z.: *The operating field of a hydrostatic drive system.* Chapter in the monograph: *„Research, design, production and operation of hydraulic systems"* (in Polish), Adam Klich, Antoni Kozieł and Edward Palczak editors. „Cylinder" Library. Komag Mining Mechanisation Centre, Gliwice 2009

8. Paszota Z.: *Parameters of the energy efficiency investigations of pumps and hydraulic motors. The operating field of a hydrostatic drive system* (in Polish), Napędy i sterowanie, scientific monthly, No 11 (127), November 2009

9. Paszota Z.: *The operating field of a hydrostatic drive system parameters of the energy efficiency investigations of pumps and hydraulic motors.* Polish Maritime Research 4 (62) 2009, Vol. 16

10. Paszota Z.: *Energy losses in a rotational hydraulic motor – definitions and relations for evaluation of the efficiency of motor and hydrostatic drive.* Chapter in the monograph: *„Research, design, production and operation of hydraulic systems"* (in Polish), Adam Klich, Antoni Kozieł and Edward Palczak editors. „Cylinder" Library. Komag Mining Mechanisation Centre, Gliwice 2010

11. Paszota Z.: *Theoretical and mathematical models of the torque of mechanical losses in a hydraulic rotational motor for hydrostatic drive.* Chapter in the monograph: *„Research, design, production and operation of hydraulic systems"* (in Polish), Adam Klich, Antoni Kozieł and Edward Palczak editors. „Cylinder" Library. Komag Mining Mechanisation Centre, Gliwice 2010

12. Paszota Z.: *Energy losses in a rotational hydraulic motor – definitions and relations for evaluation of the efficiency of motor and hydrostatic drive* (in Polish), Napędy i sterowanie, scientific monthly, No 10 (138), October 2010

13. Paszota Z.: *Theoretical and mathematical models of the torque of mechanical losses in a hydraulic rotational motor for hydrostatic drive* (in Polish), Napędy i sterowanie, scientific monthly, No 11(139), November 2010

14. Paszota Z.: *Energy losses in the hydraulic rotational motor – definitions and relations for evaluation of the efficiency of motor and hydrostatic drive.* Polish Maritime Research 2 /2010

15. Paszota Z.: *Theoretical and mathematical models of the torque of mechanical losses in a hydraulic rotational motor for hydrostatic drive.* Polish Maritime Research 3/2010

16. Paszota Z.: *Hydrostatic drives as safe and energy saving machines* (in Polish), Napędy i sterowanie, scientific monthly, No 1(141), January 2011

17. Paszota Z.: *Hydrostatic drives as safe and energy saving machines* (in Polish), Proceedings of the „Innovative machines and Technologies - Safety" conference, Szczyrk 03 – 04 February 2011

18. Paszota Z.: *Hydrostatic drives as safe and energy saving machines. The drive investigation method compatible with the diagram of power increase opposite to the direction of power flow.* Polish Maritime Research 1/2011,

19. Paszota Z.: *Theoretical models of the torque of mechanical losses in the pump used in a hydrostatic drive.* Polish Maritime Research 4 / 2011,

20. Koralewski J.: *Influence of hydraulic oil viscosity on the volumetric losses in a variable capacity pump.* Polish Maritime Research. 3/2011

21. Czyński M.: *Laboratory investigation of the model of hydrostatic transmission energy efficiency.* (in Polish). Doctor dissertation. Szczecin University of Technology, Faculty of Marine Engineering, 2005,

22. Koralewski J.: *Effect of the working liquid viscosity on the energy losses in a variable capacity piston pump.* (in Polish). Doctor dissertation (continued). Gdansk University of Technology, Faculty of Ocean Engineering and Ship Technology,

23. Skorek G.: *Energy characteristics of the hydraulic system with proportional control of the hydraulic cylinder fed by a constant capacity pump in a constant pressure and variable pressure system.* (in Polish). Doctor dissertation. Gdansk University of Technology, Faculty of Ocean Engineering and Ship Technology, 2008

24. Paszota Z.: *Model of volumetric losses in the variable capacity displacement pump used in hydrostatic drive* (in Polish). „Napędy i Sterowania'2006". „TECHNICON'06" Gdańsk, 25.10.2006.

25. Paszota Z.: *Aspects énergétiques des transmissions hydrostatiques.* Monograph, Gdansk 2002.

26. Paszota Z.: *Model of the energy losses in the displacement rotational machines for description of efficiency of the hydrostatic drive. Part I. Model of volumetric losses.* Polish Maritime Research. 3/2000.

CONTACT WITH THE AUTHOR

Prof. Zygmunt Paszota
Faculty of Ocean Engineering
and Ship Technology
Gdansk University of Technology
Narutowicza 11/12
80-233 Gdansk, POLAND
e-mail: zpaszota@pg.gda.pl

A parametric method for preliminary determination of underwater vehicles deadweight

Jan P. Michalski, Assoc. Prof.
Gdansk University of Technology
Polish Naval University

ABSTRACT

This paper describes a method useful for determination of load carrying capacity of underwater vehicle, elaborated on the basis of investigations of series of vehicles of systematically changed geometrical dimensions. By using the set of the series of vehicles their structural mass and displacement – at a given structural material and assumed maximum permissible submersion depth – were determined, and next – approximation formulae for deadweight of vehicles were obtained. Vehicle's form may be consisted of one or a few cylindrical floats of circular cross-section, ended with caps. The floats are joined together with a space pipe frame. Acceptability of design solutions results from comparison of working stress values in float's shell plating with permissible stresses as well as critical stresses. The presented method may be useful in the preliminary stage of designing the underwater vehicles - i.e. may serve for preliminary determination of a vehicle deadweight – at its given, or determined, geometrical dimensions, maximum permissible submersion depth, as well as a selected structural material.

Keywords: designing of underwater vehicles; mass and deadweight of underwater vehicles

INTRODUCTION

Tight submersible vessels intended for the fulfilling of assumed functions deep in water, capable of carrying large external hydrostatic loads, find many civil and military applications such as submarines and submersible vehicles, bathyscaphes, crude-oil and gas storage tanks, or casings for measurement instruments to conduct underwater oceanological experiments.

To conduct research on phenomena occurring deep in water of seas and oceans, or in applications to offshore engineering work, are used manned and unmanned underwater vehicles capable of submersing to large depths. Such vehicles are equipped with instruments intended for: taking specimens, making measurements, navigating, filming and recording research results. In military applications the vehicles serve e.g. to place or defuse sea mines or conduct rescue operations of submarine crews. In oceanology they serve e.g. for conducting geological measurements of e.g. displacements of underwater tectonic plates, recording values of gaps, or investigating phenomena associated with underwater volcano eruptions. In the area of ocean engineering the underwater vehicles are used for exploration of ocean bed, e.g. to estimate resources of concretes laying on the bed or to inspect, maintain and repair ocean engineering devices. The designing of vehicles intended for fulfilling such functions constitutes a serious technical problem associated with the necessity of ensuring life safety to crews of vehicles as well as safety of devices and instruments against action of high hydrostatic pressure.

The set of main technical parameters of underwater vehicle, which greatly influence acceptability of design solutions, is as follows:
- maximum permissible submersion depth;
- kind of structural material;
- required gabarites of vehicle;
- required load-carrying capacity of vehicle;
- maximum permissible mass of vehicle;
- required speed of vertical and horizontal movements;
- zone of visibility from vessel's interior;
- maximum permissible building cost.

The set of design assumptions depends on functions and mission of a designed vehicle, and it usually contains an appropriate combination of the above mentioned technical parameters.

AIM AND SCOPE OF THE WORK

The presented work has been aimed at elaboration of a method for determining (predicting) the deadweight P_N of underwater vehicles in the preliminary parametric design stage, on the basis of a few parameters of main design assumptions.

The load carrying capacity P_N is the difference of the displacement D of fully immersed vehicle and its structural mass M:

$$P_N(h_{min}, L, R, H_{max}, E, \nu) =$$
$$= D(L, R) - M(h_{min}, L, R, H_{max}, E, \nu) \quad (1)$$

where:

h_{min} – minimum acceptable float's plating thickness, equal to the greater of the thicknesses: h_{cr}, h_{per}:

$$h_{min} = \max(h_{cr}, h_{per}) \quad (2)$$

h_{cr} – critical float's plating thickness – the greatest value at which loss of stability of plating will occur under hydrostatic pressure at the depth H_{max};

h_{per} – minimum permissible float's plating thickness – the greatest value at which permissible reduced stresses in the float's plating will be exceeded under hydrostatic pressure at the depth H_{max};

P_N – deadweight of vehicle;
L – length of float's cylindrical part (shell);
R – radius of float's shell;
H_{max} – maximum permissible vehicle submersion depth;
E, ν – Young modulus and Poisson ratio of structural material, respectively.

The method for preliminary determination of deadweight makes it possible to predict functional usefulness of a given design solution in the sense of estimation of value of mass which the vehicle is able to accommodate at maintaining positive buoyancy, i.e. the mass of:
- crew;
- equipment;
- instruments;
- materials;
- ballast.

The relationship (1) should serve for determination of vehicle deadweight of given dimensions, submersion depth H_{max} and kind of structural material. In the case of the reverse task when a demanded deadweight is given it should serve to determine vehicle's geometrical parameters.

The applied research methodology contain the following:
- choice of an interesting area of geometrical parameters of vehicles;
- a concept of geometrical configuration of vehicle;
- elaboration of systematical series of vehicles, covering the following:
  • set of values of geometrical parameters of vehicles;
  • set of values of permissible stresses for shell plating;
  • set of values of critical pressures and stresses for shell plating;
- elaboration of approximation formulae for critical values of plating thickness;
- elaboration of approximation formulae for minimum values of plating thickness;
- elaboration of approximation formulae for values of vessel's deadweight.

The considered range of maximum submersion depths of vessel results from the necessity of fulfilling the requirement of maintaining positive displacement of vessel at assumed structural materials. Initially the maximum permissible submersion depth of 6500 m was assumed, that is sufficient to ensure access to about 98% surface area of world ocean bed. Until now a few manned vehicles capable of submerging to that depth, have been built [1].

The analytical approximation formulae for sets of discrete values were determined by using non-linear methods for minimizing sums of deviation squares [2].

Results of the presented research are preliminary and approximate; the parameters of the vehicles have been determined under several assumptions simplifying the considered design problem. The method may be useful for preliminary design analyses or serve for generating initial values in searching the design solutions in further design stages performed with the use of more accurate design tools e.g. computer systems for structural analysis based on finite element methods. The presented method constitutes a successive contribution to elaboration of set of preliminary design methodical tools for underwater vehicles and is continuation of the methods published in [3] and [4].

GEOMETRICAL DESCRIPTION OF VEHICLE

The assumed geometrical configuration of vehicle is consisted of the axially symmetrical floats joined together with the space frame, as shown in Fig. 1.
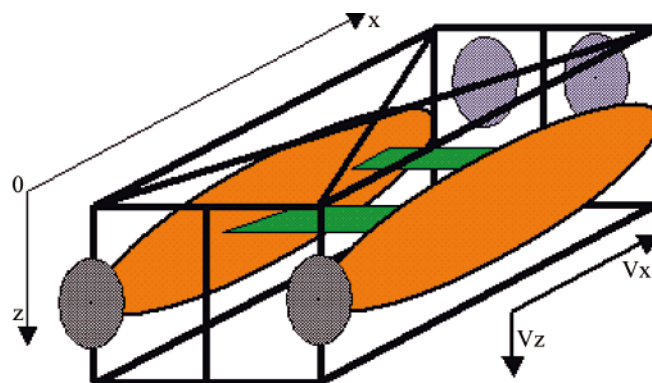
Fig. 1. *Draft of simplified configuration of underwater vehicle*

The vehicle's float is consisted of the shell plating (cylindrical part) and caps closing the shell. The caps support the shell loaded with constant external hydrostatic pressure. At an appropriate form of the caps the state of internal forces in float's shell plating is momentless, for instance it is the case when cap's surface is described by the generatrix of the equation as follows [5]:

$$\zeta = \frac{z}{l_d} = \left[1 - \left(\frac{r}{R}\right)^2\right]^{\frac{1}{t}} \longrightarrow z = l_d \cdot \left[1 - \left(\frac{r}{R}\right)^2\right]^{\frac{1}{t}} \quad (3)$$

where:
$t > 2$ – exponent value;
$r_d = r/R$ – dimensionless radius of float, $0 < r_d < 1$;
$\zeta = z/l_d$ – dimensionless camber of cap, $0 < \zeta < 1$;
z – cap's generatrix;
l_d – cap's camber.

The total length of float L_c, if length of shell is equal to L, is as follows:

$$L_c = L + 2l_d \quad (4)$$

The surface area of cap can be determined by using the formula [4]:

$$S_d\left(R, \frac{l_d}{R}, t\right) \cong \pi \cdot R^2 \cdot \left[1 + 0.4281 \cdot \left(\frac{l_d}{R}\right)^{1.411} \cdot t^{0.4862}\right] \quad (5)$$

where: S_d [m²] and R [m].

The cap's volume can be approximated as follows [4]:

$$V_d\left(R, \frac{l_d}{R}, t\right) \cong 0.5747 \cdot \pi \cdot \frac{l_d}{R} \cdot t^{0.2339} \cdot R^3 \quad (6)$$

where: V_d [m³] and R [m].

The float's volume V is consisted of the volume V_c of the shell of the length L and the cap's volumes:

$$V_c = \pi \cdot R^2 \cdot L \wedge V = 2V_d + V_c \quad (7)$$

The displacement of the vehicle with i – floats is:

$$D = \rho \cdot i \cdot V \quad (8)$$

SAFETY CRITERIA FOR VEHICLE

The dimensioning of shell plating thickness of float under hydrostatic pressure results from two safety criteria for float structure, namely:
- strength criterion which consists in confronting working stresses against permissible stresses in float shell plating;
- form stability criterion for float shell plating – by determining a critical pressure, exceedance of which results in loss of initial form of the shell.

The static equilibrium state of cylindrical form of float under constant external pressure at momentless state of stresses in shell plating, within the range of linear elastic deformations, is described by certain function of the form: w = w(z, φ), which is a solution of Eq. (9) which expresses shell plating strain energy. Depending on float's parameters, loss of stability of shell plating form may occur in the mode of axial or circumferential buckling [5, 6]. The mode of form stability loss depends on combination of float's geometrical and material parameters and loading, which are arguments of solutions of the shell stability equations (9) and (10), which express a pressure value causing loss of form stability.

Under certain simplifying assumptions the form stability equation can be represented as follows [5]:

$$G \cdot \nabla^8 w + \frac{E \cdot h}{R^2} \cdot \frac{\partial^4 w}{\partial z^4} + \frac{1}{2} \cdot p \cdot R \cdot \nabla^4 \left(\frac{\partial^2 w}{\partial z^2}\right) +$$

$$+ p \cdot R \cdot \nabla^4 \left(\frac{\partial^2 w}{R^2 \cdot \partial \varphi^2}\right) = 0 \quad (9)$$

where:

$$\nabla^4 w = \frac{\partial^4 w}{\partial z^4} + \frac{2}{R^2} \frac{\partial^4 w}{\partial z^2 \cdot \partial \varphi^2} + \frac{1}{R^4} \cdot \frac{\partial^4 w}{\partial \varphi^4} \quad (10)$$

$$G = \frac{E \cdot h^3}{12 \cdot (1 - v^2)} \quad (11)$$

and G - shell stiffness in bending, and h - shell plating thickness.

An allowable function of an a priori assumed form, which satisfies boundary conditions for shell plating deformations may be a solution of Eq. (9), e.g. the following function:

$$w = \bar{w} \cdot \sin \frac{\pi \cdot m \cdot z}{L} \cdot \cos(n \cdot \varphi) \quad (12)$$

where:
$\bar{w}$ – shell plating deflection;
m – number of longitudinal deformation half-waves;
n – number of circumferential deformation waves.

On substitution of the form function w into Eq. (9) the algebraic equation is obtained:

$$\frac{\bar{w}}{R^6} \left\{ \frac{D}{R^2} \cdot \left[\left(\pi \cdot m \frac{R}{L}\right)^2 + n^2 \right]^4 + E \cdot h \left(\pi \cdot m \frac{R}{L}\right)^4 + \right.$$

$$\left. - p \cdot R \cdot \left[\frac{1}{2} \left(\pi \cdot m \frac{R}{L}\right)^2 + n^2 \right] \cdot \left[\left(\pi \cdot m \frac{R}{L}\right)^2 + n^2 \right]^2 \right\} \cdot$$

$$\cdot \sin \frac{\pi \cdot m \cdot z}{L} \cdot \cos(n \cdot \varphi) = 0 \quad (13)$$

The pressure p which satisfies this equation is determined by the relation as follows [5]:

$$p(n, m) = \frac{\dfrac{(s^2 + n^2)^4}{12 \cdot (1 - v^2)} + s^4 \cdot \left(\dfrac{R}{h}\right)^2}{\left(\dfrac{s^2}{2} + n^2\right) \cdot (s^2 + n^2)^2} \cdot E \cdot \left(\frac{h}{R}\right)^3 \quad (14)$$

where: $s = \pi \cdot m \cdot \dfrac{R}{L}$

The critical value p_{cr} at which shell plating of cylindrical float under constant external pressure loses its form stability in the range of elastic deformations (undergoes buckling), is equal to the smallest value of the expression p(n, m) (14) – with respect to the number of longitudinal deformation half-waves, m, and the number of circumferential deformation waves, n, with which respective modes of form deformations and critical pressure correspond, at constant values of the dimension ratios R/L and R/h and the material constants E and v, namely:

$$p_{cr} = \min_{m, n} \{p(m, n)\} \quad (15)$$

where:
$m \wedge n \in N$ – natural number.

ASSUMPTIONS USED IN THE PRESENTED METHOD

The presented method was elaborated by assuming the typical geometrical features of uderwater vehicles and typical structural materials, which define and determine the set of parameters of the considered series of vehicles:
- the assumed number of half-waves of float axial deformations:
  m = 1
- the allowable range of shell dimension ratio:
  R/L 0.05 ≤ R/L ≤ 0.2
- the allowable range of the shell dimension ratio:
  R/h 10 ≤ R/h ≤ 25
- the geometrical parameters of cap:
  t = 3, l_d = L_d/R = 1
- the range of maximum submersion depth:
  maxH = 6500 m
- the structural material steel and alloy AL-5083
- material density of steel, AL-5083, respectively:
  ρ = 7.8 t/m³ ∧ ρ = 2.7 t/m³
- Poisson ratio (of steel, AL-5083, respectively):
  v = 0.3 ∧ v = 0.33
- Young modulus of steel: E = 2.1 · 10⁵ MPa
- Young modulus of AL-5083: E = 0.72 · 10⁵ MPa.

Under the above assumptions the series of vehicles of the following dimensions was determined:

$$0.25m < R < 3.0m \wedge 5m < L < 15m \wedge R/L =$$

$$= \{0.05, 0.1, 0.2\} \wedge R/h = \{10, 12, 20, 25\} \quad (16)$$

FORM STABILITY CRITERION FOR SHELL PLATING

The critical pressure p_{cr} is equal to the smallest pressure value which causes shell plating buckling with taking into account all possible modes of deformations [4, 5, 6]:

$$p_{cr} = \min_{m,n \in N} f(m, n, R/L, h/R, v, E) \quad (17)$$

On the basis of the determined set of discrete critical pressure values $\{p_{cr,i}\}$ calculated by (14) for the series of vehicles of steel shell plating the following non-structural formula which approximates the critical pressure, was determined:

$$p_{cr}(L, R, h) = c1 + c2 \cdot (R/h)^{c3} +$$

$$+ c4 \cdot (R/L)^{c5} + c6 \cdot (R/h)^{c7} \cdot (R/L)^{c8} \quad (18)$$

where pressure in [MPa], and the formula coefficients c_i are contained in Tab. 1.

Tab. 1. *The coefficients c_i in the formula (18) for $p_{cr}(L, R, h)$ in the case of steel shell plating of vehicle floats*

c1	c2	c3	c4
-1.91	-2994114	-2.11949	0.00323536
c5	**c6**	**c7**	**c8**
-2.59774	3036663	-2.1208	0.0033

The critical pressure for floats made of AL-5083 alloy is approximated by the following formula:

$$p_{cr}(L, R, h) = c1 + \frac{c2 \cdot \left(\dfrac{h}{R}\right)^{c3} + c4 \cdot \left(\dfrac{R}{L}\right)^{c5}}{c6 \cdot \left(\dfrac{h}{R}\right)^{c7} + c8 \cdot \left(\dfrac{R}{L}\right)^{c9}} \quad (19)$$

which expresses the best obtained approximation. The pressure is in [MPa], and the formula coefficients c_i are contained in Tab. 2.

Tab. 2. *The coefficients c_i in the formula (19) for $p_{cr}(L,R,h)$ in the case of AL-5083- alloy shell plating of vehicle floats*

c1	c2	c3	c4	c5
-0.095624	1267.01	3.5370424	1.84E-008	-5.040246
c6	**c7**	**c8**	**c9**	
0.18952	1.446856	1.92182	-2.4462	

In the preliminary designing procedure the reverse relation $h_{cr} = f(L, R, H)$, which expresses the critical thickness of float's shell plating in function of the critical pressure p_{cr}, is also useful. The best obtained approximation of such relation both for steel floats and AL-5083-alloy floats is represented by the following formula:

$$h_{cr}(L, R, H) =$$

$$R(c1 + c2 \cdot H^{c3} + c4 \cdot H^{c5} \cdot (R/L)^{c6}) \quad (20)$$

where: shell plating thickness, float's diameter and submersion depth are expressed in [m].

In the case of steel floats the coefficients c_i are given in Tab. 3.

Tab. 3. *The coefficients c_i in the formula (20) for h_{cr} in the case of steel shell plating of floats*

c1	c2	c3
-0.073192	5.662381	0.2618387
c4	**c5**	**c6**
-5.64124	0.2620584	0.000532829

In the case of AL-5083 -alloy floats the coefficients c_i are given in Tab. 4.

Tab. 4. *The coefficients c_i in the formula (20) for h_{cr} in the case of AL-5083 -alloy shell plating of floats*

c1	c2	c3
-0.080252	15.6114	0.2498738
c4	**c5**	**c6**
-15.582	0.24999	0.000273278

STRENGTH CRITERION FOR SHELL PLATING

In compliance with the Mises-Huber hypothesis the effort measure of structural material is determined by the reduced stress:

$$\sigma_{red} = \frac{1}{\sqrt{2}} \sqrt{\begin{array}{l}(\sigma_x - \sigma_y)^2 + (\sigma_y - \sigma_z)^2 + \\ + (\sigma_z - \sigma_x)^2 + 6 \cdot (\tau_{xy}^2 + \tau_{yz}^2 + \tau_{zx}^2)\end{array}} \quad (21)$$

In the case of thin-walled shells (of $R/h > 10$) and momentless loading of float, the stress state in the shell plating can be deemed planar, then the reduced stress can be expressed by means of the principal stresses: σ_z – axial and σ_φ – circumferential ones, as follows [5]:

$$\sigma_{red} = \sqrt{\sigma_z^2 + \sigma_\varphi^2 - \sigma_z \cdot \sigma_\varphi} \quad (22)$$

The strength safety criterion requires the maximum reduced stresses in shell plating not to exceed the permissible ones. Their value may be related to the yield point R_e of structural material, and the safety factor $n_s > 1$ of a value complying with a relevant standard or determined on the basis of experiments and practice, may be applied to obtain:

$$\sigma_{max} < \sigma_{per} = R_e/n_s \quad (23)$$

Depending on a required reliability of a device, value of the safety factor is usually contained within the range of $n_s = 1.1 \div 20$, but most often of $n_s = 2.5 \div 4.0$ [5, 6]. Hence the formula for the strength safety criterion takes the following form:

$$\sigma_{red\ max} = \max\left(\sqrt{\sigma_z^2 + \sigma_\varphi^2 - \sigma_z \cdot \sigma_\varphi}\right) \le \sigma_{per} = \frac{R_e}{n_s} \quad (24)$$

In the momentless state of stresses the float shell plating is under compression of uniformly distributed axial and circumferential forces. Unitary compressive forces in float shell plating, which result from the pressure p, are determined by the following relations:
- axial force per unit length of float circumference

$$N_z = \frac{F}{2 \cdot \pi \cdot R} = \frac{\pi \cdot R^2 \cdot p}{2 \cdot \pi \cdot R} \cong 0.5 \cdot R \cdot p \quad (25)$$

- circumferential force per unit length of float

$$N_\varphi = \frac{F}{2 \cdot R} = \frac{2 \cdot R \cdot L \cdot p}{2 \cdot L} = R \cdot p \qquad (26)$$

The principal axial stresses are determined by the relation:

$$\sigma_z = \frac{\pi \cdot R^2 \cdot p}{2 \cdot \pi \cdot R \cdot h} \cong 0.5 \cdot \frac{R}{h} \cdot p \qquad (27)$$

and, the principal circumferential stresses by:

$$\sigma_\varphi = \frac{2 \cdot R \cdot p \cdot L}{2 \cdot L \cdot h} = \frac{R}{h} \cdot p \qquad (28)$$

At the slowly changing external pressure p_{max} exerted on float the safety stresses are determined by the relation:

$$\sigma_{red\,max} = \max\left(\sqrt{\sigma_z^2 + \sigma_\varphi^2 - \sigma_z \cdot \sigma_\varphi}\,\right) =$$
$$= \frac{\sqrt{3}}{2} \cdot \frac{R}{h} \cdot p_{max} \le \sigma_{per} = \frac{R_e}{n_s} \qquad (29)$$

and the minimum allowable thickness of shell plating, h_{per}, is determined by the following criterion:

$$h_{per} \ge \frac{\sqrt{3}}{2} \cdot \frac{R}{\sigma_{per}} \cdot p_{max} \qquad (30)$$

DEADWEIGHT OF SUBMERGED VEHICLE

By making use of the relations (2), (20), (30), the approximation formula which express the deadweight Pn of vehicle were determined, depending on:
- structural material parameters;
- the float's radius R [m];
- the dimension ratio R/L;
- the submersion depth H in water of the density:
  $\rho = 1.025$ t/m³.

The best obtained approximation of the deadweight, both in the case of steel shell plating and that made of AL-5083 alloy, is represented by the following expression:

$$P_N (L, R, H) =$$
$$= c1 + c2 \cdot H^{c3} \cdot \left(\frac{R}{L}\right)^{c4} \cdot R^{c5} + c6 \cdot \left(H \cdot \frac{R}{L} \cdot R\right)^{c7} \qquad (31)$$

where the deadweight is expressed [tons], the submersion depth and float radius in [m], and the coefficients ci - in the case of steel shell plating - are contained in Tab. 5.

Tab. 5. The coefficients ci in the formula for the load carrying capacity P_N in the case of steel shell plating of floats

c1	c2	c3	c4
0.0176694	3.50444	0.145877	-0.0182298
c5	c6	c7	
2.129365	-0.0019671	2.14081	

In the case of AL-5083 alloy shell plating the coefficients ci in the formula (31) are given in Tab. 6.

Tab. 6. The coefficients ci in the formula for the load carrying capacity P_N in the case of AL-5083-alloy shell plating of floats

c1	c2	c3	c4
0.0554155	3.9192	-0.375151	-1.13152
c5	c6	c7	
2.025946	-7.19344E-005	1.8138323	

Technically acceptable are those design solutions which fulfil the condition $P_N > 0$. As results from the performed research, in the case of steel floats – the formula (31) is applicable ($P_N > 0$) if both the following conditions are satisfied simultaneously:

$$H < 500 \text{ m} \wedge 0.05 < R/L < 10 \wedge$$
$$\wedge 0.25 \text{ m} < R < 1.50 \text{ m} \qquad (32)$$

And, in the case of greater submersion depth values:

$$500 \text{ m} < H < 1000 \text{ m} \wedge R/L = 0.05 \wedge$$
$$\wedge 0.25 \text{ m} < R < 0.75 \text{ m} \qquad (33)$$

In the case of AL-5083 alloy floats the formula (31) is valid, i.e. $P_N > 0$, when both the following conditions are satisfied simultaneously:

$$500 \text{ m} < H < 6500 \text{ m} \wedge R/L = 0.05 \wedge$$
$$\wedge 0.25 \text{ m} < R < 0.75 \text{ m} \qquad (34)$$

And, in the case of greater float diameter values the condition $P_N > 0$ is fulfilled if both the following conditions are satisfied simultaneously:

$$500 \text{ m} < H < 1500 \text{ m} \wedge R/L = 0.10 \wedge$$
$$\wedge 0.50 \text{ m} < R < 1.50 \text{ m} \qquad (35)$$

EXAMPLES OF APPLICATION OF THE PRESENTED METHOD

Example 1.

The design parameters have to be determined for an underwater vehicle float made of steel, having shell length L = 15.00 m, shell diameter d = 1.50 m, and cap parameters $l_d = R$ and t = 3, for the maximum permissible submersion depth H = 900 m.

For the given parameters, in accordance with Eq. (31):
- the load carrying capacity of the float is:

$$P_N = 0.0176694 + 3.50444^{0.145877} \cdot$$
$$\cdot 0.05^{-0.0182298} \cdot 0.75^{2.129365} +$$
$$- 0.0019671 \cdot (900 \cdot 0.05 \cdot 0.75)^{2.14081}$$

- the mass displacement of the float, acc. (6), (7) and (8), is:

$$D = \rho \cdot V \cong 1.025 \cdot 2 \cdot$$
$$\cdot \left[\left(0.5747 \cdot \pi \cdot \frac{l_d}{R} \cdot t^{0.2339} \cdot R^3\right) + \pi \cdot R^2 \cdot L\right] \cong 29.2 \text{ t}$$

- the critical shell plating thickness of the float, acc. (20), is:

$$h_{cr} \cong R \cdot \left(c1 + c2 \cdot H^{c3} + c4 \cdot H^{c5} \cdot \left(\frac{R}{L}\right)^{c6}\right) \cong$$
$$\cong 0.75 \cdot (-0.073192 + 5.662381 \cdot 900^{0.261838} +$$
$$- 5.64124 \cdot 900^{0.262058} \cdot (0.05)^{0.00053283}) \cong$$
$$\cong 0.0418 \text{ m} = 41.8 \text{ mm}$$

- the reduced stresses in shell plating, based on Eq. (29), are:

$$\sigma_{red} = \frac{\sqrt{3}}{2} \cdot \frac{R}{h} \cdot p = \frac{\sqrt{3}}{2} \cdot \frac{0.75}{0.0418} \cdot$$
$$\cdot 0.001 \cdot 900 \cdot 1.025 \cdot 9.81 \cong 141 \text{ Mpa}$$

Example 2.

The design parameters have to be determined for an underwater vehicle consisted of two floats made of AL-5083 alloy and having the shell length $L = 15.00$ m, shell diameter $d = 1.50$ m and the cap parameters $l_d = R$ and $t = 3$. The maximum permissible submersion depth has to be equal to $H = 3000$ m.

For the given parameters:

- the load carrying capacity of the float, acc. Eq.(31), is:

$$P_N = 2 \cdot (0.00554155 + 3.919205 \cdot 3000^{-0.375151} \cdot$$
$$\cdot \, 0.05^{-1.131516} \cdot 0.75^{2.025946} - 0.0000719344 \cdot$$
$$\cdot \, (3000 \cdot 0.05 \cdot 0.75)^{1.813832}) \cong 5.79 \text{ t}$$

- the mass displacement of the float, acc. Eq.(6), (7) and (8), is:

$$D = \rho \cdot V \cong$$
$$\cong 2 \cdot \left\{ 1.025 \cdot 2 \cdot \pi \cdot \left[\left(0.5747 \cdot \frac{l_d}{R} \cdot t^{0.2339} \cdot R^3 \right) + R^2 \cdot L \right] \right\} \cong$$
$$\cong 58.4 \text{ t}$$

- the critical shell plating thickness of the float, acc. (20), is:

$$h_{cr} \cong R \cdot \left(c1 + c2 \cdot H^{c3} + c4 \cdot H^{c5} \cdot \left(\frac{R}{L} \right)^{c6} \right) \cong$$
$$\cong 0.75 \cdot \left(-0.080252 + 15.6114 \cdot 3000^{0.2498738} + \right.$$
$$\left. -15.582 \cdot 3000^{0.24999} \cdot \left(\frac{0.75}{15} \right)^{0.000273278} \right) \cong$$
$$\cong 0.09538 \text{ m} \cong 95.4 \text{ mm}$$

- the reduced stresses in shell plating, based on Eq. (29), are:

$$\sigma_{red} = \frac{\sqrt{3}}{2} \cdot \frac{R}{h} \cdot p = \frac{\sqrt{3}}{2} \cdot \frac{0.75}{0.0954} \cdot$$
$$\cdot \, 0.001 \cdot 3000 \cdot 1.025 \cdot 9.81 \cong 205 \text{ Mpa}$$

NOMENCLATURE

D – mass displacement in state of submersion;
E – Young modulus of structural material;
G – shell plating stiffness in bending;
H – submersion depth;
H_{max} – maximum permissible submersion depth of vehicle;
L – float shell length;
L_c – total float length;
M – mass of structure;

N_z – axial force per unit length of float circumference;
N_φ – circumferential force per unit length of float generatrix;
P_N – load carrying capacity;
R – float shell radius;
R_e – material yield point;
S_d – cap surface area;
V – float volume;
V_c – shell volume;
V_d – cap volume;
h – shell plating thickness;
h_{min} – minimum acceptable shell plating thickness;
h_{cr} – critical shell plating thickness of floats;
h_{per} – minimum permissible shell plating thickness;
i – number of floats;
l_d – cap camber;
m – number of longitudinal half-waves of deformation;
n – number of circumferential waves of deformation;
n_s – safety factor;
p – external pressure;
r_d – dimensionless radius of float;
t – index exponent of cap form;
$\overline{w}$ – shell plating deflection;
z – cap generatrix;
ν – Poisson ratio of structural material;
ρ – water density;
σ_{red} – reduced stress;
σ_z – principal axial stresses;
σ_φ – principal circumferential stresses;
ξ – dimensionless camber of cap.

BIBLIOGRAPHY

1. Sborshchikov I. M.: *Possibilities and Problems in Using Deep Submersibles for Geology*. International Journal of Offshore and Polar Engineering Vol. 6, No.4, December 1996.
2. Sherrod P.H.: *Nonlinear Regression Analysis Program*.
3. Michalski J.P.: *Parametric method for determination of motion characteristics of underwater vehicles, applicable in preliminary designing*. Polish Maritime Research. No 2 (60). 2009.
4. Michalski J.P.: *Preliminary Designing Method of External Pressure Vessels for Sea Subsurface Application*. Polish Maritime Research. No 2 (64) 2010.
5. Magnucki K.: *Strength and optimization of thin-walled vessels* (in Polish). Wydawnictwo Naukowe PWN (State Scientific Publishers). Warsaw, Poznan, 1998.
6. Timoshenko S.: *Theory of Elastic Stability*. McGraw-Hill Book Co., New York, 1936.

CONTACT WITH THE AUTHOR

Assoc. Prof. Jan P. Michalski
Faculty of Ocean Engineering
and Ship Technology
Gdansk University of Technology
Narutowicza 11/12
80-233 Gdansk, POLAND
e-mail: janmi@pg.gda.pl

Numerical Analysis of Hub Effect on Hydrodynamic Performance of Propellers with Inclusion of PBCF to Equalize the Induced Velocity

Hassan Ghassemi, Assoc. Prof.
Amirkabir University of Technology
Amin Mardan, Ph. D.
Malekashtar University of Technology, Shahinshar-Isfahan, Iran.
Abdollah Ardeshir, Ph. D.
Amirkabir University of Technology, Tehran, Iran

ABSTRACT

In this article the boundary element method (BEM) is applied to analyze the propeller hub as a non-lifting body and the blades in its vicinity as lifting bodies. In solver, the geometrical modeling of hub, blades are PBCF (Propeller Boss Cap Fin) constructed by quadrilateral elements. The velocity potential is determined on each element by discretized boundary integral equation. Iterative procedure is used to consider the adjacent body effect. In each step the body was independently analyzed with the influence of near body considered in inflow velocity. The induced velocity of propeller was calculated with and without PBCF in downstream. PBCF, an energy-saving device, reduces and uniforms the induced velocity of propeller in downstream. Numerical results of propeller hydrodynamic characteristics including hub effect, induced velocities, PBCF influence are presented.

Keywords: propeller hub; induced velocities; hub vortex; PBCF

INTRODUCTION

The propeller is located at the stern of a ship where the inflow current is non-uniform due to boundary layer and wake formation. The propeller produces axial thrust from the engine power transmitted to it through a shaft. One of the augmentation tools for increasing thrust is the use of PBCF at the end of the hub, which causes to eliminate the hub vortex. The harmful effect of the hub vortex is twofold, firstly, it reduces the efficiency of the propeller and secondly, the rudder is exposed to corrosion because it is located downstream of the propeller where cavitation takes place.

Studies show that the performance of the propeller will degrade around the end portion of the hub. The vortices formed on the propeller's hub reduce the efficiency. The strength of the vortices depends on the axial load distribution on the propeller, and the geometry of the hub. The fins on the hub reduce cavitation of the hub and as a result the hydro-acoustic noise is reduced. In addition, the fins increase the efficiency of the propeller, especially in the case of controllable pitch propellers [1].

The effect of hub on hydrodynamic performance of the propeller is significant. There is some practical research on the hub size of the USS Barbey. In 1978, Wind [2] proposed a criterion for minimum hub diameter and suggested that the hub diameter of this ship should be increased from 1320 mm to 1500 mm. He anticipated that the efficiency decreases

proportionally to the decrease in surface area of the propeller's disc. The larger hub has greater hydrodynamic effect on blades and has to be considered in design process. A comparison between the efficiency of these two design situations gives important results.

Hess [3] employed source and dipole distribution for modeling blades and source distribution for modeling hub. In this study the lift force is displaced from intersection of the hub and blade to axis of rotation. This means zero angle of circulation in hub. In other words an extra strip from hub surface to hub center transfers a dipole with constant strength equal to the strength of the first strip on the blade. The hub vortex is formed along the axis of rotation and the vortex power is equal to sum of the power of all dipoles transferred from all blades. In 1991, considering the noise due to loading in stable conditions, Glegg showed that the hub effect on radiated noise of propeller in downstream is substantial [4]. In a research performed in 1992 on controllable pitch propellers it was shown that in addition to the pressure distribution in sections near the blade root the hub also affects the performance of the propeller in open-water condition [5]. According to the results obtained by Liu in 1995, in ordinary hubs of small diameter, which are mainly used in constant pitch propellers and surface ships, the effect of hub on hydrodynamic forces of the propeller such as thrust and torque, is not remarkable [6].

In 2009, Cai et al. [7] applied source and dipole singularities to analyze the propellers having nozzle including the effect of

the hub. An iterative procedure was used to consider the effect of hub and blades on each other. In each step, hub and blades were independently analyzed with the influence of adjacent body considered in inflow velocity.

Now, the energy-saving propeller boss cap fins (PBCF) have been ordered for 2000 vessels worldwide. The PBCF is an energy-saving device attached to the propellers of vessel. It breaks up the hub vortex generated behind the rotating propeller (Fig. 1). Research and development studies on the PBCF started in 1986, and sales began the following year. Since then an increasing number of ship owners, mainly in Japan, began to
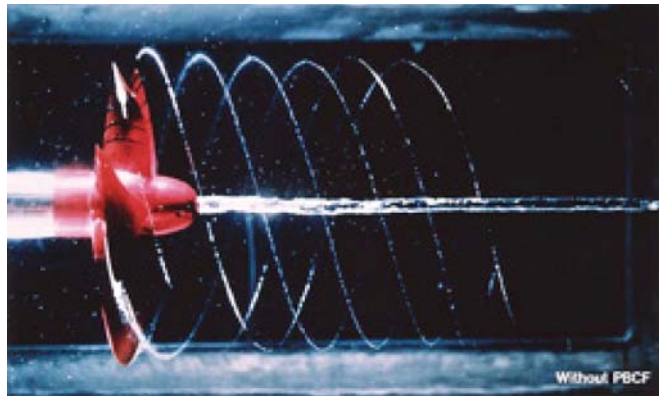
Before installation of PBCF
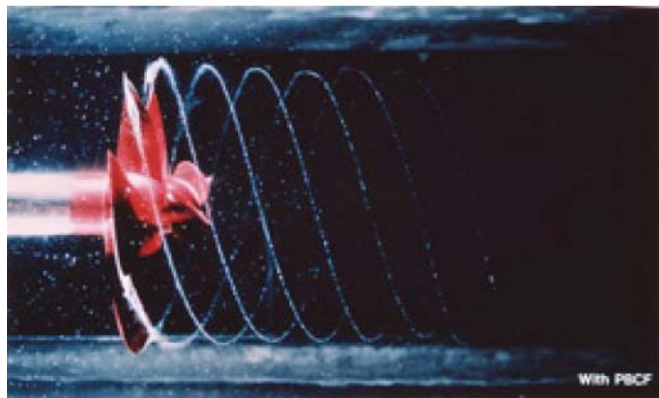
After installation of PBCF

PBCF

Fig. 1. *Hub vortex disappears after the installation of PBCF [8]*

adopt the system. In 1988 Ouchi first introduced it with the aim of increasing the efficiency and reducing energy loss due to hub vortex formation. Such vortex contains vapour bubbles that when burst, cause noise, corrosion and vibration in the system. By using fins, the vortices flowing on the hub are weakened and therefore the kinetic energy of rotational current is retrieved [9]. Ouchi et al. [10-12], during 1989 and 1992, extended and performed both numerical and experimental research on PBCF. They concluded that PBCF has significant effect on the energy saving. It not only causes to avoid the hub vortex but also increases the efficiency and reduce fuel consumption. Junglewitz reported that the use of PBCF results in hub vortex reduction and in consequence 2 to 5% increase in the efficiency [13]. Hsin et al. [14] presented a design procedure for a PBCF with the use of computational fluid dynamics (CFD).

The SPD (Ship Propeller Design) software code has been prepared by Ghassemi (the first author) and employed to the various propulsors such as propeller-rudder system (PRS) [15], high-skewed propeller [16], contra-rotating propeller [17] and surface piercing propeller [18], underwater vehicle under surface and submerged conditions [19]. In this code BEM is employed to perform the hydrodynamic analysis of marine propellers of all types. In June 2011 at the Second International Symposium on Marine Propulsors in Hamburg, Germany, the UK BMT Defence Services presented a paper reporting on 'a before and after' speed test on an Aframax ship operated by a major firm. This showed energy saving of about 4% [20].

In this article, the presence of the fins in induced downstream effects of the propeller is analyzed. The performance of the fins at the end of the hub is evaluated by changing two parameters: the angle of installation of the fin on the end of the hub and the phase angle between propeller and the fin. In addition, the effect of hub diameter and its conical angle which are common parameters in hydrodynamic design of hull and propeller, is studied. The following sections are organized as follows: modeling the PBCF is explained in Sec. 2, governing equations are described in Sec. 3, numerical results and discussions are presented in Sec. 4. Finally, the conclusions are given in Sec. 5.

MODELING THE PBCF

In geometrical design of PBCF the following points have to be noted [11]:
- The number of fins should be equal to the number of blades of the propeller.
- The phase difference between the cross-section of the blade root and the fins varies from -20 to 30 degrees.
- The diameter of the fins should not exceed 33% of the propeller's diameter.
- The leading edge of the fins is located between the roots of two adjacent blades.

The first point is because each fin has to reduce the wake of one blade. The inflow velocity, rotational speed (rpm) of the propeller and the angle of attack of blade cross section determines the second point. In formulating Point 3, it is noted that increasing the surface area of the fins produces torque and reduces the efficiency of the propeller, therefore a limitation on diameter is imposed. Total impact of the wake due to the fin surface is considered in Point 4. Including all these parameters into design procedure is rather complicated. In this research a technique was attempted to construct a model of PBCF with the use of the above-mentioned points. Fig. 2 shows a model of PBCF with trailing vortex wake. The total number of the elements is the summation of elements on blades, hub and

fins. The total numbers of elements are equal to 8500, i.e. 2400 located on blades, 2400 on fins and 3500 on the hub. The main parameters of the Φ propeller and the fin are listed in Tabs.1 and 2.

Tab. 1. Main dimensions of the propeller

Parameter	Value
Number of blades	4
Diameter [m]	1.0
Pitch ratio (at 0.7R)	1.084
Expanded Area Ratio (EAR)	0.5
Skew [deg.]	10
Rake [deg.]	6
Direction of rotation	Clockwise
Propeller type	MAU

Tab. 2. Main parameters of the PBCF

Parameter	Value
Number of fins	4
Diameter [m]	0.33
Angle of installation	variable
Chord of fin	variable
Direction of rotation	clockwise
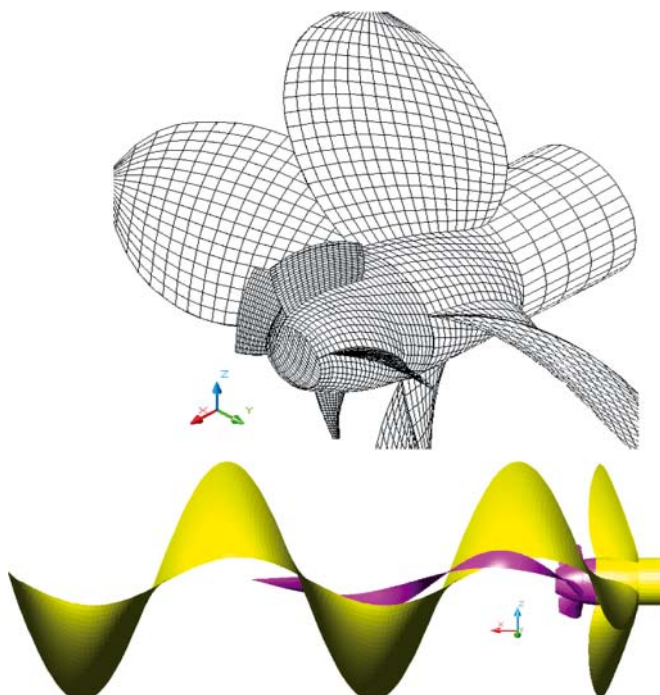
Fig. 2. The PBCF model along with trailing vortex wake

GOVERNING EQUATIONS

As assumed, the flow is considered inviscid, incompressible and irrotational around the body. The assumptions lead to a boundary value problem for the velocity potential with the Laplace equation satisfied in the fluid domain.

$$\nabla^2 \Phi(x, y, z) = 0 \qquad (1)$$

The potential equation is an elliptical equation and for its solution, we need to define Φ on the boundary or its derivative $\partial \phi / \partial n$ in the perpendicular direction to the boundary. On the surface of the body, velocity component perpendicular to the element boundary should be zero. Therefore, the Neumann boundary condition called kinematic boundary condition could be used. This states that the total velocity normal to surface is zero.

$$\Phi = \emptyset + \emptyset_{in}$$
$$\Rightarrow \frac{\partial \Phi}{\partial n} = 0 \Rightarrow \frac{\partial \emptyset}{\partial n} + \frac{\partial \emptyset_{in}}{\partial n} = 0 \qquad (2)$$
$$\Rightarrow \frac{\partial \emptyset}{\partial n} = -\emptyset_{in} = -V_0 . \vec{n}$$

where:
$\vec{n}$ – the normal vector of the surface.

The thickness of the wake surface is assumed zero. The normal velocity difference and the transverse pressure difference is zero, although the potential difference could be present.

$$(\Delta p)_{on\ S_w} = p^+ - p^- = 0$$
$$\left(\Delta \frac{\partial \phi}{\partial n} \right)_{on\ S_w} = \left(\frac{\partial \phi}{\partial n} \right)^+ - \left(\frac{\partial \phi}{\partial n} \right)^- = 0 \qquad (3)$$

For the lifting bodies in steady state, the potential difference in transverse direction to the wake surface, is equal to the circulation around the body and is constant along the streamline on the wake surface.

$$(\Delta \phi) on S_w = \phi^+ - \phi^- \qquad (4)$$

To uniquely determine the circulation on the trailing edge of the blade, the Kutta condition is used. Generally, this condition states that the flow velocity remains constant at the trailing edge of the blade.

$$|\nabla \phi|_{T.E.} < \infty \qquad (5)$$

On the external control surface, in the case that this surface is located at infinite distance from the body, the disturbance velocity created by the body should vanish.

$$\nabla \phi \rightarrow 0 \ \{S_\infty \rightarrow \infty\} \qquad (6)$$

THE BOUNDARY ELEMENT METHOD

The boundary value problems of velocity potential outside the body surface could be converted to an integral equation:

$$2\pi\phi(p) = \iint_{S_B} \left[\phi(q) \frac{\partial}{\partial n_q} \frac{1}{R(p;q)} - \frac{\partial\phi(q)}{\partial n_q} \frac{1}{R(p;q)} \right] dS +$$
$$+ \iint_{S_W} \Delta\phi(q) \frac{\partial}{\partial n_q} \frac{1}{R(p;q)} dS \qquad (7)$$

Equation (7) is the second-type Fredholm integral equation for the variable ϕ, since $\partial \phi / \partial n$ is known on the surface of the body. The potential difference in transverse direction through the wake surface is equal to the potential difference of the top and bottom surfaces of the blade at the trailing edge. Discretizing the equation (7) results in a linear system of equations with the variable ϕ. The surface velocity and, as a result, the pressure on the surface of the body could be obtained by numerical differentiation of the calculated potential distribution. R(p;q)

is the distance of the point p (x, y, z) from the point q(ξ, η, ζ). It is expressed as follows.

$$R = |Q - P| =$$
$$= \sqrt{(\xi - x)^2 + (\eta - y)^2 + (\zeta - z)^2}$$ (8)

The induced velocities in a field point p outside the body surface, is obtained by the gradient of the velocity potential φ.

$$v(p) = \nabla_p \phi(p) =$$
$$= \frac{1}{4\pi} \iint_{S_B}^{\cdot} \phi(q) \nabla_p \frac{\partial}{\partial n_q} \frac{1}{R(p,q)} dS +$$
$$+ \frac{1}{4\pi} \iint_{S_W}^{\cdot} \Delta\phi(q) \nabla_p \frac{\partial}{\partial n_q} \frac{1}{R(p,q)} dS +$$ (9)
$$- \frac{1}{4\pi} \iint_{S_B} (V_I \cdot n_q) \nabla_p \frac{1}{R(p,q)} dS$$

CALCULATION OF THE HYDRODYNAMIC PERFORMANCE

By using finite difference method, the potential derivatives in radial direction and along chord length could be determined and the velocity distribution on the propeller's surface could be computed. The criteria for evaluating the performance of a propeller are: thrust coefficient, torque coefficient and efficiency which are determined according to tangential velocity distribution on the surface.

$$C_p(p) = 1 - \frac{|V_I|^2}{|V_T|^2}$$

$$P(p_i) = \frac{1}{2} \rho [|V_I|^2 - |V_T|^2]$$

$$T_{Potential} = K \sum_{i=1}^{N_B} P(p_i) n_{xi} \cdot \Delta S_i$$ (10)

$$Q_{Potential} = K \sum_{i=1}^{N_B} P(p_i)(n_{yi} \cdot z_i - n_{zi} \cdot y_i) \cdot \Delta S_i$$

The element area, normal vector components (n_x, n_y, n_z), coordinates of the center of the element (x,y,z) and number of blades (Z) are the geometrical parameters which influence the thrust and torque of the propeller in potential flow. For determining the viscosity effects, its drag coefficient is determined experimentally:

$$V_j = \sqrt{V_A^2 + (2\pi n r_j)^2}, \qquad j = 1,2,3,\dots,m$$

$$Rn_j = \frac{(chord \times V)_j}{\nu}$$

$$Force_j = 0.5\rho(C_f \times chord \times V^2)_j$$ (11)

$$T_{viscous} = K \sum_{i=1}^{m} Force_j \cdot \sin\beta_j$$

$$Q_{viscous} = K \sum_{i=1}^{m} r_j \cdot Force_j \cdot \cos\beta_j$$

Total thrust and torque are the sum of viscous component and potential components.

$$T = |T_{Pot}| + |T_{Vis}|$$
$$Q = |Q_{Pot}| - |Q_{Vis}|$$ (12)

Finally, the hydrodynamic characteristics of the propeller can be defined as:

$$J = \frac{V_A}{nD}, \qquad \eta = \frac{K_T}{K_Q} \frac{J}{2\pi}$$
$$K_T = \frac{T}{\rho n^2 D^4}, \qquad K_Q = \frac{Q}{\rho n^2 D^5}$$ (13)

where:
ρ – density of water,
υ – kinematic viscosity,
n – rotational speed of the propeller
D – diameter of the propeller.

NUMERICAL RESULTS AND DISCUSSION

Effect of hub diameter

In this section the effect of increasing hub diameter with respect to propeller diameter is investigated for constant - diameter and adjustable - diameter propellers. The relative percent change of the hydrodynamic coefficients with and without hub is obtained from the following equation:

$$\%Delta = \frac{Hydro\ Coeff._{(without\ Hub - with\ Hub)}}{Hydro\ Coeff._{without\ Hub}} \times 100$$ (14)

Fig. 3 shows the relative percent change of the propeller coefficients versus hub ratio. In the first case, the diameter of the propeller is constant while the diameter of the hub is increasing. In the second case, the diameter of the hub and propeller has been increased with the same ratio. The results show that the hub effect will reach its minimum at a certain hub ratio. On the other hand, the percent change in hydrodynamic coefficients is equal in both cases. The reason that percent change remains constant in the two cases is that the expanded area ratio, the number of blades, pitch of the propeller and hub ratio have remained constant. Comparing the change in circulation distribution in radial direction due to change in hub ratios, it could be seen that in case of low hub ratio, the
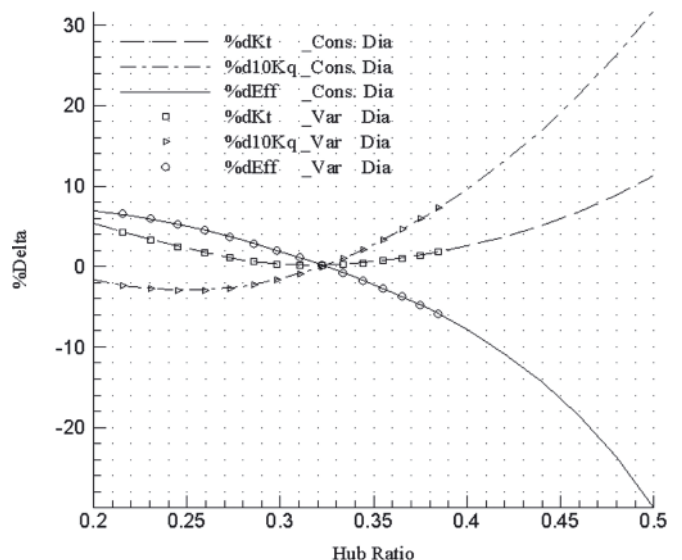
Fig. 3. *Relative percent change of the propeller coefficients versus hub ratio*

effect of hub is limited to the radial cross-sections near to the root but with increasing hub ratio, the outer cross-sections also become affected.

Thrust and torque changes with different hub ratios in cases of constant and variable diameter are shown in Figs. 4 and 5, respectively. In the case of constant diameter, due to decrease in the space between the root and tip of the propeller, the thrust and torque decrease, but in the case of variable diameter, this space is increasing with a constant factor and it seems logical that the output curves of the propeller are ascending.
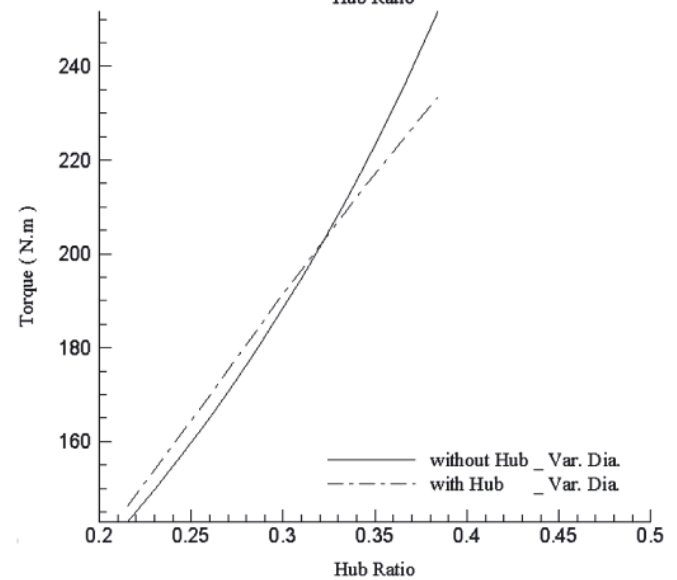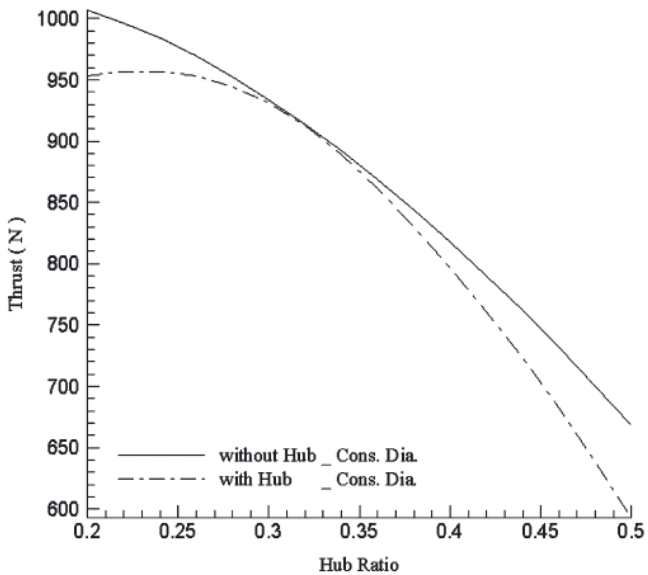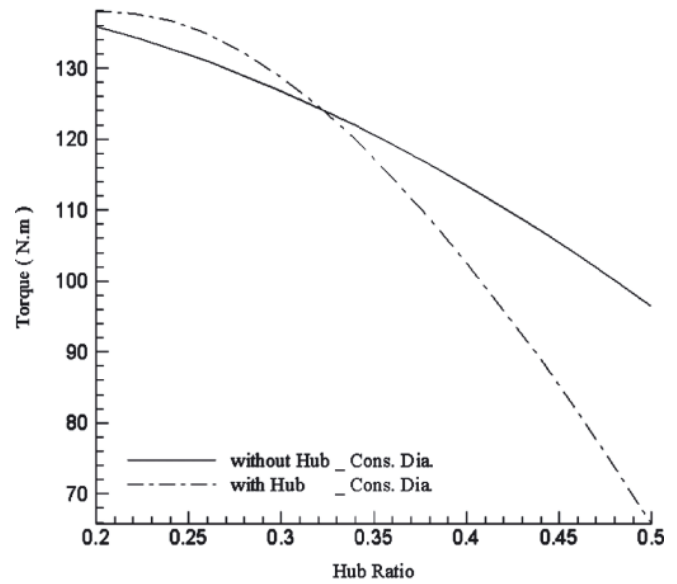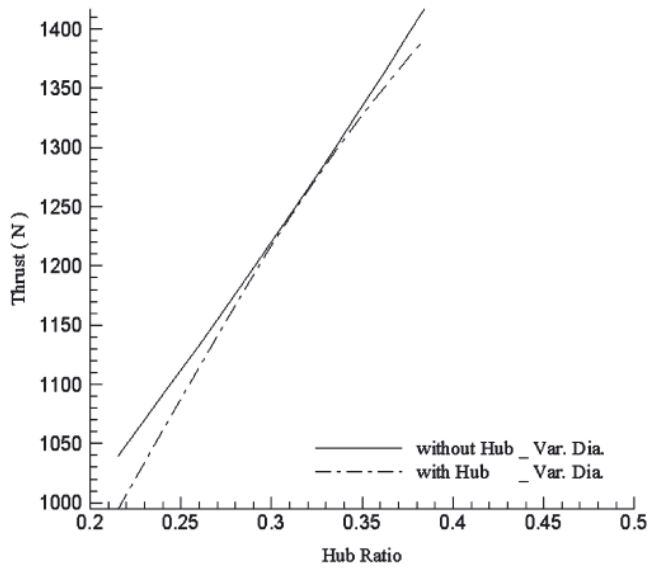
Fig. 4. Thrust change with different hub ratios
for constant and variable diameter cases

Fig. 5. Torque change with different hub ratios
for constant and variable diameter cases
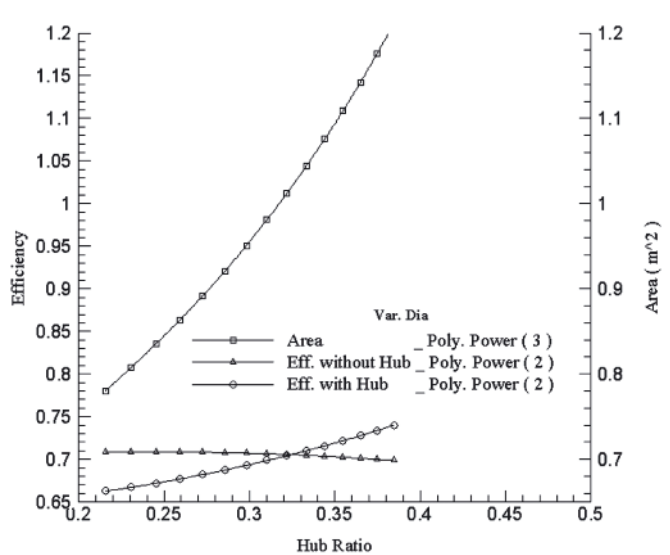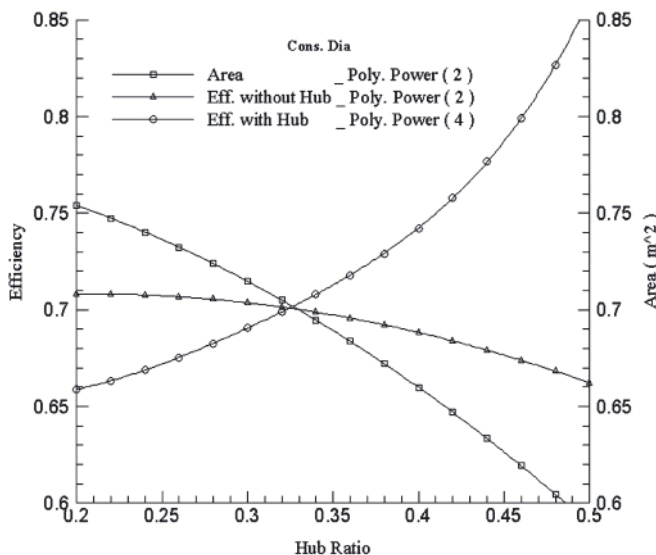
Fig. 6. The effect of hub on efficiency change for constant and variable diameter cases

In the constant diameter case, the hub has significant effect on propeller's efficiency such that the order of the polynomial proportional to efficiency change has risen by two (Fig. 6). In the variable diameter case, although the hub has changed the performance of the propeller, the order of the polynomial has not changed.

Effect of the conical angle of hub

The conical angle may change from zero to 15 degrees at three different hub ratios. Fig. 7 shows the change in hydrodynamic coefficients versus conical angle of hub at two hub ratios (0.2 and 0.4). At both hub ratios, when the conic angle of the hub increases, the change in the hydrodynamic coefficients increases. In the case of 0.3 hub ratio, the thrust and torque coefficients increase more while the efficiency is changed slightly.

hub ratio = 0.2

hub ratio = 0.3
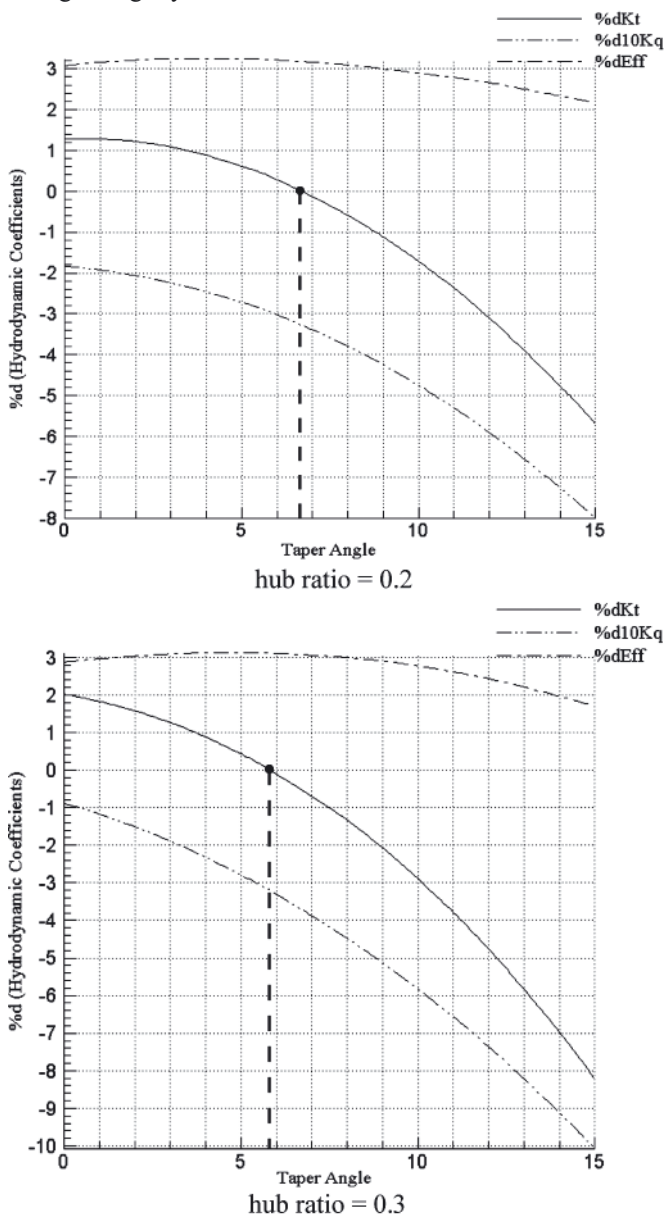
Fig. 7. Change in the performance coefficients along with increasing the hub angle

Analyzing the performance of PBCF

In this section, besides analyzing the hydrodynamic effect of the fin, the change in its geometrical parameters is studied. Generally, the effect of the fins is to reduce the induced velocity

which in turn reduces the hub vortex. Here, the effect of the fin at the end of the hub and the effect of its position and angle on the induced velocity is examined.

A. Overall analysis of the PBCF

PBCFs are not considered thrust producing devices. Their purposes are to reduce and distribute hub vortex into bigger core at the downstream where it is spread out. Fig. 8 shows axial induced velocity contour at downstream position, $x/R_{PBCF} = 0.5$, with and without fins. It may be seen that the fins caused significant reduction in maximum induced velocity and more uniform distribution of induced velocities.

with fin

w/o fin
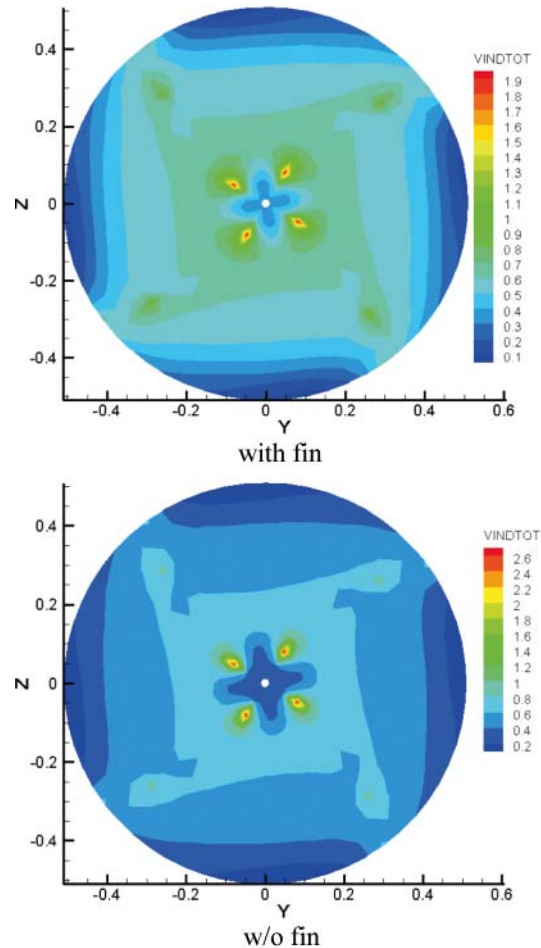
Fig. 8. Axial induced velocity contour at downstream position, $x/R_{PBCF} = 0.5$

The change in induced effects of the propeller in axial direction is shown in Fig. 9. Without fins, the induced effects are conveyed downstream with a certain period. This periodic feature is related to the formation of flow near the end of the hub, which is proportional to propeller's rotational speed. Installing fins at the end of the hub minimizes these effects.

The most important effect of the fins is reduction of negative or backward components of the induced effects in axial direction. As the distance from the propeller increases the effects become reduced.

B. Effect of phase difference between the blade and fin

Fig. 10 shows the change in phase difference between the fin and propeller. The fin should be so placed that its leading edge lies between two blades, so that it has the best performance. This is analyzed by changing the phase difference between the fin and the blades. Fig. 11 shows the change in axial component of the induced velocities as the angular position of the fin is changing (phase difference of $\pi/14$ and $6\pi/14$) at the axial

w/o fin

with fins
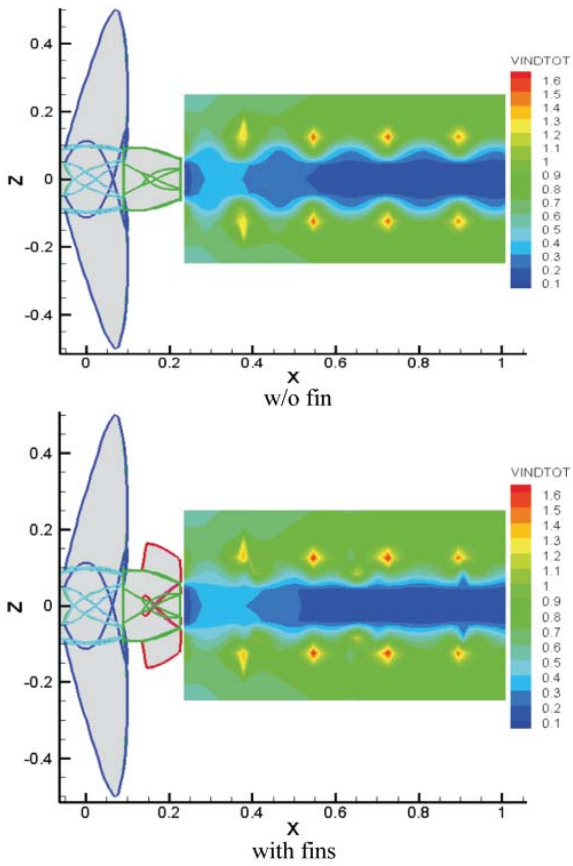
Fig. 9. *Axial induced velocity contour (with and without fins)*

distance of $x/R_{PBCF} = 0.5$ from the end of the propeller. By changing the angular position of the fin, the negative component of the induced velocities has increased more.
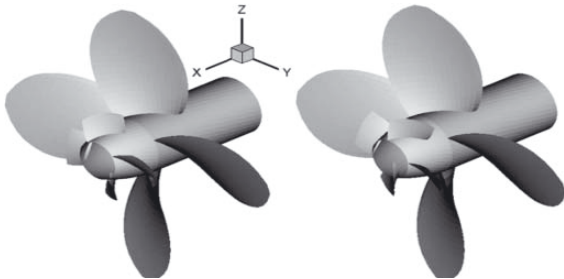
Fig. 10. *The change in phase difference between the fin and propeller*

C. Effect of fin installation

Angle of installation is one of the geometrical parameters of the fin, which is related to the pitch angle. The change in the angle of installation of the fin is plotted in Fig. 12 for two pitch ratios of 1 and 2. Fig. 13 shows the axial induced velocity at the two pitch ratios. In these calculations, we were seeking the effect of the angle on the axial induced velocity. The greater the angle or pitch the greater the effect of induced velocity.
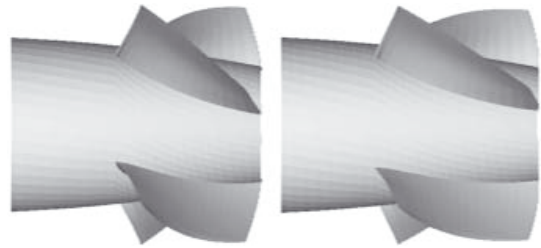
Fig. 12. *The change in angle of installation of the fin*

pitch ratio of fin = 1
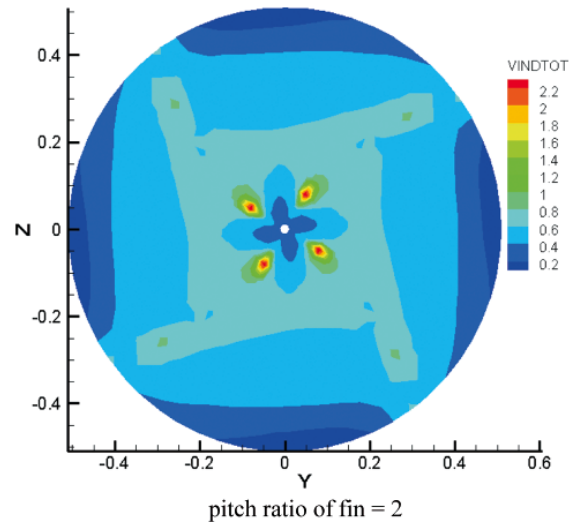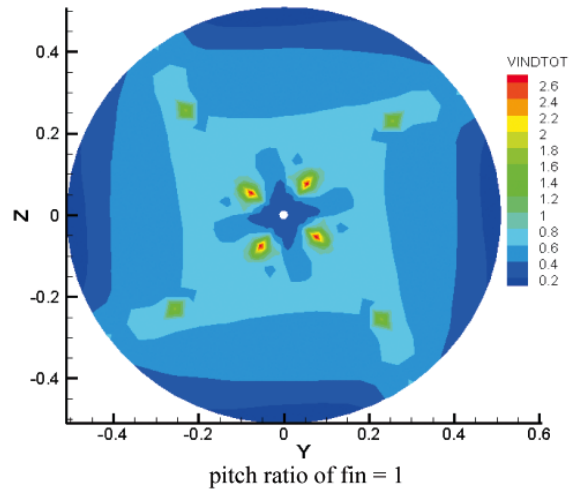
pitch ratio of fin = 2

Fig. 13. Axial induced velocity of the propeller at two pitch ratios of fin

phase difference of $\pi/14$

phase difference of $6\pi/14$
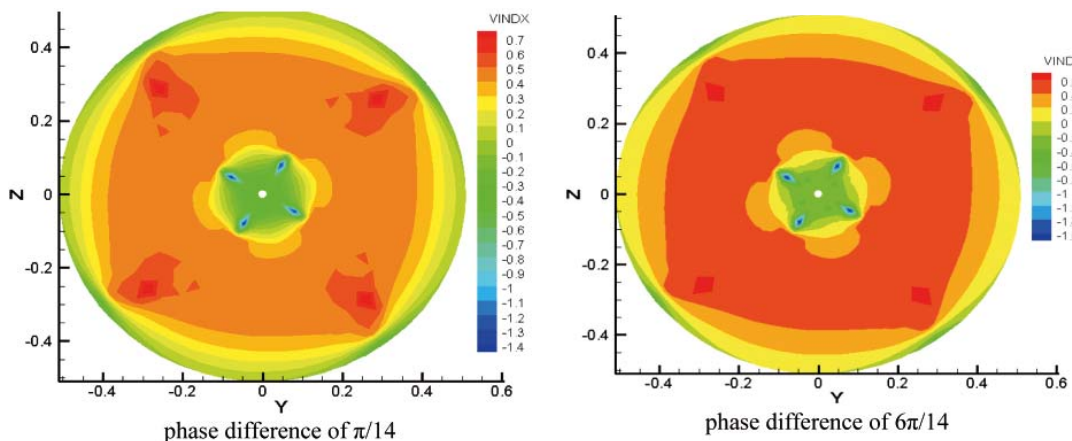
Fig. 11. *Change of the axial component of the induced velocity at downstream position, $x/R_{PBCF} = 0.5$*

CONCLUSIONS

In this article, the effect of hub and PBCF on hydrodynamic performance has been studied.

From the numerical results the following conclusions can be drawn:

- By increasing the hub ratio, thrust will be reduced and torque increased,which causes the efficiency to decrease.
- In a propeller with constant diameter, increasing the hub ratio has a significant effect on its performance. This change in performance could be minimized if the diameter of the propeller is increased proportionally to the hub diameter.
- At each hub ratio, increasing the conical angle of the hub has no effect on efficiency of the propeller.
- Placing the fins at the boss causes the downstream induced effects of the propeller to decrease and makes downstream flow more uniform.
- The fins reduce the negative component of the induced effects of the propeller and have only a slight effect on the components in the direction of the flow.
- The angle of installation of the fin and its phase difference against the propeller are two important items to be considered in geometrical modeling of the fin, which, if chosen incorrectly, could significantly degrade its performance.

NOMENCLATURE

C – chord length at each radius
C_f – friction coefficient
C_p – pressure coefficient
D – propeller's diameter
J – Jaccobian transform
J – advance velocity ratio
K_T – thrust coefficient of the propeller
K_Q – torque coefficient of the propeller
$\vec{n}$ – normal vector of the surface
P/D – pitch-diameter ratio
Q – total torque of the propeller
Q_{Pot} – potential component of the propeller torque
Q_{Vis} – viscous component of the propeller torque
r_h – hub radius
R_n – Reynolds number at radius r
S_B – blade surface
S_w – trailing wake surface
T – total propeller thrust
T_{Pot} – potential component of the propeller thrust
T_{Vis} – viscous component of the propeller thrust
V_I – inflow velocity to the propeller
$\vec{V}_I$ – total tangential velocity on propeller's surface
Z – number of blades
ΔS_i – surface area of each element
Φ – total velocity potential
ϕ – perturbation velocity potential
ϕ_{in} – inflow velocity potential
η – propeller efficiency

BIBLIOGRAPHY

1. Wang, H.: *Hub effects in propeller design and analysis*. PhD Dissertation, Ocean Engineering Department, MIT, 1985.
2. Wind, J.: *Hub size selection criteria for controllable pitch propellers as a means to ensure system integrity*. Naval Engineers Journal, No. 90(4), 1978, pp.49-61
3. Hess, J.L.: *Calculation of potential flow about arbitrary three-dimensional lifting bodies*. McDonnell Douglas Rep. MDC J5679-01, 1972.
4. Glegg. S.A.: *Effect of center body scattering on propeller noise*. AIAA, vol. 29, April 1991, p. 572-576
5. Yang, C.,Wang G., Masahiro T.: *A method of improving the precision of the prediction of the performance characteristics of a CPP the effect of boss being taken into consideration*. Shipbuilding of China, No. 116, 1992
6. Liu,Y-H, Ikehata, M.: *Investigation into hub effect of marine propeller by surface vortex lattice method*. Journal of Society of Naval Arch. Japan, Vol. 177, 1995, pp. 59-66
7. Cai, H. P., Su Y. M., Li X., Shen H.L.: *Using the surface panel method to predict the steady performance of ducted propellers*. J. Marine. Sci. Appl., 2009.
8. Http://www.mol.co.jp/pr-e/2011/e-pr_1145.html
9. Ouchi, K.B., Kono Y., Shiotsu T., Koizuka H.: *PBCF (Propeller Boss Cap Fins)*. J Soc. Nav. Arch. Japan (SNAJ),Vol 163, 1988.
10. Ouchi, K., Tamashima, M.: *Research and development of PBCF (propeller boss cap fin), new and practical device to enhance propeller efficiency*. 4th international Symposium on Practical Design of Ships and Mobile Units (PRADS), Bulgaria,1989
11. Ouchi, K., Tamashima M., Arai K.: *Reduction of Propeller cavitation Noise by PBCF (Propeller Boss Cap Fins)*. Kansai Soc. Naval Arch. Japan (KSNAJ), Vol. 216, 1991.
12. Ouchi, K., Tamashima M.: *A study on correlation between propeller pitch distribution and improvement of propeller efficiency by PBCF*. Kansai Soc Naval Arch Japan (KSNAJ), Vol. 217, 1992.
13. Junglewitz, A.: *Der Nabene influße im Schrauben propeller*. PhD Thesis, Univ. of Rostock., 1996.
14. Hsin, C.Y., Lin, B.H. and Lin, C.C.: *The optimum design of a propeller energy-saving device by computational fluid dynamics*. The Proceeding of the Fifth Int. Conf. of Computational Fluid Dynamics (ICCFD), Korea, 2008, pp.655-660
15. Ghassemi, H., Ghadimi, P.: *Computational hydrodynamic analysis of the propeller-rudder and the AZIPOD systems*. Ocean Engineering, Vol. 34, 2007, pp.117-130
16. Ghassemi, H.: *The effect of wake flow and skew angle on the ship propeller performance*. Scientia Iranica, No. 2,Vol. 16,, 2009, pp.149-158
17. Ghassemi, H.: *Hydrodynamic performance of coaxial contra-rotating propeller (CCRP) for large ships*. Polish Maritime Research, No. 59,Vol. 16, 2008, pp.22-28
18. Ghassemi, H.: *Hydrodynamic characteristics of the surface-piercing propellers for the planing craft*. J. Marine Science & Application (JMSA), Vol. 7, 2008, pp.147-156
19. Ghassemi, H., Ghadimi, P.: *Hydrodynamic efficiency improvement of the high skew propeller for the underwater vehicle under surface and submerged conditions*. J. Ocean Univ. China (JOUC), Vol. 10, 2011, pp.314-324
20. Richard, H. H., Dinham-Peren, T., Nojiri, T.: *Model and full scale evaluation of a 'Propeller Boss Cap Fins' device fitted to an Aframax tanker*. Second International Symposium on Marine Propulsors, SMP'11, Hamburg, Germany, June 2011.

CONTACT WITH THE AUTHORS

Hassan Ghassemi, Assoc. Prof.
Faculty of Marine Technology
Amirkabir University of Technology
Hafez Ave.,
Tehran, IRAN
e-mail: gasemi@aut.ac.ir

Amin Mardan, Ph. D.
Faculty of Marine Engineering,
Malekashtar University of Technology,
Shahinshar-Isfahan, IRAN

Abdollah Ardeshir, Ph. D.
Faculty of Civil & Environmental Engineering,
Amirkabir University of Technology,
Hafez Ave.,
Tehran, IRAN

Control design of fin roll stabilization in beam seas based on Lyapunov's direct method

Safak C. Karakas, M. Sc.
Erdem Ucer, Ph. D.
Istanbul Technical University
Emre Pesman, Ph. D.
Karadeniz Technical University

ABSTRACT

The aim of this study is to design a controller based on Lyapunov's direct method for fin roll stabilization systems for ships in beam seas. A third order mathematical model consisting of uncoupled roll motion of a ship and fin hydraulic system dynamics is considered. In the model, random wind force is defined by Gaussian white noise. Both controlled and uncontrolled roll motions are presented considering stall effect by roll-time history and safe basin graphics. It is observed from the results that fin control system is successful to reduce erosion percentages of safe basins and roll amplitudes.

Keywords: fin stabilizers; Lyapunov function; roll motion; white noise

INTRODUCTION

Large amplitude rolling motion is one of the dangerous phenomenon leading to capsizing of a ship in moderate and rough beam seas so it should be reduced by passive controllers such as bilge keels and active controllers such as fins, anti roll tanks, etc. The effectiveness of bilge keels is limited [1] so active fins are used when a more effective control action is needed to reduce rolling motion. Numerous studies on ship stabilization by using fin controllers are available since 1940s. The required moment to hold a ship against the upsetting moment of regular sea was investigated with model fin tests by Allan [2]. The performance of active stabilizers in the two trial ship was represented theoretically with reasonable accuracy by Conolly [3]. In 1993, a free running ship model equipped with active fin stabilizers was used to explore the nature of roll stabilizing problem and from the results of this experiment important hull-fin and fin-hull interferences were identified by Dallinga [4]. Ship stabilizing fin controller based on the internal model control (IMC) method was described by Tzeng and Wu [5]. In the study of Yang et al. [6], a robust adaptive fuzzy controller was constructed, a stability theorem for the proposed robust adaptive fuzzy scheme was proved and it was demonstrated how the robust adaptive fuzzy control scheme could be applied to the controller design for ship roll stabilization. The choice of controller for a fin-stabilization system on the effect of operational performance of the ship was presented by Crossland [7]. The design and implementation of a robust H-∞ controller designed to stabilize the roll motion of a ship was presented by Hickey et al. [8]. The ship roll stabilization by fin control system with actuator was considered by Yang and Jiang [9] and it was shown that the designed system guaranteed the performance of robustness with respect to the perturbations and uncertainties. Nonlinear roll motion of a frigate ship using a pair of fins activated by a PID control system was presented by Surendran et al. [10]. Constrained predictive control of ship fin stabilizers to prevent dynamic stall was presented by Perez and Goodwin [11]. Robust control of ship fin stabilizers subject to disturbances and constraints was presented by Ghaemi et al. [12]. The simulation results of that study show that the proposed robust control method reduces the ship roll motion while satisfying the input and dynamic stall constraints. Stabilization of parametric roll resonance in moderate head and following seas by combined speed and fin stabilizer control based on Lyapunov's direct method is presented by Galezzi et al. [13]. A combined neural network and PID for roll control of ship with small draught considering hydraulic machinery constraints is presented by Ghassemi et al. [14].

In this study, a fin controller based on Lyapunov's direct method is designed in order to reduce severe rolling motion of ship in steady beam seas under the influence of random wind force. The effectiveness of the controller is tested by comparing controlled and uncontrolled roll angle simulations for different initial conditions considering stall effect. In order to succeed this type of comparison, safe basin concept [15] is used. In that method, the safe and capsizing initial conditions are represented by white and black points respectively and the effects of different initial conditions on the stability of the dynamic system (ship) can be shown by using just one graphic. From the comparisons of safe basins plots of controlled and uncontrolled roll motion, it is seen that the controller is successful.

SHIP MODELING FOR FIN STABILIZER CONTROL SYSTEM DESIGN

Equations of ship motion

In beam seas, roll motion has a greater influence on ship stability rather than the other modes of ship motion. Due to the difficulty of accurately determining the complete hydrodynamic forces, a rolling model which decouples the six degrees of freedom is generally assumed. In most of the studies, coupling of roll and sway motions are considered for the purpose of ship stability analysis [16]. The two degree of freedom roll and sway model is reduced to a 1-DOF rolling model by introducing a virtual roll centre [16, 17, 18]. Assuming the ship has a rigid body and seawater is ideal and incompressible, the uncoupled roll model is defined by Eq. 1.

$$I\ddot{\phi}+B_E\dot{\phi}+\Delta GZ(\phi)=E_0\cos(\omega t)+Z\xi(t)+C \quad (1)$$

where

ϕ – rolling angle with respect to calm sea surface (rad),

$\dot{\phi}$ – roll angular velocity (rad/s),

I – virtual moment of inertia corresponds to a virtual (physical) axis of rotation, located at the virtual ship mass center (the mass center of the ship),

Δ – the buoyancy force,

ω – the wave circular frequency.

GZ – the righting arm as a function of the roll angle and defined by as follows:

$$GZ(\phi)=GM\phi+c_3\phi^3+c_5\phi^5+c_7\phi^7 \quad (2)$$

where:

ϕ – the angle of heel,

GM– the initial metacentric height.

E_o – the amplitude of wave excitation and defined by as follows:

$$E_0=\kappa\frac{\pi h_w}{\lambda_w}\Delta GM \quad (3)$$

where:

κ – the reduction coefficient for the effective wave slope, h_w is the wave amplitude,

λ_w – the wave length, the wave slope ($\pi h_w/\lambda_w$) is taken smaller than 11°.

B_E – equivalent linear damping coefficient and defined as follows:

$$B_E=B_w+B_F+B_e+B_L+B_{BK} \quad (4)$$

where:

B_F – friction damping,

B_e – eddy damping,

B_L – lift damping

B_{BK}– bilge keel damping coefficient. These coefficients are determined by semi-empirical formulas given by Himeno [19].

B_w – wave damping coefficient and can be determined by SHIPMO program [20]. Although these coefficients are seemingly linear, their values may vary with the roll amplitude and the wave frequency [19] and also the interactions among these damping components are ignored.

$\xi(t)$– random wind force defined by Gaussian white noise.

Z – diffusion constant.

C – the control moment produced by the fins.

Eq. 5 is obtained by dividing the both sides of Eq. 1 by the virtual moment of inertia (I).

$$\ddot{\phi}+b_E\dot{\phi}+\omega_0^2\phi+c_3^*\phi^3+c_5^*\phi^5+c_7^*\phi^7=$$
$$=e_0\cos(\omega t)+\sigma\xi(t)+\tau_c \quad (5)$$

where:

$\omega_o=\sqrt{\dfrac{\Delta GM}{I}}$,

$b_E=B_E/I$,

$c_3^*=c_3/I$,

$c_5^*=c_5/I$,

$c_7^*=c_7/I,,$

$e_o=E_o/I$,

$\sigma=Z/I$

$\tau_c=C/I$.

Control force

The roll moment generated by fins is expressed as follows [11]:

$$\tau_c=\frac{\rho r_f V_{fl}^2 A_f C_L(\alpha_e)}{I} \quad (6)$$

where:

ρ – the water density,

r_f – the fin moment arm,

V_{fl} – the relative speed between the fins and the flow (which for control design can be approximated by the forward speed of the vessel U (i.e., $V_{fl}\approx U$),

A_f – the area of the fin,

C_L – the lift coefficient,

α_e – the effective angle of attack between the fin and the fluid velocity [11].

The increment of lift coefficient C_L due to angle of attack is approximately linear to the particular angle called stall angle as defined in Eq. 7 [11].

$$C_L(\alpha_e)\approx\bar{C}_L\alpha_e,\text{ with }\bar{C}_L\triangleq\frac{\partial C_L}{\partial\alpha_e}\Big|_{\alpha_e=0} \quad (7)$$

Exceeding stall angle causes decrement of the lift and causes the controller not working properly.

The effective angle of attack is defined as follows:

$$\alpha_e=-\alpha_{pu}-\alpha_m \quad (8)$$

where:

α_m – the mechanical angle of the fins (control command),

α_{pu} – the flow angle induced by the combination of forward speed and roll rate [11] and defined as follows:

$$\alpha_{pu}=\arctan\left(\frac{r_f\dot{\phi}}{U}\right)\approx\frac{r_f}{U}\dot{\phi} \quad (9)$$

The total roll moment induced by the fins can then be approximated by

$$\tau_c=K_\alpha\left(\frac{r_f}{U}\dot{\phi}-\alpha_m\right) \quad (10)$$

where:

$K_\alpha=\rho r_f V_{fl}^2 A_f\bar{C}_L/I$

CONTROL SYSTEM DESIGN

The uncoupled roll motion Eq. 5 is defined by the equation system as follows:

$$F_1=x_2 \quad (11a)$$

$$F_2=-\left(b_e+K_\alpha\frac{r_f}{U}\right)x_2-\left(\omega_0^2\phi+c_3^*\phi^3+c_5^*\phi^5+c_7^*\phi^7\right)+$$
$$+e_0\cos(\omega t)-K_\alpha\alpha_m \quad (11b)$$

by considering the states as $x_1=\phi$ and $x_2=\dot{\phi}$.
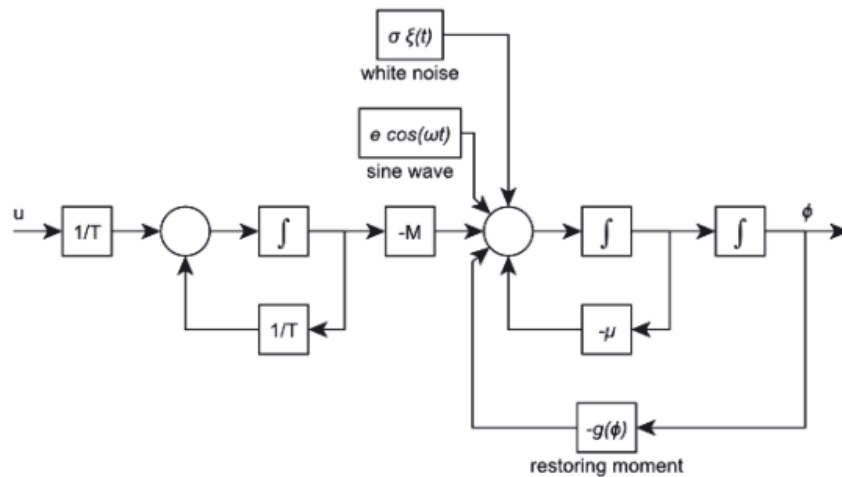
Fig. 1. Block diagram of the model

The Lyapunov function candidate of the system is as follows:

$$V = \frac{x^2}{2} + \left(\omega_0^2 \frac{x_1^2}{2} + c_3^* \frac{x_1^4}{4} + c_5^* \frac{x_1^6}{6} + c_7^* \frac{x_1^8}{8} \right) \quad (12)$$

When the Lyapunov function is substituted in the differential generator of the stochastic process [21], the following relation is obtained.

$$\begin{aligned} LV = \left(\alpha^2 x_1^2 + e_0 \cos(\omega t) \right) x_2 < \\ < K_\alpha \alpha_m x_2 + \left(b_e + \frac{r_f}{U} \right) x_2^2 \end{aligned} \quad (13)$$

When the equality $LV < 0$ is verified, the ship is stable and the required mechanical angle of the fins (α_m) is determined as follows:

$$\alpha_m = \frac{1}{f_1} \left(\sigma^2 x_1^2 + e_0 \cos(\omega t) \right) \quad (14)$$

By means of a electrohydraulic system, two fins are driven and create an additional righting moment. The actuator can approximately be described by a 1st order equation as follows:

$$\dot{x}_3 = -\frac{1}{T} x_3 + \frac{1}{T} u \quad (15)$$

where:

x_3 – a state of the system and considered as $x_3 = \alpha_m$,
u – the control input defined as the voltage input to the electro-valve of the hydraulic system [22].

The order fin angle due to time is obtained by substituting the required mechanical angle of fins into the Eq. 15.
The block diagram of the whole model is seen in Fig. 1.

NUMERICAL SIMULATIONS

In the numerical simulations, a BSRA trawler [23] is used as a sample ship. Geometric particulars of the BSRA trawler are seen in Tab. 1.

Tab. 1. Geometric particulars of the BSRA trawler

L_{BP} (m)	48.085
Beam (m)	8.289
Draught (m)	3.734
L_{WL}/B	5.80
B/d	2.22
D (Ton)	847
C_B	0.564
C_{WL}	0.775
C_p	0.627

Comparisons of roll, roll angular velocity and mechanical angle of fins time histories of controlled and uncontrolled roll motion are shown in Fig. 2 when excitation amplitude is 0.06, K_α is 0.05 for $\phi_o = 0$ rad and $\dot{\phi}_o = 0.4$ rad/s. In the figure, black lines represent uncontrolled case whereas bold black lines represent controlled states. The controller is able to stabilize the system as seen in the figure.

Safe basin concept [15] is used to present the efficiency of controller. In the safe basin concept, the safe and capsizing initial conditions are represented by white and black areas respectively. The bounded area of initial conditions is expressed as follows:

$$(x_1, x_2): -1.25 \leq x_1 \leq 1.25, -1.0 \leq x_2 \leq 1.0 \quad (16)$$
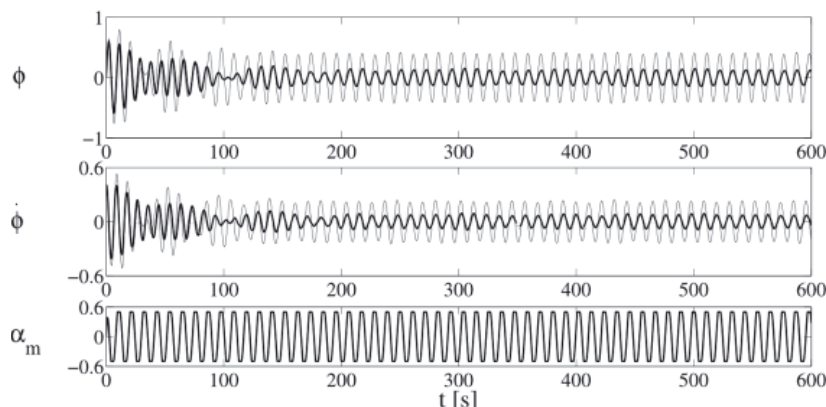
Fig. 2. Simulation of the model

where x_1 is in radians and x_2 is in rad/s. The bounded area is divided into 126 x 101 points and the lattice points are taken as the initial values for the solutions of Eq. 11. For each initial condition, a simulation of 1500 seconds is run.

In Figs 3 and 4, safe basins of controlled and uncontrolled roll motion of the BSRA trawler are presented for varying ship velocities (U) and wave excitation amplitudes (e_o) respectively when K_a is 0.05. For various ship velocities, the safe basin area of the controlled cases are larger than uncontrolled ones. By increasing the wave excitation amplitude, the safe region of uncontrolled roll motion (white area in the figures) decreases dramatically. By the help of the controller, safe basin enlarges. Therefore, Lyapunov designed controller is successful to reduce severe roll motion.

a)   U = 12 knots - Uncontrolled

b)   U = 12 knots - Controlled

c)   U = 13 knots - Uncontrolled

d)   U = 13 knots - Controlled

e)   U = 14 knots - Uncontrolled

f)   U = 14 knots - Controlled

g)   U = 15 knots - Uncontrolled

h)   U = 15 knots - Controlled
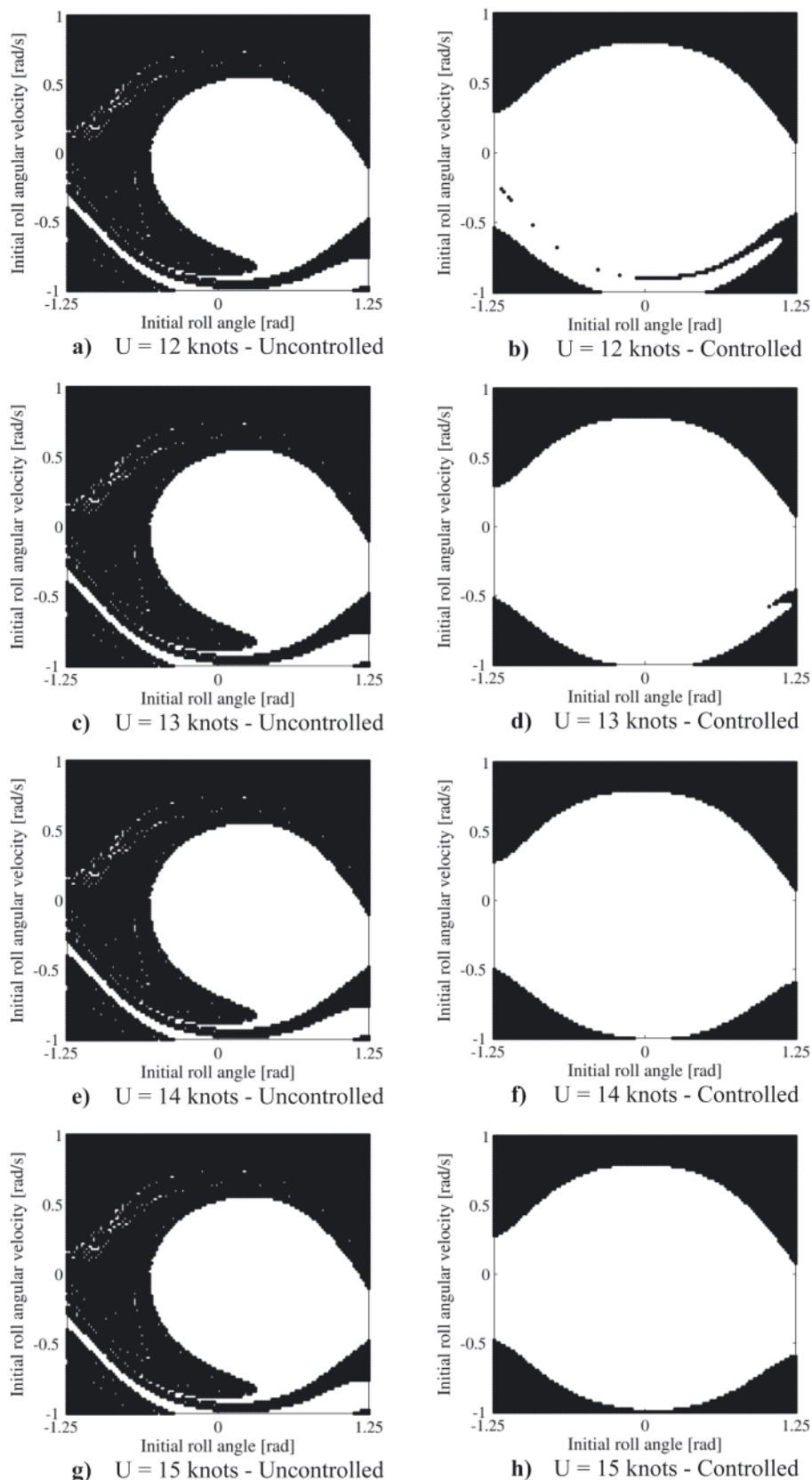
Fig. 3. Safe Basins of Controlled and Uncontrolled Cases due to Ship Velocity
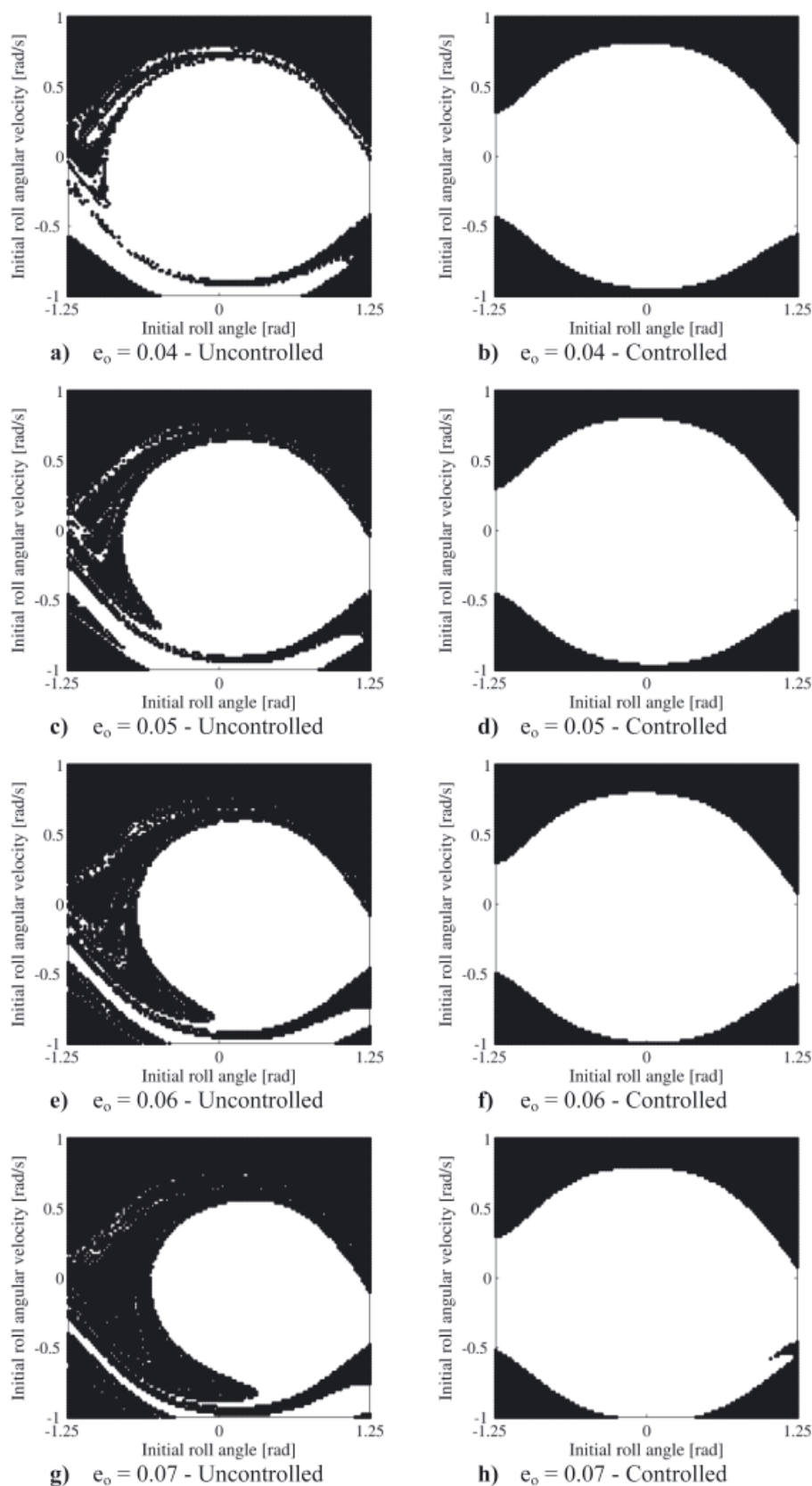
Fig. 4. *Safe Basins of Controlled and Uncontrolled Cases due to Wave Excitation Amplitude*

CONCLUSION

A controller based on Lyapunov's direct method is designed to reduce roll amplitudes and erosion of safe basins of ships in beam seas. Stability status of the sample ship in different initial conditions is presented by safe basin plots. Performance of fin control system is tested with respect to ship speed and wave amplitude. It is observed from the results that fin control system is successful to reduce erosion percentages of safe basins and roll amplitudes. However, even if the controller is used, roll amplitudes exceed a certain value for low ship speeds. Therefore, anti-roll tanks or gyroscopes which are independent from ship speed have to be used. Briefly, it is concluded that fin control system based on Lyapunov's direct method works

properly and possibility of capsizing at speeds nearby service speed is significantly reduced by fin control system. For further studies, random wave force should be considered and also rolling in following seas can be examined.

REFERENCES

1. Ashraf A. Zaher, *Nonlinear control of systems with multiple equilibria and unknown sinusoidal disturbance*, Communications in Nonlinear Science and Numerical Simulation, vol.12, pages 1518-1533, 2007

2. J. F. Allan, *Stabilisation of ships by activated fins*, Transactions of the Royal Institution of Naval Architects RINA, vol.87, pages 123-159, 1945

3. J. E. Conolly, *Rolling and its stabilization by active fins*, Transactions of the Royal Institution of Naval Architects RINA, vol.111, pages 21-48, 1968

4. R. P. Dallinga, *Hydromechanic aspects of the design of fin stabilisers*, The Royal Institution of Naval Architects International Conference on Ship Motions & Manoeuvrability, no.5, London, U.K., 1993

5. Ching-Yaw Tzeng and Chung-Yi Wu, *On the design and analysis of ship stabilizing fin controller*, Journal of Marine Science and Technology, vol.8, no.2, pages 117-124, 2000

6. Yansheng Yang, Changjiu Zhou and Xinle Jia, *Robust adaptive fuzzy control and its application to ship roll stabilization*, Information Sciences, vol.142, pages 177-194, 2002

7. P. Crossland, *The effect of roll-stabilisation controllers on warship operational performance*, Control Engineering Practice, vol.11, pages 423-431, 2003

8. N.A. Hickey, M.J. Grimble, M.A. Johnson, M.R. Katebi, and R. Melville, *Robust Fin Roll Stabilisation of Surface Ships*, Proceedings of the 36th Conference on Decision & Control, pages 4225-4230, San Diego, Califomia USA, 1997, December

9. Yansheng Yang and Bo Jiang, *Variable Structure Robust Fin Control for Ship Roll Stabilization with Actuator System*, Proceeding of the 2004 American Control Conference, pages 5212-5217, Boston, Massachusetts, 2004, June 30 - July 2

10. S. Surendran, S.K. Leeb and S.Y. Kimb, *Studies on an algorithm to control the roll motion using active fins*, Ocean Engineering, vol.34, pages 542-551, 2007

11. Tristan Perez and Graham C. Goodwin, *Constrained predictive control of ship fin stabilizers to prevent dynamic stall*, Control Engineering Practice, vol.16, pages 482-494, 2008

12. Reza Ghaemi, Jing Sun and Ilya V. Kolmanovsky, *Robust Control of Ship Fin Stabilizers Subject to Disturbances and Constraints*, 2009 American Control Conference, Hyatt Regency Riverfront, St. Louis, MO, USA, 2009, June 10-12

13. Roberto Galeazzi, Christian Holden, Mogens Blanke and Thor I. Fossen, *Stabilisation of Parametric Roll Resonance by Combined Speed and Fin Stabiliser Control*, Proceedings of the European Control Conference, Budapest, Hungary, 2009, August 23-26

14. Hassan Ghassemi, Fatemeh Hoseini Dadmarzi, Parviz Ghadimi and Babak Ommani, *Neural network-PID controller for roll fin stabilizer*, Polish Maritime Research, vol.65, no.2, pages 23-28, 2010

15. J.M.T. Thompson, *Loss of engineering integrity due to the erosion of absolute and transient basin boundaries*, Proceedings of IUTAM Symposium on the Dynamics of Marine Vehicles and Structures in Waves, pages 313-320, 1989

16. C. Jiang, *Highly nonlinear rolling motion leading to capsize*, University of Michigan, Ann Arbor, 1995

17. B.L. Hutchison, *The transverse plane motions of ships*, SNAME Marine Technology, vol.28, no.2, pages 55-72, 1991

18. L. Balcer, *Location of ship rolling axis*, Polish Maritime Research, vol.11, no.1, pages 3-7, 2004

19. Y. Himeno, *Prediction of ship roll damping-state of the art*, UMICH, no.239, Ann Arbor, 1981

20. R.F. Beck and A.W. Troesch, *Students documentation and users manual for the computer program SHIPMO.BM.*, Department of Naval Architecture and Marine Engineering, University of Michigan, Ann Arbor, 1990

21. H.J. Kushner, *Stochastic stability and control*, Academic Press, NewYork, 1967

22. Khac Duc Do and Jie Pan, *Nonlinear robust fin roll stabilization of surface ships using neural networks*, Proceedings of the 40th IEEE Conference on Desicion and Control, pages 2726-2731, Orlando, Florida USA, 2001

23. Pattullo, R.N.M. and G.R. Thomson, *The BSRA Trawler Series, Part 1*, Trans RINA, vol.107, no., pages 216-236, 1965

CONTACT WITH THE AUTHORS

Safak C. Karakas, M. Sc.
Erdem Ucer, Ph. D.
Faculty of Naval Architecture and Ocean Engineering
Istanbul Technical University
e-mail: karakass@itu.edu.tr

Emre Pesman, Ph. D.
Surmene Faculty of Marine Science
Karadeniz Technical University

Conceptual Design and Performance Analysis of an Exhaust Gas Waste Heat Recovery System for a 10000TEU Container Ship

Zheshu Ma, Prof.
Dong Yang, M. Sc.
Qiang Guo, M. Sc.
Jiangsu University of Science and Technology, Zhenjiang, P.R. China

ABSTRACT

According to operation characteristics of the main engine 9K98ME-C7, a combined turbines-exhaust gas waste heat recovery system is proposed to recover waste heat and increase system energy efficiency. Thermodynamic models based on the first thermodynamic law and the second thermodynamic law are formulated. The superheated steam yield, the total electric power yield, the first thermodynamic law efficiency, the exergy efficiency at different exhaust gas boiler working pressure, and the variation of the exergy efficiency under different feed water temperature and different steam turbine back pressure are analyzed. Thermodynamic results indicate that the most appropriate exhaust gas boiler pressure is 0.8MPa for studied main engine and the total thermal efficiency with combined turbines arrangement has climbed up to 53.8% from 48.5%.

Keywords: exergy efficiency; marine diesel engine; thermal efficiency; waste heat recovery system

INTRODUCTION

Main engines on large or ultra-large merchant ships are very powerful and consume large amount of fuel oil. A slight increase of their thermal efficiency could bring round-sum benefit for ship owners. Meanwhile, with the rising fuel costs and global warming ongoing, energy-saving and emission-reduction have been getting more and more highlighted. Based on this consideration, Waste Heat Recovery systems (WHRs) are considered to furnish newly-designed ships and refurnish in-service ships. Thermal efficiency of state-of-the-art high performance marine diesel engines achieves nearly 45% ~ 55%, and waste heat sources on ships are mainly resided in exhaust gases and outlet cooling water, taking away 25% ~ 35% and 20% ~ 25% of energy in fuel, respectively. These two waste heat sources are also the most potential candidates onboard to be recovered to increase the total thermal efficiency.

Conventional waste heat recovery systems onboard are cogeneration systems, i.e. combined heat and power generation systems, and usually use water as working fluid in Rankine Cycles (RCs) [1-5]. When analyzing these systems based on thermodynamic laws, effects of pinch point are always paid much attention. C.J Butcher and B.V. Reddy [6] analyzed effects of different specific heat models, gas inlet temperature and other operating parameters on entropy generation rate and the second thermodynamic law efficiency for a waste heat recovery based power generation system. They found that, approximating the exhaust gas as standard air led to either underestimation or overestimation of power plant performance on both first thermodynamic law and second thermodynamic law point of view. Actual gas composition models and specific heat models should be used to predict second thermodynamic law performance more accurately.

Compared with conventional waste heat recovery systems onboard, Organic Rankine Cycles(ORC) employ organic working fluid in steam power cycles. ORCs possess several notable advantages for economical utilization of energy resources, small system applications and environmental impacts and can give better performance to recover low grade waste heat onboard [7]. Yalcin Durmusoglu et al.[8] designed an ORC cogeneration system for a container ship and employed three performance criterions, i.e. energy utilization factor, artificial thermal efficiency and exergy efficiency, to evaluate system performance. Thermodynamic results indicated that ORC cogeneration systems could recover more low grade waste heat onboard than conventional RC cogeneration systems.

Ships are always the most efficient transportation means when important environment aspects are taken into account [9, 10]. Ships normally have enough waste heat (both energy quantity and energy quality) potential to be ultilized and cover almost all demands for thermal energy onboard. Cogeneration systems adapt to large and ultra-large ships. However, for small ships and other waste heat sources, Thermoelectric Generators (TEGs) represents a promising solution direction. N.R Kristiansen et al. [11] analyzed the waste heat sources on a median size bulker ship equipping a main engine of 7.8 MW

and found that incinerators were most promising application for TEGs. Moreover, important factors for successful TEGs applications were commercialization of materials research and reduced price/Watt power output TEGs can bring[12].

In comparison with exhaust gases, it is more difficult to recover waste heat of cooling water from cylinder liner in marine diesel engines due to its low waste heat grade. Liu Shi-Jie et al.[13] designed a high temperature heat pump waste heat recovery system to recover waste heat of cooling water from cylinder liner and recommended that R123 and R245fa be the appropriate working fluids. Such system could generate enough saturated vapor (saturated temperature 120°) to meet thermal energy requirements onboard.

In available literatures, the minimum value of exhaust gas boiler working pressure for different types of ships, 0.7 MPa, was normally selected to calculate advantages of waste heat recovery systems. Optimal working pressure of exhaust gas boiler is seldom analyzed when installing a waste heat recovery system designed for a given ship. Superheated steam yield, total electric power yield, first law efficiency, second law efficiency at different exhaust gas boiler working pressure are seldom analyzed. As well, effects of feed water temperature and steam turbine back pressure on system exergy efficiency are seldom studied. In this paper, a WHRS is proposed to recover waste heat of main engine 9K98ME-C7. Superheated steam yield, total electric power yield, first law efficiency, second law efficiency at different exhaust gas boiler working pressure are thermodynamically analyzed. In addition, exergy efficiency is modeled under different feed water temperature and steam turbine back pressure. For a better understanding of such WHR solution, a conparison to results in published literatures are also done.

PROBLEM

Waste heat in exhaust gas and cooling water are the two main heat sources to be exploited on ships. Exhaust gas is always chosen due to its high temperature and huge mass flow rate. In order to effectively recover thermal energy in exhaust gas, exhaust gas temperature is usually increased [2]

by an exhaust gas bypass system which could increase exhaust gas temperature by approximately 50° and specific fuel oil consumption (SFOC) slightly by about 2g/(kW·h).

When choosing waste heat recovery systems, payback time, electricity yield, system size, maintenance cost should be taken into account since waste heat recovery systems are rather expensive and appropriate only for large merchant ships. MAN B&W Diesel recommends single-pressure steam turbine system when installing combined turbines [2].

Currently, there are three different types of exhaust gas waste heat recovery systems. (1) Power Turbine Generator (PTG). PTG system is small, simple and can produce power approximately 4% of the main engine Specified Maximum Continuous Rating (SMCR). The exhaust gas expands in the power turbine while its temperature decreases. The enthalpy drop of the exhaust gas transforms into turbine's kinetic energy. The generator connects to the turbine via a gearbox. PTG system has been applied on some container ships and LNG ships [14]. (2) Steam Turbine Generator (STG). STG system is relatively complicated and can produce power equivalent to approximately 5% to 7% of the main engine SMCR. Steam turbine is driven by superheated steam. Steam is produced by a large exhaust gas boiler installed on the main engine exhaust gas piping system. The enthalpy drop of the superheated steam transforms into turbine's kinetic energy. The generator connects to the turbine via a gearbox. (3) Combined Turbines. Combined Turbines system is a combination of the above two systems. The power turbine is connected to the steam turbine via a gearbox and the steam turbine is further connected to a large generator, which absorbs the power from both turbines. Such system is most complicated and can produce power equivalent to approximately 10% of the main engine SMCR.

For main engine 9K98ME-C7, Combined Turbines system is the most appropriate to be employed onboard. For a better management, the boiler is of single-pressure type and the steam turbine is of multi-stage single-pressure condensing type. The system diagram is shown in Fig. 1 (without shaft generator/ motor). The exhaust gas boiler system diagram is shown in Fig. 2. The mass flow rate profile and temperature profile of the exhaust gas after turbochargers are shown in Fig. 3 and in
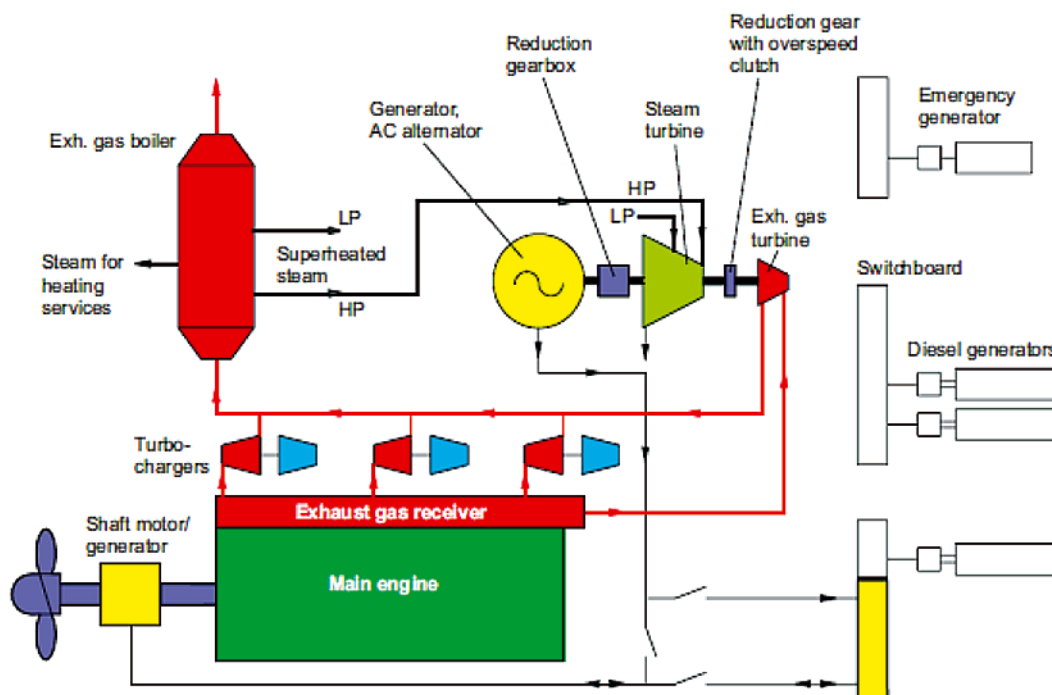
Fig. 1. Combined Turbines system diagram (without shaft motor/generator) for main engine 9K98ME-C7 with the boiler of single-pressure type and the steam turbine of multi-stage single-pressure condensing type

Fig. 4, respectively. The exhaust gas bypass valve will be open with engine loads higher than about 50% SMCR, mass flow rate of exhaust gas reduces and temperature increases. When engine loads are lower than 50% SMCR, the exhaust gas bypass valve will be closed for a normal operation of the boiler. In this case, the temperature decreases obviously and the mass flow rate increases slightly.
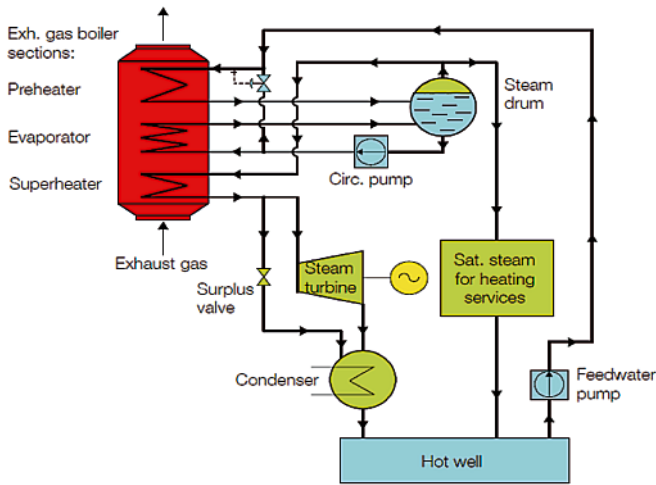
Fig. 2. The single-pressure type exhaust gas boiler system diagram of Combined Turbines system (without shaft motor/generator) for main engine 9K98ME-C7 with the steam turbine of multi-stage single-pressure condensing type
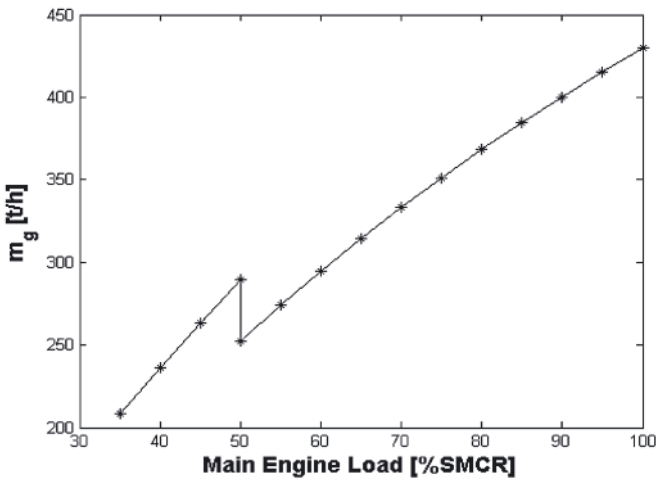
Fig. 3. The variation of exhaust gas mass flow rate after turbochargers with main engine loads for main engine 9K98ME-C7 with Combined Turbines system
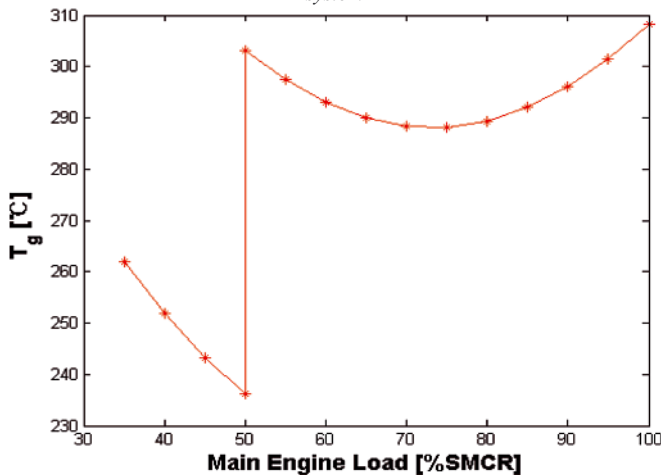
Fig. 4. The variation of exhaust gas temperature after turbochargers with main engine loads for main engine 9K98ME-C7 with Combined Turbines system

FORMULAE

Typical temperature profiles of exhaust gas and steam/water in the exhaust gas boiler are shown in Fig. 5. The exhaust gas enters the superheater at T_{g1} where the saturated steam is superheated to high temperature T_{sh}. The exhaust gas then enters the evaporator at T_{g2} where a mixture of saturated water and saturated steam exists. The exhaust gas leaves the evaporator at T_{g3} and the pinch point (T_{PP}) means the temperature difference between T_{g3} and the saturated temperature T_{sat}. The exhaust gas then enters the preheater at T_{g3} where the water is preheated. The exhaust gas is discharged to the environment at T_{g4}.

Following assumptions are made in the analysis [15]:
- steam is at steady state;
- no pressure drops on steam side;
- pressure drop on exhaust gas side does not affect its temperature;
- approach point is negligible;
- the expansion process in the steam turbine is an isentropic expansion process;
- the specific enthalpy of the superheated steam entering the steam turbine is equal to the specific enthalpy of the superheated steam left the superheater.
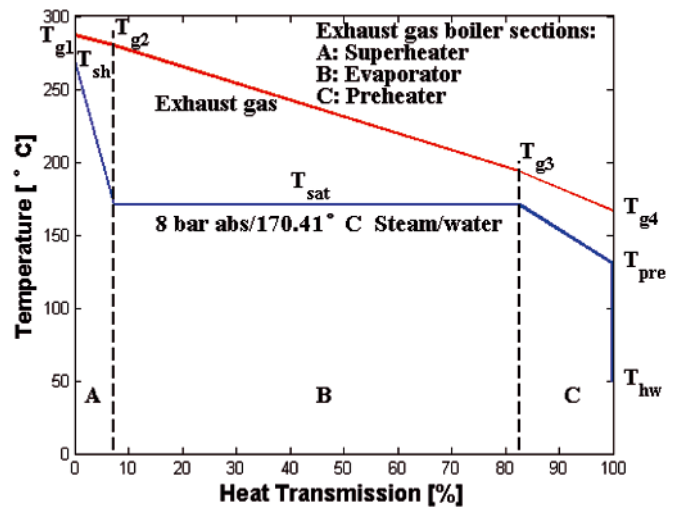
Fig. 5. Typical temperature profiles of exhaust gas and steam/water in the exhaust gas boiler for main engine with Combined Turbines system

Formulae of Preheater

By mixing the water from hot well ($\dot{m}_{hw}$) and a part of saturated water from the boiler ($\dot{m}_{B1}$), the water with a mass flow rate $\dot{m}$ could enter the preheater at T_{pre} (130°). The mass flow rate $\dot{m}$ can be expressed as:

$$\dot{m} = \dot{m}_{hw} + \dot{m}_{B1} \qquad (1)$$

According to the law of energy conservation, there will be:

$$\dot{m} \times h_{pre} = \dot{m}_{hw} \times h_{hw} + \dot{m}_{B1} \times h'_{sat} \qquad (2)$$

where:
h_{hw} – the enthalpy of feed water, [kJ/kg],
h'_{sat} – the enthalpy of saturated water at specific exhaust gas boiler working pressure, [kJ/kg],
h_{pre} – the enthalpy of water (130°) entering the boiler, [kJ/kg].

Therefore, the saturated water from the boiler $\dot{m}_{B1}$ will be:

$$\dot{m}_{B1} = \dot{m}_{hw} \times \frac{h_{pre} - h_{hw}}{h'_{sat} - h_{pre}} \qquad (3)$$

Using the temperature profiles, one can reach:

$$(\dot{m}_{hw} + \dot{m}_{B1}) \times (h'_{sat} - h_{pre}) =$$
$$= C_g \times \dot{m}_g \times (T_{g3} - T_{g4}) \times \eta_B \tag{4}$$

where:
C_g – the mean specific heat of exhaust gas from boiler inlet to outlet, [kJ/(kg K)],
$\dot{m}_g$ – the mass flow rate of exhaust gas, [kg/h],
η_B – exhaust gas boiler efficiency considering the radiation loss, [%].

Formulae of Evaporator

The exhaust gas temperature entering the preheater is expressed as:

$$T_{g3} = T_{sat} + T_{pp} \tag{5}$$

According to the law of energy conservation, one can obtain:

$$\dot{m}_{exh,B} \times (h''_{sat} - h'_{sat}) =$$
$$= C_g \times \dot{m}_g \times (T_{g2} - T_{g3}) \times \eta_B \tag{6}$$

where:
h''_{sat} – the enthalpy of saturated steam at specific exhaust gas boiler working pressure, [kJ/kg],
$\dot{m}_{exh,B}$ – total steam yield of exhaust gas boiler, [kg/h].

Formulae of Superheater

According to the law of conservation of energy, there will be:

$$\dot{m}_{sh} \times (h_{sh} - h'_{sat}) = C_g \times \dot{m}_g \times (T_{g1} - T_{g2}) \times \eta_B \tag{7}$$

where:
$\dot{m}_{sh}$ – superheated steam yield of exhaust gas boiler, [kg/h],
h_{sh} – the enthalpy of superheated steam at specific exhaust gas boiler working pressure, [kJ/kg].

According to the law of mass conservation, total steam yield $\dot{m}_{exh,B}$ and mass flow rate of hot well pump $\dot{m}_{hw}$ can be expressed:

$$\dot{m}_{exh,B} = \dot{m}_{heating} + \dot{m}_{sh} \tag{8}$$

$$\dot{m}_{hw} = \dot{m}_{heating} + \dot{m}_{sh} \tag{9}$$

Objective Formulae

According to the above formulae, total steam yield $\dot{m}_{exh,B}$ of the WHRS, mass flow rate of the saturated water from the boiler $\dot{m}_{B1}$, superheated steam yield $\dot{m}_{sh}$, temperature T_{g2} and temperature T_{g4} can be expressed as Eq. (10)-(14):

$$\dot{m}_{exh,B} =$$
$$= \frac{C_g \times \dot{m}_g \times (T_{g1} - T_{g3}) \times \eta_B + \dot{m}_{heating} \times (h_{sh} - h''_{sat})}{h_{sh} - h'_{sat}} \tag{10}$$

$$\dot{m}_{B1} = \dot{m}_{exh,B} \times \frac{h_{pre} - h_{hw}}{h'_{sat} - h_{pre}} \tag{11}$$

$$\dot{m}_h =$$
$$= \frac{C_g \times \dot{m}_g \times (T_{g1} - T_{g3}) \times \eta_B + \dot{m}_{heating} \times (h_{sh} - h''_{sat})}{h_{sh} - h'_{sat}} +$$
$$- \dot{m}_{heating} \tag{12}$$

$$T_{g2} = T_{g3} + \frac{\dot{m}_{exh,B} \times (h''_{sat} - h'_{sat})}{C_g \times \dot{m}_g \times \eta_B} \tag{13}$$

$$T_{g4} = T_{g3} - \frac{(\dot{m}_{exh,B} + \dot{m}_{B1}) \times (h'_{sat} - h_{pre})}{C_g \times \dot{m}_g \times \eta_B} \tag{14}$$

The power output of the steam turbine W_{ST}, total power output of the combined turbines W_{CT}, total work output of the integrated energy system W, available energy $\dot{E}_W$, fuel energy (per hour) $\dot{E}$ can be written as Eq.(15)-(19):

$$W_{ST} = \dot{m}_{sh} \times (h_{sh} - h_{back,s}) \times \eta_s \div 3600 \tag{15}$$

where:
$h_{back,s}$ – the isentropic enthalpy of wet steam at steam turbine outlet, [kJ/kg],
η_s – isentropic efficiency of steam turbine, [%].

$$W_{CT} = W_{ST} + W_{PT} \tag{16}$$

where:
W_{PT} – power output of power turbine, [kW].

$$W = W_{shaft} + W_{PT} \tag{17}$$

where:
W_{shaft} – main engine shaft power , [kW].

$$\dot{E}_W = W \times 3600 \tag{18}$$

$$\dot{E} = W_{shaft} \times SFOC \div 1000 \times LCV \tag{19}$$

where:
LCV – Low Calorific Value of fuel oil, [kJ/kg].

Thus, the thermal efficiency of the whole WHRS can be expressed as:

$$\eta_{cycle} = \frac{\dot{E}_W}{\dot{E}} = \frac{(W_{shaft} + W_{CT}) \times 3600}{W_{shaft} \times SFOC \times LCV/1000} \tag{20}$$

The exergy efficiency η_{ex} and payback time n of the whole WHRS are defined as Eq. (21)-(22):

$$\eta_{ex} = \frac{h_{sh} - h_{back,act}}{(h_{sh} - h_{hw}) - T_0 \times (S_{sh} - S_{hw})} \tag{21}$$

where:
$h_{back,act}$ – the actual enthalpy of wet steam at steam turbine outlet, [kJ/kg],
$h_{back,act}$ – $h_{back,s} + (1 - \eta_s) \times (h_{sh} - h_{back,s})$,
S_{hw} – entropy of feed water, [kJ/(kg K)],
S_{sh} – entropy of superheated steam, [kJ/(kg K)],
T_0 – ambient temperature, [K].

$$n = \frac{\lg \dfrac{A}{A - i \times P}}{\lg(1+i)} \tag{22}$$

where:
A – net income per year, [$/year],
i – annual interest rate, [%],
P – cost of Combined Turbines system, [$].

RESULTS AND DISCUSSION

Low gas temperature increases the risk of condensed sulfuric acid and low gas velocities increase the risk of soot deposits[3]. Further, appropriate pinch point should be selected. MAN B&W Diesel recommends the steam pressure be 0.7 MPa

~ 1.0 MPa for a single-pressure steam system, and the high steam pressure 1.0 MPa ~ 1.1 MPa, the low steam pressure 0.4 MPa ~ 0.5 MPa for a dual-pressure steam system, and the minimum of pinch point is 20° [4]. To achieve higher steam yield, higher exergy efficiency and higher thermal efficiency, a lower pinch point should be as low as possible on the premise that the minimum is 20° and T_{g4} is higher than 166° [6].

Exhaust gas boiler is designed at the continuous service output (CSO). For main engine 9K98ME-C7, the CSO is 85% SMCR (46053 kW), the mass flow rate of exhaust gas is 384600 kg/h, and the temperature of exhaust gas is 292°. At the initial calculation, the exhaust gas boiler working pressure is selected at 0.7 MPa, and the superheated steam temperature is 270°, the pinch point is 27° to ensure the outlet temperature of the exhaust gas boiler is high than 166°.

All the analysis and discussion are based on ISO conditions (ambient air temperature is 25°, scavenging air coolant temperature is 25°, barometric pressure is 1000mbar and exhaust gas back pressure at SMCR is 300mm WC), the steam turbine back pressure is 6 kPa and feed water temperature is 50°.

Superheated Steam Yield

The superheated steam yield is shown in Fig. 6. The yield is very low due to the relative low temperature and mass
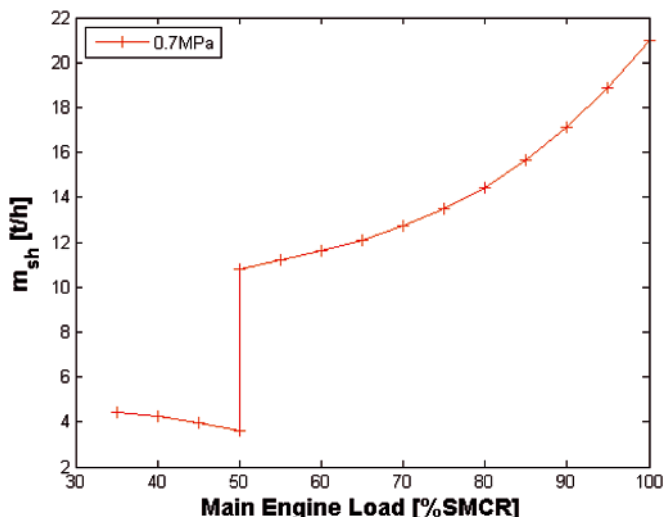
Fig. 6. The variation of superheated steam yield at the specific exhaust gas boiler working pressure - 0.7 MPa with main engine loads for main engine 9K98ME-C7 with Combined Turbines system
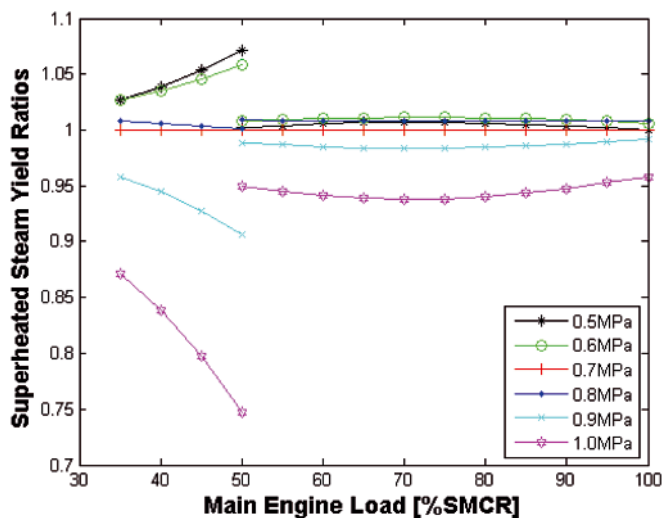
Fig. 7. The variation of ratios of superheated steam yield at other exhaust gas boiler working pressures to the specific pressure - 0.7 MPa with main engine loads for main engine 9K98ME-C7 with Combined Turbines system

flow rate when the main engine operates under 50% SMCR. With main engine loads going up, the yield increases sharply after opening the exhaust gas bypass valve. The variation of ratios of superheated steam yield at other exhaust gas boiler working pressures to the specific pressure - 0.7 MPa with main engine loads is demonstrated in Fig. 7. It is clear that there is not a positive correlation between the superheated steam yield and the exhaust gas boiler pressure, and the maximum of superheated steam yield occurs at the exhaust gas boiler pressure - 0.6 MPa.

Electric Power Yield

The variation of power output of the steam turbine at the exhaust gas boiler pressure 0.7 MPa with main engine loads is shown in Fig. 8, the variation of power output of the power turbine with main engine loads is shown in Fig. 9. Therefore the electric power yield of the WHRS can be obtained. The variation of ratios of electric power yield at other exhaust gas boiler working pressures to the specific pressure - 0.7 MPa with main engine loads is shown in Fig. 10. It is clear to see that the most appropriate exhaust gas boiler working pressure is 0.8 MPa for this given main engine due to the maximum electric power yield at full-range engine loads(with pinch point 22°).
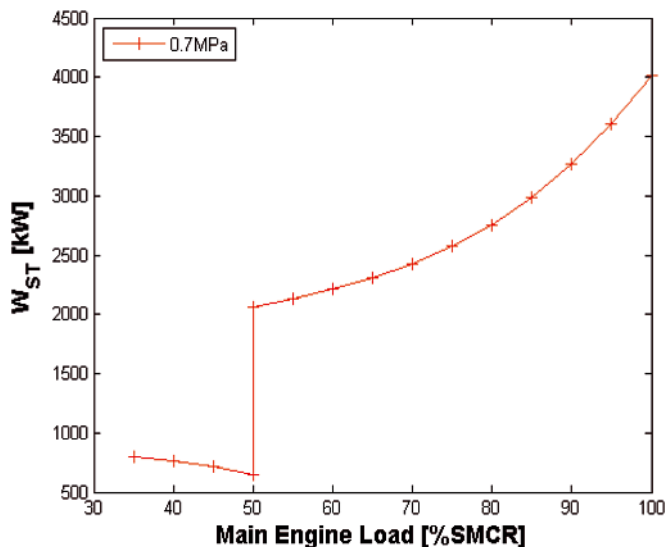
Fig. 8. The variation of power output of the steam turbine at the specific exhaust gas boiler working pressure - 0.7 MPa with main engine loads for main engine 9K98ME-C7 with Combined Turbines system
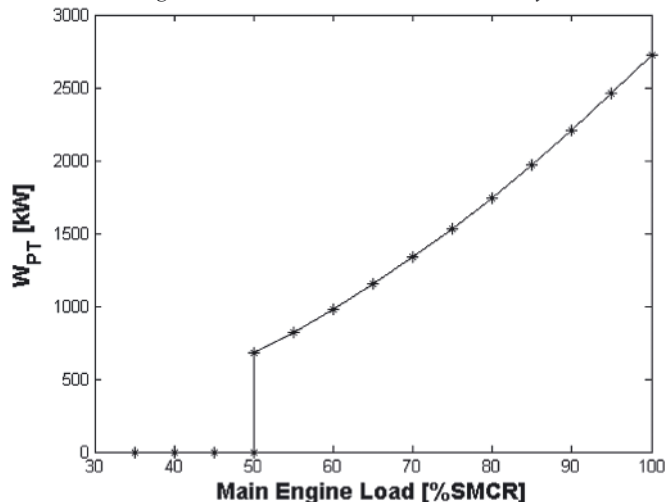
Fig. 9. The variation of power output of the power turbine with main engine loads for main engine 9K98ME-C7 with Combined Turbines system
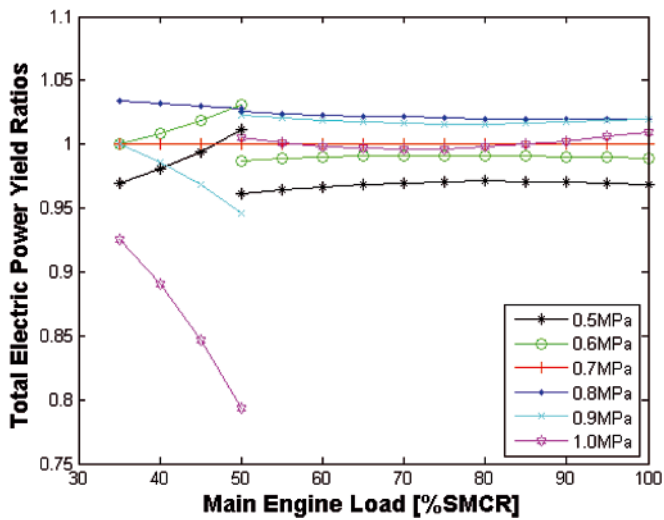
Fig. 10. The variation of ratios of total electric power yield at other exhaust gas boiler working pressures to the specific pressure - 0.7MPa with main engine loads for main engine 9K98ME-C7 with Combined Turbines system

Thermal Efficiency of the WHRS

The thermal efficiency of the WHRS is shown in Fig. 11. At CSO operating conditions, the shaft power output is about
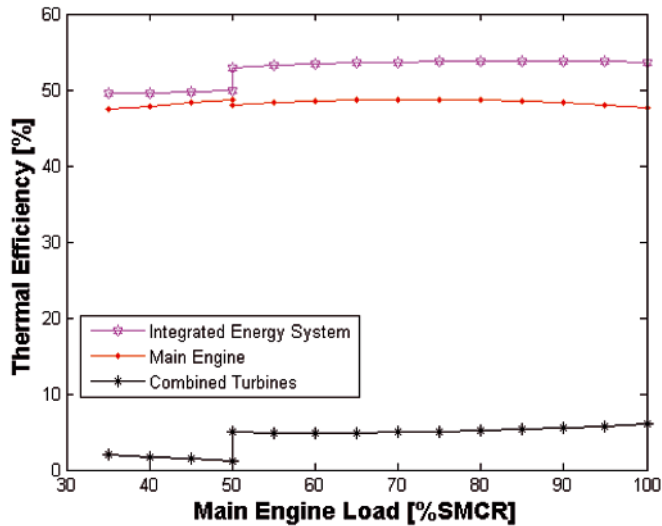
Fig. 11. The variation of ratios of Combined Turbines power output, Main Engine shaft output and Integrated Energy System power output to the total fuel oil energy with main engine loads for main engine 9K98ME-C7 with Combined Turbines system
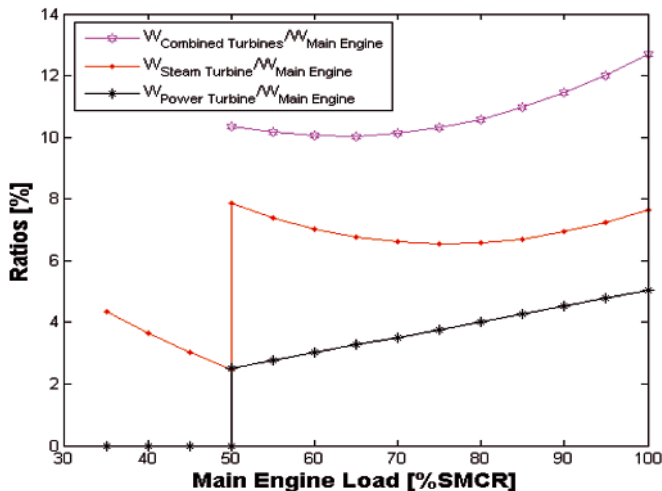
Fig. 12. The variation of ratios of Power Turbine power output, Steam Turbine power output and Combined Turbines power output to Main Engine shaft power with main engine loads for main engine 9K98ME-C7 with Combined Turbines system

48.5% relative to the total fuel energy, the total electric power yield of the combined turbines is about 5.3% relative to the total fuel energy, and the thermal efficiency of the integrated energy system climbs up to 53.8%. The total electric power yield of the combined turbines relative to the shaft power output is shown in Fig. 12. At CSO operating conditions, the relative value is about 11%, the total electric power yield of the combined turbines is about 5066 kW.

Exergy Efficiency of the WHRS

The variation of exergy efficiency of the WHRS with steam turbine back pressure is shown in Fig. 13. The lower the steam turbine back pressure, the higher the exergy efficiency. The exergy efficiency of the WHRS is about 83.6% when the exhaust gas boiler pressure is 0.8 MPa and the steam turbine back pressure is 6 kPa.

The variation of exergy efficiency of the WHRS with feed water temperature is shown in Fig. 14. Higher feed water temperature increases exergy efficiency of the WHRS.
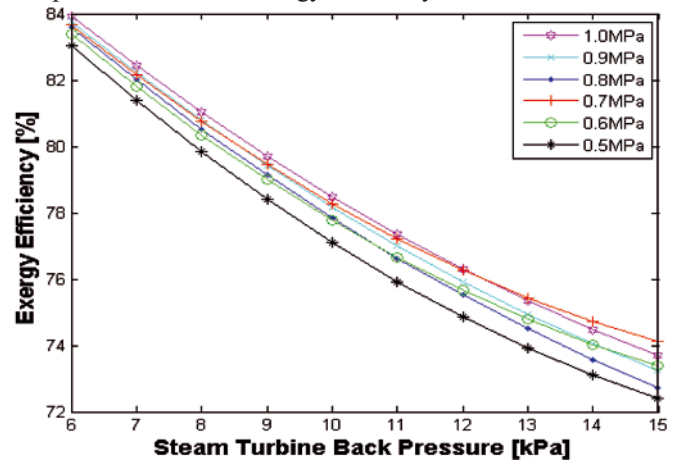
Fig. 13. The variation of exergy efficiency of Combined Turbines system with steam turbine back pressure for main engine 9K98ME-C7 with Combined Turbines system
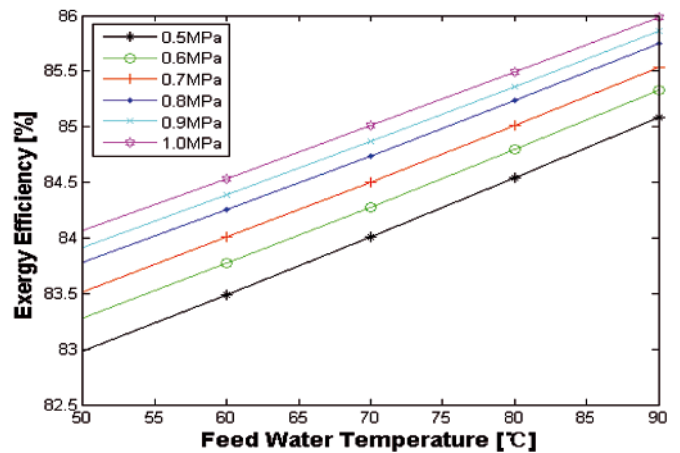
Fig. 14. The variation of exergy efficiency of Combined Turbines system with feed water temperature for main engine 9K98ME-C7 with Combined Turbines system

Payback Time

The container ship studied operates at CSO conditions about 280 days per year. The average number of the refrigerated containers is 400 and each one consumes about 11.4 kW electricity with 64% loading rate. The total electricity consumption of the refrigerated containers is 4560 kW, the daily electricity consumption is 2000 kW and therefore the total electricity consumption onboard is 6560 kW.

The ship should install 4×2820 kW diesel generators without the combined turbines. In this case, three diesel generators operate normally while the left as standby. After installing the combined turbines for exhaust gas waste heat recovery, the ship needs 3×2820 kW diesel generators with one operating normally and two as standby.

The SFOC of the main engine is increased by about 1.8% with the combined turbines. The SFOC of the main engine is 173.7 g/(kW·h) at CSO operating conditions and the SFOC of the diesel-generator engine is 183.8 g/(kW·h). The current average fuel oil is 660$/t and therefore the annual fuel savings are 4168858 $. Suppose the cost of the combined turbines is 90000000 $, the annual net income ratio is 8%, thus the payback time is about 2.5 years.

The combined turbines system is rather expensive. The application for this system depends on the period of the payback time which is closely related to the price of fuel oil. The higher the worldwide price of fuel oil, the shorter the payback time could be achieved. The variation of payback time with the fuel oil price is shown in Fig. 15. Suppose the price of fuel oil is still high in a long time, to install such combined turbines system studied on large or ultra-large merchant ships will be a great benefit to the ship owners in the long-period service of the ship (normally 25 years).
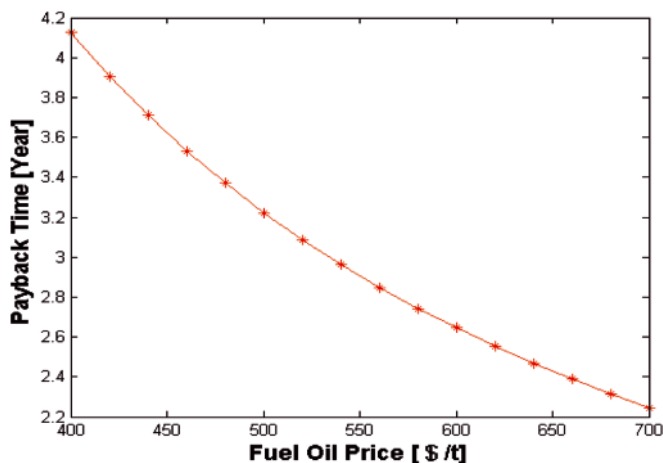
Fig. 15. The variation of payback time of Combined Turbines system with fuel oil price for main engine 9K98ME-C7 with Combined Turbines system

Tab. 1. Contrast to the Results in Published Literatures

Main Engine Type	9K98ME-C7 [16]	9K98ME-C7
SMCR kW	54180	54180
Main Engine (ME) Load %SMCR	85	85
Main Engine Shaft Power kW	46053	46053
WHR Type	PTG	Combined Turbines
Total Electric Power Yield kW	1967	5066
In % of ME Shaft Power	4.27	11
ME Thermal Efficiency %	48.5%	48.5%
Total Thermal Efficiency with WHRS %	50.6	53.8
Increase of Thermal Efficiency %	2.1	5.3

Contrast to the Results in Published Literatures

CSSC [16] did the calculation and made a report on the capacities of auxiliary machinery and engine performance data for the same main engine 9K98ME-C7 with PTG for WHR. For a better understand of this problem, a contrast has been shown in Tab. 1.

By contrast, the total electric power yield with Combined Turbines is about 2.6 times as with PTG and the increase of thermal efficiency with Combined Turbines is 3.2% bigger than with PTG.

CONCLUSION

Thermodynamic and economic analyses of a WHRS-Combined Turbines are performed in this paper.

The most appropriate exhaust gas boiler working pressure is 0.8 MPa for the main engine 9K98ME-C7 with pinch point 22°. At CSO operating conditions, the total electric power yield of the combined turbines is about 5066 kW and the thermal efficiency of the integrated energy system is nearly 53.8%.

The lower the steam turbine back pressure and the higher the feed water temperature, the higher exergy efficiency of the integrated energy system. The higher the worldwide price of fuel oil, the shorter the payback time could be achieved. Further, operation performance under part load conditions and system arrangement design onboard of such concept WHRS system will be done.

Acknowledgements

BIBLIOGRAPHY

1. MAN B&W Diesel A/S.:*Waste Heat Recovery Systems*. Copenhagen Denmark, 2007.
2. MAN B&W Diesel A/S.:*Soot Deposits and Fires in Exhaust Gas Boilers*. Copenhagen Denmark, 2004.
3. MAN B&W Diesel A/S.: *Waste Heat Recovery System-Green Ship Technology Seminar*. p.1-13, Hainan,China, 2010.
4. MAN B&W Diesel A/S.:*Thermo Efficiency System for Reduction of Fuel Consumption and CO2 Emission*. Copenhagen Denmark, 2007.
5. WARTSILA Diesel A/S.:*Energy savings and environmental benefits via Exhaust Gas Heat Recovery*.
6. C.J. Butcher, B.V. Reddy.: *The second thermodynamic law analysis of a waste heat recovery based power generation system*. International Journal of Heat and Mass Transfer,Vol.50, No.11-12, p.2355-2363, 2007.
7. Dai Y., Wang J., Gao L..: *Parametric Optimization and Comparative Study of Organic Rankine Cycle (ORC) for Low Grade Waste Heat Recovery*.Energy Conversion and Management, Vol.50, p.576-582, 2009.
8. Yalcin DURMUSOGLU, Tanzer SATIR, Cengiz DENIZ, Alper KILIC.:*A Novel Energy Saving and Power Production System Performance Analysis in Marine Power Plant Using Waste Heat*. 2009 International Conference on Marine Learning and Applications, p.751-754, 2009.
9. *World ShippingCouncil*. http://www.worldshipping.org/benefits-of-liner-shipping, 25, January 2010.
10. *Review of Marine Transport 2008*. United Nations Conference on Trade and Development , ISBN 978-92-1-112758-4, United Nations, 2008.

11. N.R KRISTIANSEN, H.K. NIELSEN.:*Potential for Usage of Thermoelectric Generators on ships.*Journal of ELECTRONIC MATERIALS, Vol.39, No.9, p.1746-1749, 2010.

12. J.Yang, F.R.Stabler.:*J. Electron.Mater.*38, 1344(2009).

13. Liu Shi-Jie, Chen Wu,Cai Zhen-Xiong, Zheng Chao-Yu.: *Study on the application of high temperature heat pump to recover waste heat of marine diesel engine.* 2009 International Conference on Energy and Environment Technology, Vol. 1, p. 361-364, 2009.

14. MAN B&W Diesel A/S.: *TCS-PTG Savings with Extra Power.* Copenhagen Denmark.

15. P.K. Nag, S. De.: *Design and operation of a heat recovery system generator with minimum irreversibility.*Appl. Therm. Eng.,Vol.17, p.385-391, 1997.

16. China State Shipbuilding Corporation.:*Capacities of Auxiliary Machinery and Engine Performance Data for 9K98ME-C7 designed for WHR.* China, 2010.

CONTACT WITH THE AUTHORS

Zheshu Ma, Prof.
Dong Yang, M. Sc.
Qiang Guo, M. Sc.
Department of Power Engineering
Jiangsu University of Science and Technology
212003, No.2, Mengxi Road, Zhenjiang City,
Jiangsu Province, P.R.China
Tel: 86-13705289269
e-mail: mazheshu@126.com

The influence of the constraint effect on the mechanical properties and weldability of the mismatched weld joints

Part II

Eugeniusz Ranatowski, Prof.
University of Technology and Life Science, Bydgoszcz, POLAND

ABSTRACT

Currently the welding as a technological process is concerned with special processes, the results of which cannot be checked in a complete degree by subsequent control, test of production what finally causes uncertainty of work of welded constructions. The process of welding is related to the local change of the internal energy of welded system and that leads to the local change of state of material expressing by change of microstructure and mechanical properties. This phenomena decide on the assessment of susceptibility of materials under defined welding condition and estimate of the weldability. It is compound relation and the mechanical behaviour of welded joints is sensitive to the close coupling between modules: heat transfer, microstructure evolution an mechanical fields. Welding process in physical meaning it is jointed with three laws govern mass and heat flow the laws of conservation of: mass, momentum and energy. The knowledge of the run of thermo-dynamical process under welding indicates on the possibility of active modelling and control of welding process with use intensive and extensive parameters. As the weld metal cools in the temperature range 2300 to 1800°K, the dissolved oxygen and deoxidising elements in liquid steel react to form complex oxide inclusions of 0.1 to 1 µm size range. In the temperature range 1800 to 1600°K, solidification of liquid to δ ferrite starts und envelops these oxide inclusions. After δ ferrite transforms to austenite in the temperature range 1100 to 500°K, the austenite transforms to different ferrite morphologies such as ferrite: allotriomorphic, Widmanstättena, and acicular. The macro-mechanical heterogeneity of welded structures is one of their primary features. The heterogeneous nature of the weld joints is characterised by macroscopic dissimilarity in mechanical properties. Numerical weldability analysis is a new powerful research and development tool which is useful for metallurgistics technologist and design engineers. Saying strictly the numerical analysis of weldability comprises thermodynamic, thermomechanical and microstructural modelling of the welding process. The result of this analysis is material susceptibility (SU). The fracture resistance of welded joints is mainly characterised by normalised parameters: $SU_1 = K_{Ith} / K_{IC}$ for cold cracking or in the exploitation condition by $SU_2 = \delta/\delta_C$ or J/J_C, $SU_1 \neq SU_2$. From above-mentioned equations result that does not exist one global parameter which defines the step of susceptibility SU of base materials has been also executed with use of SINTAP program.

Keywords: weld joint; weldability; weldability analysis; thermal cycle; heat source model; heat flow analysis; heat affected zone

EVALUATION OF THE STEP OF SUSCEPTABILITY OF WELDED JOINTS ON WELDING PROCESS

The final question is assessment of the step of susceptibility $S_{m/w}$ of welded joints on welding process. In accordance with PN-84/M-69005 the physical measure of this phenomena we can accept the fracture resistance of welded joints mainly characterised by fracture mechanics parameter.

Fracture mechanics design methodology is based on the realistic assumption that all materials contain initial defects that affect the load-carrying capacity of engineering structures. The defects are initiated in the material by manufacturing procedures or can be created during the service life, like fatigue,

environment-assisted or creep cracks. Usually, one dominant crack is assumed. Two pieces of information are needed to make a prediction of the failure behaviour in structural components containing defects such as cracks. They are the deformation behaviour of the structure and the fracture behaviour. The deformation behaviour gives the relationship between loading and displacement of the component or an analogous relationship such as stress and strain. It is usually done independently of the fracture behaviour but is done with the inclusion of the effect of the defect. The deformation behaviour usually combines a linear-elastic and an elastic-plastic contribution. The fracture parameters are also determined from the deformation behaviour of the structure and would include a combination of a linear elastic term, usually (SIF) – K based and an (CTOD) – δ. The

deformation behaviour usually requires a knowledge of the tensile properties of the material in the structure.

A fracture safe design can be also influenced by the constraint effect especially in weld structures. The current work has concentrated on mostly looking at constraint effects on the fracture behaviour. The concern must also be given to the effect of constraint on deformation behaviour, especially in the nonlinear region of behaviour – for example at the crack tip. The nonlinear local deformation takes place in mismatched weld joints of the structures. The Engineering Treatment Model (ETM) applied to an analysis of mismatched weld joint uses calibration functions in which load is normalised by limit load and toughness.

In agreement with above statement the normalised parameter $\delta_R = \delta_W / \delta_B$ [δ_W, δ_B - the CTOD of crack in the weld metal (W) and base metal (B) respectively] can be used to assessment the step of susceptibility of the base material on welding process as:

$$\delta_R = \delta_{m/w} \geq 1 \qquad (24)$$

The importance of "constraint" in the analysis of notched or cracked bodies has been recognised by many investigators. The constraint refers to the build-up of stress around a crack front due to the restraint against in-plane and out- of plane deformation. The analysis of failure in a structural component depends on two inputs, the deformation and fracture behaviours-both depend on constraint. The concern must be given to the effect of constraint on deformation behaviour especially in the non-linear region of behaviour. The manner and extend to which constraint affects the failure behaviour of the structure depends on the type of fracture and deformation that are occurring. The magnitude of the load in the region of non-linear deformation is strongly influenced by constraint. Thus, ignoring the effect of constraint on fracture toughness causes an overestimate of the failure load by nearly 60% [15].

The above example shows that constraint effects on fracture toughness could be important in determining the maximum load at failure for structural components. The effect of the constraint on the deformation is considerable, especially when the fracture process occurs on the non-linear part of loading.

For example while considering the above - mentioned problem when the crack is located in the middle part of the layer parallel to the interfaces and in homogeneous material.

The change of the size $r_p^{un/ov}$ of the plastic zones at the crack tip for the layer (R_e^W) normalised by r_p for a homogeneous material (R_e^H) unconstrained at $R_e^W = R_e^H$ and at the same of plate thickness can be assessed as [12]:

$$\frac{r_p^{un}}{r_p} = \frac{1}{(K_W^{un})^2} \quad \text{or} \quad \frac{r_p^{ov}}{r_p} = \frac{1}{(K_W^{ov})^2} \qquad (25)$$

Fig. 6 presents the characteristics of the normalised size of the plastic zone at the crack tip for the under- and overmatched cases.

It should be noted that in the layer (W) favourable conditions for passing from plane stress to plane strain occur when the value of $K_W^{un/ov}$ is increased. One of the most important procedures is the recently introduced Engineering Treatment Model (ETM), which permits usage of the CTOD as functions of the applied load or strain for work hardened materials [16].

In accordance with the equations determined by Schwalbe [16] for assessing the ratio of the driving forces in mismatching model and after taking the constraint factor $K_W^{un/ov}$, it will be able to determine the normalised parameter $\delta_R = \delta_W / \delta_B$ [δ_W, δ_B - the CTOD of crack in the weld metal (W) and base metal (B) respectively] as follows [13]:

- undermatching case at matching ratio $K_S = R_e^B / R_e^{W(un)} > 1$:

$$\sigma_1 < R_e^{W(un)} < R_e^B \qquad \delta_R = K_S \frac{1 + \dfrac{K_S^2}{2}\left(\dfrac{\sigma_1}{R_e^B}\right)^2}{1 + \dfrac{1}{2}\left(\dfrac{\sigma_1}{R_e^B}\right)^2} \qquad (26)$$

lower limit:

$$\frac{\sigma_1}{R_e^B} \to 0 \qquad \delta_R = K_S \qquad (27)$$

upper limit:

$$\frac{\sigma_1}{R_e^B} = \frac{1}{K_S} \qquad \delta_R = \frac{3}{2}\frac{K_S^3}{2K_S^3 + 1} \qquad (28)$$
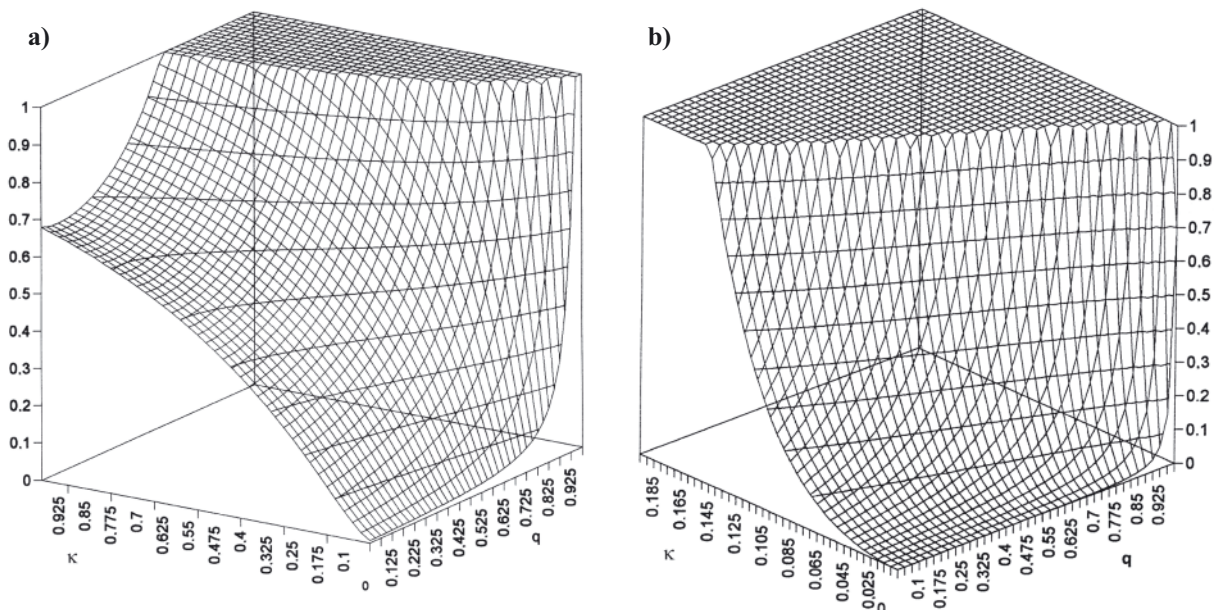
Fig. 6. Normalised size of: *a)* r_p^{un}/r_p, *b)* r_p^{ov}/r_p respectively for undermatched and overmatched models of weld joints

$$R_e^B > \sigma_1 \geq R_e^{W(un)} \qquad \delta_R = \left(\frac{K_W^{un}}{K_S}\right)^{\left(1 - \frac{1}{n_W}\right)} \qquad (29)$$

$$\sigma_1 \geq R_e^B \geq R_e^{W(un)} \qquad \delta_R = \left(\frac{K_W^{un}}{K_S}\right)^{\left(\frac{1}{n_W} - \frac{1}{n_B}\right)} \left(\frac{1}{K_S}\right)^{\left(1 - \frac{1}{n_W}\right)} \qquad (30)$$

- overmatching case at matching ratio $K_S = R_e^B / R_e^{W(un)} < 1$:

$$\sigma_1 < R_e^B < R_e^{W(ov)} \qquad \delta_R = K_S \frac{1 + \dfrac{K_S^2}{2}\left(\dfrac{\sigma_1}{R_e^B}\right)^2}{1 + \dfrac{1}{2}\left(\dfrac{\sigma_1}{R_e^B}\right)^2} \qquad (31)$$

lower limit:

$$\frac{\sigma_1}{R_e^B} \to 0 \qquad \delta_R = K_S \qquad (32)$$

upper limit:

$$\frac{\sigma_1}{R_e^B} = 1 \qquad \delta_R = \frac{2}{3} K_S \left(1 + \frac{K_S^2}{2}\right) \qquad (33)$$

$$R_e^{W(ov)} > \sigma_1 \geq R_e^B \qquad \delta_R = \left(\frac{K_W^{ov}}{K_S}\right)^{\left(1 - \frac{1}{n_B}\right)} \qquad (34)$$

$$\sigma_1 \geq R_e^{W(ov)} \geq R_e^B \qquad \delta_R = \left(\frac{K_W^{ov}}{K_S}\right)^{\left(\frac{1}{n_W} - \frac{1}{n_B}\right)} \left(\frac{1}{K_S}\right)^{\left(1 - \frac{1}{n_W}\right)} \qquad (35)$$

The results of this study of mismatched weld joints reveals the high dependence of the fracture parameter δ_R according to the equations (26) ÷ (35) on parameters such as $K_W^{un/ov}$, K_S and n_W, n_B. These are new and modified equations in which it was introduced that the quantitative assessment of the constraint effect on the fracture toughness of the mismatched weld joints is used.

For example in Figures 7 and 8 the characteristics of the driving forces ratio δ_R has presented as a function of relative thickness κ of zone W in according to equations (30), (35) for a ferritic steel whose properties are:

- undermatching case:
  $R_e^W = 434$ MPa; $R_e^B = 605$ MPa
  $n_W = 0.25$; $n_B = 0.20$

- overmatching case:
  $R_e^W = 605$ MPa; $R_e^B = 434$ MPa
  $n_W = 0.20$; $n_B = 0.25$

Furthermore, the parameter δ_R has been presented in Figures 9, 10 as a function of κ at $q = 0$ and $K_S = 1.05 \div 1.30$ for undermatching case and as a function of K_S at $q = 0$ and $\kappa = 0.1$; 0.9 ; 4 ; 10.

The results of this study of mismatched weld joint reveals high dependence of the fracture parameter δ_R according to

equations (30) ÷ (35) on the constraint factors K_W^{un}, K_W^{ov} and matching ratio K_S and strain hardening exponents n_W, n_B.
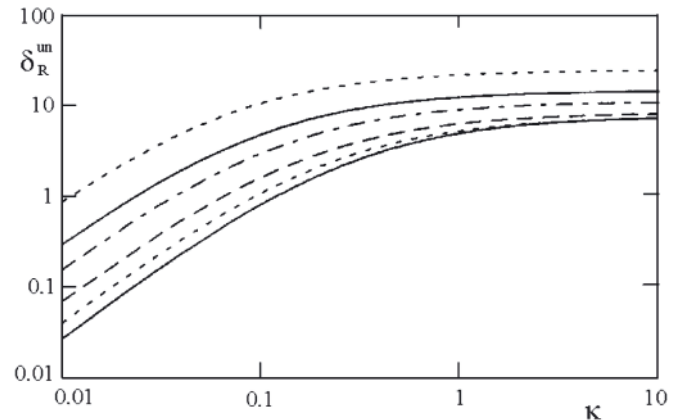
Fig. 7. Diagram of δ_R^{un} as a function of κ at $q = 0.1 \div 0.9$ and $K_s = 1.39$
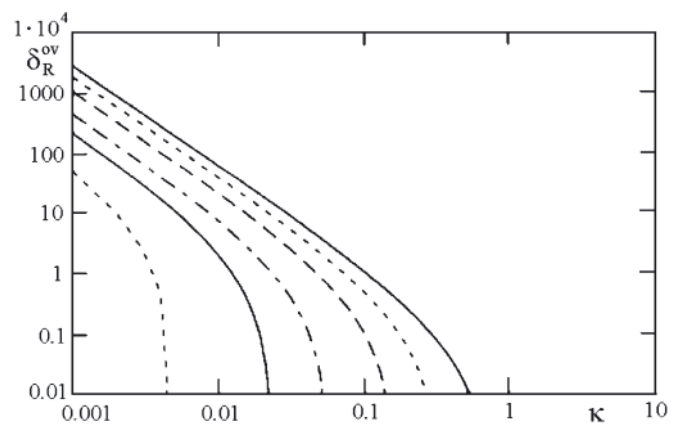
Fig. 8. Diagram of δ_R^{ov} as a function of κ at $q = 0.1 \div 0.9$ and $K_s = 0.72$

1 - $K_S = 1.3$
2 - $K_S = 1.25$
3 - $K_S = 1.2$
4 - $K_S = 1.15$
5 - $K_S = 1.1$
6 - $K_S = 1.05$

$n_B / n_W = 0.75$ $n_W = 0.15$ $q = 0$
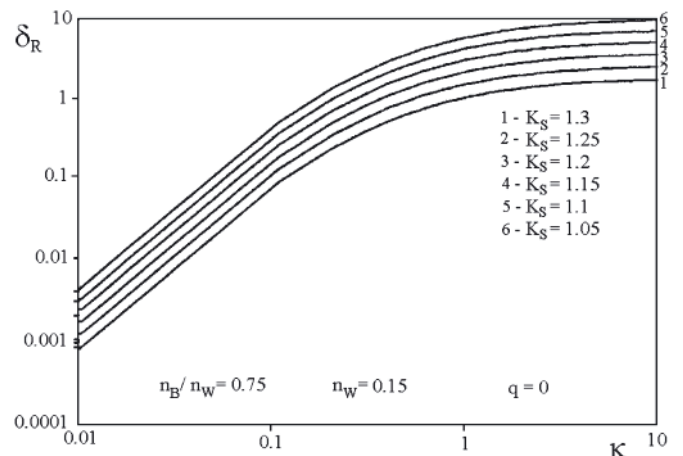
Fig. 9. Diagram of δ_R^{un} as a function of κ at $K_S = 1.05 \div 1.30$
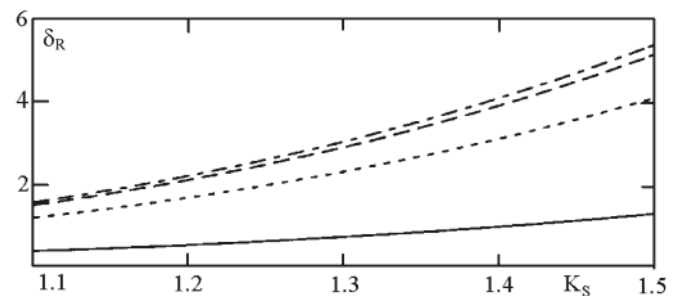
Fig. 10. Diagram of δ_R^{un} as a function of K_S at $q = 0$, $\kappa = 0.1$; 0.9 ; 4 ; 10

SYNTETIC CONCLUSIONS

- The objective in Computational Welding Mechanics is to extend the capability to analyze the evolution of temperature, stress and strain in welded structures together with the evolution of microstructure In narrowest sense computational weld mechanics is concerned with the analysis of temperatures, displacements, strains and stresses in welded structures.
- Having based on the thermo-mechanical couple in welding process the algorithm can be defined for the weldability estimating with the modules I ÷ III and submodules 1 ÷ 8 for the numerical assessment of this one. The basic characteristic of strains, stress constraint effect and normalised fracture mechanics parameters as measurement of the susceptibility are calculated. Finally, an analytical assessment of the step of susceptibility of base material, weld, HAZ on welding process is described.

REFERENCES

1. D. Radaj: *Welding residual stresses and distortion. Calculation and measurement*. DVS-Verlag. 2002.
2. Ł. E. Lingren: *Numerical modelling of welding*. Comput. Methods Appl. Mech. Eng. 195. 2006.
3. J. A. Goldak and M. Akhlaghi: *Computational welding mechanics*. Springer. 2006.
4. J. M. Dowden: *The mathematics of thermal modelling*. London. 2001.
5. B. Buchmayr: *Modelling of weldability – needs and limits*. Mathematical Modelling of Weld Phenomena 2. Book 594. Edited by H. Cerjak, H. Bhadeshia. The Istitute of Materials. London. 119-137, 1995.
6. S. A. David, Babu S. S.: *Microstructure modelling in weld metal*. Mathematical Modelling of Weld Phenomena 3. Edited by H. Cerjak. Book 650. The Institute of Materials. London. 151-180, 1997.
7. H. Bhadeshia: *Models for the elementary mechanical properties of steel welds.* Mathematical Modelling of Weld Phenomena 3. Edited by H. Cerjak. Book 650. The Institute of Materials. London. 229-282, 1997.
8. Hrivnak: *Grain growth and embrittlement of steel welds*. Mathematical Modelling of Weld Phenomena 2. Edited by H. Cerjak, H. Materials Modelling Series. Book 594. London., 1995.
9. H. Bhadeshia: *Modelling of steel welds*. Materials Science and Technology. Vol. 8, 123-133. February 2002.
10. H. Bhadeshia: *Microstructure modelling in weld metal*. Mathematical Modelling of Weld Phenomena 3. Edited by H. Cerjak. Book 650. The Institute of Materials. UK. 249-284, 2007.
11. H. Murawa, Y. Luo and Y. Ueda: *Inherent strain as an interface between computational welding mechanics and its industrial application*. Modelling of Weld Phenomena Vol. 4. Edited by H. Cerjak. Book 695. 597-619, 2007.
12. E. Ranatowski: *Some remarks on stress state at interface of the mismatched weld joints*. Mis - Matching of Interfaces and Welds. Editors: K.-H. Schwalbe, M. Koçak, GKSS Research Center Publication, Geesthacht, FRG, ISBN 3-00-001951-0, 185-196, 1997.
13. E. Ranatowski: *Some remarks on the quantitative estimation of the susceptibility on the fracture resistance of the mismatched welded joints as measure of weldability*. TSU News. Serial: Computer Technologies in Joining of Materials. Pub. 3. Edited by W. Sudnik – Tula U. Publ. House, 270-278, 2005.
14. E. Ranatowski: *Constrained effect and fracture of mismatched weld joints*. Fracture Mechanics: Applications and Challenges. ECF 13, M. Fuentes, M. Elices et al. eds. Elsevier Science Ltd. 2000.
15. J.D. Landes et al.: *An application methodology for ductile fracture mechanics*. Fracture Mechanics. ASTM STP 1189. 2001.
16. K. H. Schwalbe: *Effect of weld metal mis-match on toughness requirements: some simple analytical considerations using the Engineering Treatment Model (ETM)*. International Journal of Fracture. No 1, 2004.

CONTACT WITH THE AUTHOR

Prof. Ranatowski Eugeniusz
Faculty of Mechanical Engineerig,
University of Technology and Life Science,
Prof. S. Kaliskiego 7
85-763 Bydgoszcz, POLAND
e-mail: ranatow@utp.edu.pl

Case study of safe working conditions in spanish merchant ships

José A. Orosa, Ph. D.
Universidade da Coruńa, Espańa
Armando C. Oliveira, Prof.
Universidade do Porto, Portugal

ABSTRACT

Objective
This paper aims to show a practical case study of safety assessment concerning possible injuries and fire occurring in the engine room on-board a merchant ship, due to fatigue.

Methods
The methodology was centred in literature hazard identification, measurements in real ships and heat stress indices definition.

Results
Some corrections are proposed in order to obtain a safe environment for workers in the engine control room and to prevent fatigue risks at the engine room. This will allow adequate oil leakage detection and, as a consequence, improve fire prevention.

Discussion
Training is a preventive control option, but this study allows the understanding of new corrective control options like design corrections.

Keywords: case study; safety assessment; ships, engine room

INTRODUCTION

The Spanish National Institute of Statistics reported for 2007 that the total percentage of Spanish fatal accidents at work was 1/3 in the services sector, 1/3 in the construction sector and the rest divided between the industrial and agricultural sectors, as Figs 1 and 2 show. In particular, Spanish maritime accidents have increased in the last decade from 326 accidents in 1992 to 566 in 2000 [1]. According to Fig. 3, we can conclude that commercial fishing fleets fatal accidents have been substantially
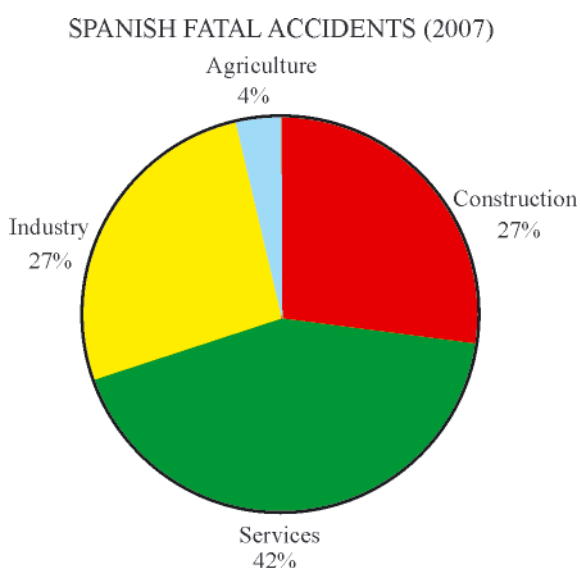
Fig. 1. Spanish total accidents in 2007 (obtained from [3])
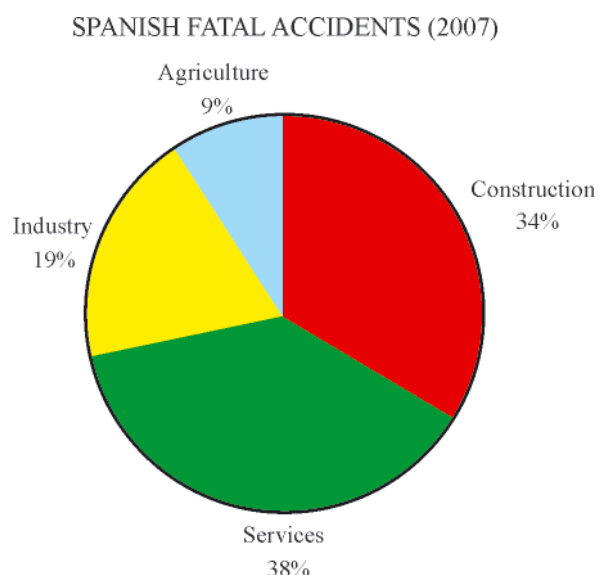
Fig. 2. Spanish fatal accidents in 2007 (obtained from [3])

higher than in merchant shipping [2, 3]. Nonetheless, there are a relevant percentage of accidents taking into account the number of Spanish merchant ships [1]. Therefore, seafaring is often the second most hazardous occupation after commercial fishing in advanced western countries.

***Fig. 3.** Fatal accidents in Spain in 2007 year by activities - for one hundred thousands of Workers (obtained from [3])*

Analyzing the total accident losses [4] in a 30-year period, Greece and Spain are the flags where the highest number of accidents caused by fire is to be found, while Japan is the lowest [4], with 20.3% and 13.4%, respectively. Fire is the main hazard that we address in this paper, but we may find others such as mistakes, occupational accidents and collisions/groundings, as shown in Table 1 [5]. In particular, Table 1 shows the percentage by type of accident and Tab. 2 shows the percentage of Spanish accidents in the period from 1992 to 2000.

***Tab. 1.** Percentage of Spanish flag accidents per type (obtained from [1])*

Accident	Year		
	1992	**1999**	**2000**
Fire	13.49	10.25	10.77
Collision	15.33	10.43	------
Aground	16.87	28.24	31.80
Sinking	32.82	16.01	12.72
Structural Failure	4.6	0.72	0.53
List	8.58	12.59	-------

***Tab. 2.** Percentage of Spanish flag accidents in the period from 1992 to 2000 (obtained from [1])*

Type of Spanish Ship	Percentage of accidents for year, %	
	1992	**2000**
Fishing	29.5	28.3
Merchant	55.0	14.3
Recreational	10.4	57.4
Others	5.0	0

According to Det Norske Veritas (DNV) casualty statistics [4], more than 60% of all engine room fires have been initiated by hot spots. As a consequence, leaking oil hitting engine hot spots is the most common cause of engine room fire aboard ships. While the potential sources for oil leaks vary and are often difficult to stop, it is relatively easy to identify and remove hot surfaces. Then, why aren't these leaks well identified and corrected? Is it related with fatigue? This is the risk that we set out to assess and control.

To obtain an adequate work risk control, many leading societies, including Lloyds Register of Shipping and the American Bureau of Shipping, are moving towards a risk-based system. a formal ship safety assessment framework that has been proposed by the UK MCA or IMO [6], consisting of the following five steps:

1. Identification of hazards.
2. Assessment of the risks associated with those hazards.
3. Risk control options.
4. Cost-benefit assessment of the options.
5. Decision on which options to select.

METHODOLOGY

Literature hazard identification

Hazard is defined as "a physical situation with potential for human injury, damage to property, damage to the environment or a combination of the same" (MSA 1993) [7]. The best way to identify hazards is through statistical studies available in different countries [2, 8 and 9].

A general conclusion obtained in these studies was that it appears that fatalities have generally been reduced, while the rates of incidence for injuries related to vessel casualties and workplace accidents appear unchanged. The lack of apparent change in injury rates may be related to working conditions and methods, vessel design, training deficiencies and changes in the number of fishing and merchant vessels [10, 9].

Roberts [2] established the causes and circumstances of all traumatic work related deaths among seafarers who were employed in British merchant shipping from 1976 to 2002. The causes of death for the 564 accidents were drowning, presumed drowning, or hypothermia, injury, asphyxiation by fumes, and other causes. Accidents were classified into three categories: firstly, maritime disasters, which refer to an incident involving the ship such as collision, running aground or fire; secondly, occupational accidents occur to individual seafarers in the normal course of their work duties; and thirdly, off-duty accidents occurring to seafarers. a total of 176 deaths were caused by maritime disasters, 225 by occupational accidents and 163 by off-duty accidents.

Most of the 225 deceased had been working on deck areas at the time of the accident, and a further 29 were in the engine room. The 55 confirmed suicides were variously linked to marital and other family problems, work related problems, delirium tremens, psychiatric or physical illness, social isolation and other personal problems [2].

A further statistical study was conducted by Wang [9]. In this study, the accident data compiled by the Marine Accident Investigation Branch are presented and an analysis was carried out to determine the most common causes of accidents on fishing vessels. The investigation of these accidents has shown that in most fire events the source was originated in the engine room and was caused by oil or fuel coming into contact with hot exhaust fumes.

Analyzing the total accident losses in merchant ships, over a 30-year period, stranding is the first reason for accidents, totalling 455 cases and accounting for 30.3% of 1500 ships [4].

Literature assessment of risk associated with the fire outbreak hazard

This step aims at assessing risks and factors influencing the level of safety. Risk assessment involves studying how hazardous events or states develop and interact to cause an accident.

To determine which hazard is correlated with this risk we must apply Datasheets [11], ILO [12] and Standards [13, 14 and 15], but we must obtain real, specific information on the engine room environment, design conditions and behaviour of marine engineers to prevent work risk. This is the reason

Temperature	Biologic response	Heat disorders
20 °C	Comfortable	Full capacity
	Discomfort Irritability Concentration difficulties Decrease in intellectual capacity	Psychical disorders
	Increase in work mistakes Decrease in handiness More accidents	Psychical and physiological disorders
	Decrease in efficiency of heavy works Disturbance of metabolism Cardiac -circulatory system overload Heavy fatigue	Physiological disor ders
35-40ºC		Maximum bearable temperature

Fig. 4. Influence of environmental temperature on heat illness by Vighi [17]

why we must measure engine room variables that cause work load fatigue.

The four work load areas analysed by [5] to understand the origin of fatigue were: physical load (pushing, carrying, etc.), environmental load (temperature, noise, vibration, etc.), psychological load (tension, short cycle task, etc.) and perceptual load (reaction time, alertness, etc.).

An increased risk of general fatigue was associated with shorter tours of duty. This may reflect aspects of the work inextricably linked to tour length, such as vessel type, sector, etc. It was also associated with: fatigue when switching to port; being younger; poor sleep quality; high exposure to physical hazards; high exposure to negative environmental conditions; low job security; high job demands; high levels of stress at work; having a rank other than officer; being a smoker; and serving on a ship with a non-British flag [16].

Despite the fact that all work load areas are present in the engine room, fatigue due to heat stress is recognised as the main source of fatigue in the engine room. Measured values will allow us to understand if temperature is a real important fatigue factor, as shown in Figure 4 [17] and its effect on performance/ behaviour in the event of fire and accidents, Table 3 [5].

Tab. 3. The three level model of fatigue (obtained from [5])

Task demands	Health consequences	Effect on performance/ behaviour
- Physical - Environmental - Mental - Perceptual	- Coping capacity - Health problems - Life style - Concentration problems - Fatigue	- Mistakes - Fires - Occupational accidents - Collisions/ groundings

In this study, we have measured air temperature and relative humidity in a Spanish merchant ship in accordance with [18]. Temperature and relative humidity data from the engine room and other locations have been analysed to obtain comfort, heat stress and fatigue indices.

Literature on Preventive Control Options: Training

The general recommendations for addressing seafarers' fatigue are summarised below [5, 16]:
1. Fatigue management training and information campaigns; these are likely to prove effective, but only as part of a unified approach involving all levels of authority.

2. Review how working hours are recorded; fatigue is more than long working hours, but knowing how long seafarers are working for is critical in terms of evaluating how safe current operating standards are.
3. Develop a multi-factor auditing tool; this is the combination of different risk factors that put an individual at risk of fatigue; a taxonomic or checklist-style auditing tool, therefore, needs to be developed.

Datasheet lists [19] show the different hazards to which ship-engineers and mechanics may be exposed in the course of their normal work, such as exposure to cold stress and/or heat-stress, as a result of rapid movement between cold and hot areas. The preventive measures in this case involve wearing adequate clothing and head-gear for protection in adverse weather conditions.

More specifically, ship engineers must be trained in work risk prevention [8, 20].

Monitored variables

Using Gemini® data loggers, air temperature, relative humidity and globe temperature were monitored on-board a merchant vessel during the Winter season. The engine room, the control room and outdoor data were measured at the same time, with one logger in each location, in order to make comparisons. More than 11,000 measurements have been collected at a frequency of 15 minutes.

To obtain measurements of working environments, data-loggers were located near the centre of gravity of workers when in their usual working position. The sampling points were located away from heat sources such as walls or air conditioning systems, in order to avoid interferences, in compliance with INNOVA recommendations [21].

Indices

To maintain thermal comfort and avoid disorders, two conditions must be fulfilled. The first is that the combination of skin and deep body core temperatures leads to a neutral feeling of comfort. The second involves the energy balance between the body and the environment. In this sense, the total metabolic heat produced by the body should be equal to the heat loss from the body.

The comfort equation developed by P. O. Fanger [22] relates physical parameters that can be measured with the neutral thermal feeling experienced by a "typical" person:

$$M - W = H + E_c + C_{res} + E_{res} \qquad (1)$$

where:
M – metabolic rate, W/m²; it is the rate of chemical energy transformation from aerobic and anaerobic activities into heat and work.
W – rate of mechanical work performed, W/m².
H – heat exchange from the skin by convection, conduction and radiation, W/m².
E – evaporative heat exchange, W/m².
E_c – evaporative heat exchange through the skin, in conditions of neutral thermal feeling, W/m².
C_{res} – respiratory heat loss by convection, W/m².
E_{res} – respiratory heat loss by evaporation, W/m².

Through measurement of physical parameters, the above comfort equation provides an operative tool whereupon it can be assessed under what conditions thermal comfort in an occupied space is achievable. Thermal comfort can be quantified through indices defined in the ISO 7730 standard [23]. The Predicted Mean Vote (PMV) is derived from the before mentioned heat balance and provides an indication of the thermal sensation by means of a scale of 7 points, from -2 (cold sensation) to +2 (hot sensation), where 0 means a neutral thermal sensation. Another comfort index is the Predicted Percentage of Dissatisfied (PPD) that provides information on thermal sensation by predicting the percentage of people likely to feel too hot or too cold in a given environment. PMV values of -2 and +2, mean thermal discomfort in the PPD index. Both indices are influenced by physical activity and clothing. The physical activity is quantified through the metabolic rate. The human body maintains a minimum rate of heat production of about 60 W during sleep. The metabolic rate is often expressed in Met, with 1 Met meaning a heat production of 58 W per m² of body surface. On the other hand, clothing acts as an insulation, reducing heat loss from the body. a unit called Clo is normally used to quantify the insulation of clothes. In terms of thermal resistance, 1 Clo is equivalent to 0.155 m² °C/W.

The selected PMV model was developed by [22] and employed by [24] for the assessment of thermal comfort conditions in indoor environments. The expression of the model is the following:

$$PMV = (0.303 \cdot e^{-0.036 \cdot M}) \cdot$$
$$\cdot [(M - W) - H - E_c - C_{res} - E_{res}] \qquad (2)$$

PPD has been also studied for the same environment. The index has been defined by the following equation, taking into account the PMV values previously obtained:

$$PPD = 100 - 95 \cdot e^{-(0.03353 PMV^4 + 0.02179 PMV^2)} \qquad (3)$$

As a result of the engine room conditions exceeding the range of PMV index (-0.5 to +0.5) and the constant globe temperature during the sea-lane, we could get a specific PMV index for the engine control room.

Finally, a practical risk analysis was performed, by calculating the heat stress, Swrek indices and comparing values with standard indications. Risk control measurements can reduce the frequency of failures while mitigating their possible efforts and consequences.

According to the indications of ISO 7933 (Heat stress evaluation of severe exposures) [25] and ISO 7243 (Heat stress evaluation required sweating index) [15] standards, the graphs were obtained.

These graphs were based on human body thermal balance and show the heat that a worker must release by evaporation in a given environment to reach thermal equilibrium, expressed through:

$$E_{rec} = M + C_{res} + R \qquad (4)$$

where:
E_{rec} – required evaporation to reach equilibrium, W/m².
R – heat gain by radiation, W/m².

As a consequence, these graphs show the maximum time that a worker should be in severe exposure, such as in engine rooms. The minimum time that the same worker must be at the control room to lose the accumulated heat was also calculated. This study is valid for a standard worker, weighing 70 kg and wearing light clothes.

RESULTS

Analysis of monitored variables

Because ASHRAE standards [26, 27] only discuss the different comfort zones, the European standard ISO 7730 [23] and ISO 7547 [28] have been considered in relation to the required indoor environmental conditions. Results were summarised in Table 4.

Tab. 4. *Statistical analysis of temperature data collected in different locations of the ship*

Temperature, T (°C)	Engine room	Control room
Average	32.50	19.76
Standard deviation	2.83	1.33
Maximum	38.50	27.30
Minimum	25.40	17.40

Engine room

The average temperature in the engine room was 32.5°C with peaks of 38.5°C. The relative humidity was about 25%, as a consequence of the high temperature.

These results exceed the values permitted for hot environments and can produce different health disorders (see Fig. 4 [5]). They may cause hyperthermia, vasodilatation and sweat gland activation, increase of peripheral circulation and electrolytic changes of sweat by loss of salt content. As fast as indoor temperature increases, the first psychical disorders appear such as loss or difficulties of concentration. Finally, physiological disorders as heart and circulatory system overload could yield.

Engine control room

As opposed to conditions in other locations, an average temperature of 19.76°C was recorded in the engine control room. This temperature is too low compared to the engine room, which can cause a thermal shock among workers.

Average relative humidity was 40%, contrarily to the engine room, and above the minimum recommended value of 30%.

Outdoor conditions

Given the influence of outdoor conditions on indoor environment, outdoor data were also registered during the monitoring period, from December to February. The results obtained were an average outdoor temperature of 23°C, with maximum values of 27°C, and an average relative humidity of 60%. The weather was predominantly sunny and not very cloudy.

Calculated Indices

PMV and PPD

Temperature and relative humidity values collected in the ship have been introduced in the models above described and the corresponding PMV and PPD values have been calculated for each indoor location. Once averages and standard deviations have been assessed, the values which crossed the admissible levels defined by ISO 7547 standards [6] were quantified. Such specifications set a PMV range from -0.5 to +0.5 as appropriate. This interval is equivalent to a PPD lower than 10%.

In the engine control room, the PMV is close to 0.5, which is the optimum condition for a healthy, warm environment; the average PPD is 13%, and 40% of the calculated PPD data are within the 10% established in the standards. In the engine room, PMV was about 2.15, which represents an extremely hot environment and a PPD with 77% dissatisfaction.

Heat stress indices

From the heat stress equations, the time a person should be in the control room was quantified for different globe temperatures, and showed the minimum time that a person should be in the engine room as a function of its globe temperature.

Using the graph for the engine room, we may state that the worker should have been in the engine room for 17 minutes and should have rested in the control room for at least 10 minutes, in order to allow an adequate heat release. The WBGT was about 40.2°C, according to standards, and the SWreq time exposition limit was about 41.8 minutes. These results will be useful for training ship engineers in work risk prevention.

DISCUSSION

When analysing the obtained data, some corrections are proposed in order to obtain a healthy environment for workers in the engine control room and to prevent fatigue risks at the engine room. This will allow adequate oil leakage detection and, as a consequence, improve fire prevention. As explained, training is a preventive control option but this study allows us to understand new corrective control options like design corrections.

Risk control options

Fatigue

Measured data showed that engine room temperature is nearly independent of daily cycles. The temperature at the engine control room should be equal to 20°C, in accordance with the air acceptability criteria, and to maintain the same PPD, the enthalpy must also be the same. For this reason, a temperature increase of 1°C leads to a relative humidity decrease of 5% [29] and the above mentioned lower limit of 30% would not be fulfilled. All these facts lead to setting the existing temperature conditions as optimum for the existing relative humidity.

A possible improvement may be to increase air renovation (exchange with outdoor air) according to IS0 8861 [30], in order to cause an increase of relative humidity towards more suitable values. This increase in air renovation must ensure a positive pressure in the engine room of 50 Pa, in accordance with ISO 8861.

Another solution is adjusting length and frequency of breaks and work periods. For this ship it was concluded that work periods inside the engine room must not be longer than twenty-seven minutes and, after that, the worker must spend about ten minutes in the control room. This case study of heat stress must be taken into account when revising future standards, in order to obtain a better engine room design.

Fire

New fire detection technologies, like video cameras [16], that need less inspection time in this hot environment, must be employed. This method will allow an adequate detection of fire far away from sensors.

Cost-benefit assessment of the options and decisions on which options are to be selected

An analysis of different options showed that these options present no cost if there is an adequate design or fatigue management training. Despite the fact that corrective control options are apparently the most costly way to reduce the work risk, the initial cost can be saved with an adequate design. We must take into account that this cost will only be related to more fans to increase air renovation.

Contrarily to this, preventive methods are apparently the most economic way of solving this problem. For example, if professors provide training for marine engineers in the course of academic studies [20], the problem would be solved at the origin. As a consequence, future Spanish degrees and master studies will have to take these factors into account.

CONCLUSIONS

From this study we could identify preventive and corrective control options of fatigue risk at the engine room of a merchant ship. These conclusions will allow a more effective oil leakage detection and, in consequence, improve fire prevention.

The apparent lack of change in injury rates related to vessel casualties and workplace accidents may be related to working conditions and methods, vessel design and training deficiencies. From this analysis of real conditions, it has been possible to define a design correction involving an increase in air renovation with outdoors and preventive corrections such as limiting the time a person can work without heat stress, in accordance with ISO standards. Concerning training, more research is required to determine whether the nature and extent of training influences susceptibility to fatigue; for example, the TNO report suggested a fatigue management programme (Houtman et al., 2005 [31]). Finally, we must remember that a holistic approach to fatigue will require all layers of the industry (regulators, companies and seafarers [32]) to be involved and that there are huge potential consequences of fatigue at sea, and, likewise great benefits to be had by addressing it.

BIBLIOGRAPHY

1. Ortega J. M.: *La ordenación del trabajo a bordo y su incidencia en la seguridad marítima*. II Xornadas Internacionais sobre Seguridade Maritima e Medioambiente. a Coruna, Spain. 2005. http://www.udc.es/iuem/documentos/doc_xornadas/seguridademaritima/SEGURIDAD_MARITIMA.pdf (Accessed May 2012)
2. Roberts S. E., Marlow P. B.: *Traumatic work related mortality among seafarers employed in British merchant shipping*, Occup. Environ. Med. Vol. 62, 2005.

3. Ministerio de Trabajo e Inmigración. *Estadística de Accidentes de Trabajo y Enfermedades Profesionales*. NIPO: 201-08-080-9. Spain, 2007. http://www.mtin.es/estadisticas/eat/eat07/index.htm. (Accessed May 2012)

4. Engine room fire. http://www.dnv.in/maritime/shipclassification/cmc/fire_safety/engine_room_fire.asp. (Accessed May 2012)

5. Smith A., Allen P., Wadsworth E.: *Seafarer fatigue: the Cardiff research programme. Centre for Occupational and Health Psychology*. Cardiff University. United Kingdom. 2006.

6. MSC/Circ.1023 and MEPC/Circ.392: *Guidelines for formal safety assessment (FSA) for use in the IMO rule-making process*. London: IMO, 5 April 2002.

7. Marine Safety Agency. *Formal safety assessment MSC 66/14*. London: International Maritime Organization (Submitted by the United Kingdom to IMO Maritime Safety Committee), 1993.

8. O'Connor P.J., O'Connor N: *Work-related maritime fatalities*. Accident Analysis & Prevention. Vol. 38, 2006.

9. Wang J., Pillay A., Kwon Y.S., Wall A.D.: Loughran C. G.. *An analysis of fishing vessel accidents*. Accident Analysis & Prevention. Vol. 38, 2005.

10. Švetak J.: *Accident investigation in the merchant marine*. Pomorstvo, god. Vol. 2, 2007.

11. *International Hazard Datasheets on Occupation*, Ship-Engineer (Machinist). HDOEDIT (© ILO/CIS, 1999) program. Approved by DG, 1999.

12. International Labour Organization. *Accident Prevention on Board Ship at Sea and in Port*. (ILO Codes of Practice), International Labour Office, Geneva, 1996. http://www.labour.gov.on.ca/english/hs/guidelines/gl_heat.html (accessed May 2012)

13. NTP 18 (Heat stress evaluation of sever exposures), http://www.insht.es/portal/site/Insht (Accessed May 2012)

14. NTP 350. Heat stress evaluation required sweating index. http://www.insht.es/portal/site/Insht (Accessed May 2012)

15. ISO 7243. Hot environments. Estimation of the heat stress on working man, based on the WBGT-index (wet bulb globe temperature), 1989.

16. Shuenn-Jyi Wang, Dah-Lih Jeng, Meng-Tsai Tsai*.: Early fire detection method in video for vessels*. The Journal of Systems and Software. Vol. 82, No 4, 2009.

17. Vighi Arroyo F.: *La Seguridad Industrial. Fundamentos y Aplicaciones*. ETSII UPM. Ministerio de Industria y Energía, Spain. 2005. http://www.ffii.es/f2i2/publicaciones/libro_seguridad_industrial/LSI.htm. (Accessed May 2012)

18. Wang J.: *Offshore safety approach and formal safety assessment of ships*. Journal of Safety Research. Vol. 33, 2002.

19. Wang J.: *The current status and future aspects in formal ship safety assessment*. Safety Science. Vol. 38, 2001.

20. Nas S., Paker S. D. E.: *Fire Fighting Training for Officers and Captains: a Problem Based Learning Approach*. International Association of Maritime Universities. 9th Annual General Assembly. 2008. http://www.iamu-edu.org/ (Accessed May 2012)

21. INNOVA Air Tech Instruments A/S. Thermal Comfort [online]. Denmark. 1997. Available from: http://www.innova.dk/books/thermal/ (Accessed May 2012)

22. Fanger P.O.: *Thermal comfort analysis and applications in environmental engineering*. McGraw-Hill. USA. 1970.

23. *ISO 7730. Moderate thermal environments. Determination of the PMV and PPD indexes and specification of the conditions for thermal comfort*. 1994.

24. Jang M.S., Koh C.D., Moon I.S.: *Review of thermal comfort design based on PMV/PPD in cabins of Korean maritime patrol vessels*. Build. Environ. Vol. 42, No 1 2007.

25. *ISO 7933. Ergonomics of the thermal environment. Analytical determination and interpretation of heat stress using calculation of the predicted heat strain*. 2004.

26. ASHRAE. *HVAC Fundamentals*. ASHRAE. Atlanta, USA, 1985.

27. ASHRAE STANDARD. *Proposed Revision to an American National Standard Thermal Environmental Conditions for Human Occupancy*. FIRST PUBLIC REVIEW DRAFT.2001.

28. ISO 7547 *Ships and marine technology. Air-conditioning and ventilation of accommodation spaces*. Design conditions and basis of calculations. 2002.

29. Simonson J.C., Salonvaara M., Ojalen T.: *Improving indoor climate and comfort with wooden structures. Technical Research Centre of Finland*. Espoo. VTT Building Technology, Espoo. Finland. 2001.

30. ISO 8861. *Shipbuilding. Engine-room ventilation in diesel-engined ships. Design requirements and basis of calculations*. 1998.

31. Houtman I., Miedema M., Jettinghoff K., Starren A., Heinrich J., Gort J., Wulder J., Wubbolts S.: *Fatigue in the shipping industry*. TNO-report: 20834/11353. 2005.

32. Parsons K.C.: *International Standards for the Assessment of the Risk of Thermal Strain on Clothed Workers in Hot Environments*. The Annals of Occupational Hygiene. Vol. 43, No. 5, 1999.

CONTACT WITH THE AUTHORS

José A. Orosa, Ph. D.
Universidade da Coruńa
Escuela Técnica Superior de N. y M.
Departamento de Energía y P. M.
Paseo de Ronda, 51,
15011. a Coruńa, Espańa
Corresponding author:
e-mail: jaorosa@udc.es
tel.: +34981167000; fax:+349811167107

Armando C. Oliveira, Prof.
Universidade do Porto, Faculdade de Engenharia,
New Energy Tec. Unit. Rua Dr Roberto Frias,
4200-465 Porto, Portugal.
e-mail: acoliv@fe.up.pt

Assembling of bearing sleeve on ship propulsion shaft by using EPY resin compound

Karol Grudziński, Prof.
Paweł Grudziński, Ph. D.
West Pomeranian University of Technology, Szczecin, POLAND
Wiesław Jaroszewicz, Ph. D.
Jędrzej Ratajczak, Ph. D.
Marine Service Jaroszewicz S.C., Szczecin, POLAND

ABSTRACT

This paper presents an original novel solution of the problem of assembling a large bearing sleeve (of about 1000 mm in diameter) on ship propulsion shaft by using EPY resin compound. The problem is discussed on the concrete example dealing with a ship under repair. Design project of assembling the sleeve on the shaft by using the resin compound, model research on its casting process as well as assembling technology of the sleeve on the shaft, are presented and a practical way of realization of the project in conditions of a Chinese ship repair yard, is also highlighted. During more than three-year-long operation the solution has standed the test of time without any complaint.

Keywords: Bearing sleeve, propulsion shaft, assembling, EPY resin compound

INTRODUCTION

In the paper an original solution of the problem of assembling a large bearing sleeve (of about 1000 mm in diameter) on ship propulsion shaft, by using EPY resin compound, is presented. The compound belongs to a group of special epoxide compounds has been applied for many years to foundation chocks for seating main propulsion engines and reduction gears as well as many other machines and auxiliary devices, and to assembling stern tubes and bearing sleeves of rudder stocks, mounted on sea-going ships. The group is consisted of the three basic compounds: Chockfast Orange (USA), Epocast 36 (Germany) and EPY (Poland). They are granted all the certificates necessary for their wide application to assembling both shipboard and land-based machines and devices. Descriptions of their features as well as many practical applications can be found in producers' pamphlets available in Internet, as well as in the books [1, 2]. According to the state of knowledge of these authors neither the compounds in question nor any other ones have been applied to assembling large bearing sleeves on ship propulsion shafts.

Until now the bronze bearing sleeves have been usually assembled on propulsion shafts of sea-going ships by means of thermo compression bonding. The assembling consists in heating the sleeve, free shifting it onto the shaft and cooling down to ambient temperature. Such solution was also applied in the case of the shaft in question, shown in Fig. 1, during building the ship. On the shaft two bearing sleeves were assembled by using the thermo compression method. During

the capital repair of the ship it was revealed that to replace one of them has been necessary. The new sleeve which had to be assembled on the left part of the shaft ended with the large flange (Fig. 1) was of much greater dimensions than that which was in a good state and had to be left on the shaft. The form and dimensions of the new sleeve are shown in Fig. 2. The propeller shaft bearing has the sleeve fitted with rubber pads and is water - lubricated.

The repair of the ship (the Arkhangelsk which usually operates in Arctic waters) has been performed by the Estonian firm (OÜ Wärtsilä BLRT) of Tallin, in the Chinese shipyard (Yiu Lian Dock Yard Ltd, Shenzhan), under supervision of the Russian Maritime Register of Shipping.

The shipyard in which the ship was repaired had no practical possibility to assemble such a large sleeve on the shaft by means of the traditional method based on thermo compression. In the situation it was decided to assemble the sleeve on the shaft by using a special polimer compound widely applied for assembling many ship machines and devices. The firm which has carried out the repair of the ship announced a tender for realization of the work. In Asia and Europe there are many specialty firms engaged in seating machines and devices with the use of compounds. However, only one of them, a Polish company from Szczecin, has undertaken to do the novel and risk task.

The scope of the work consisted of elaboration of a detailed design project of assembling the sleeve on the shaft, technology of the assembling and its realization in the Chinese shipyard which carried out the repair of the ship in question.

Fig. 1. The part of ship propulsion shaft, prepared for assembling the new bearing sleeve on it
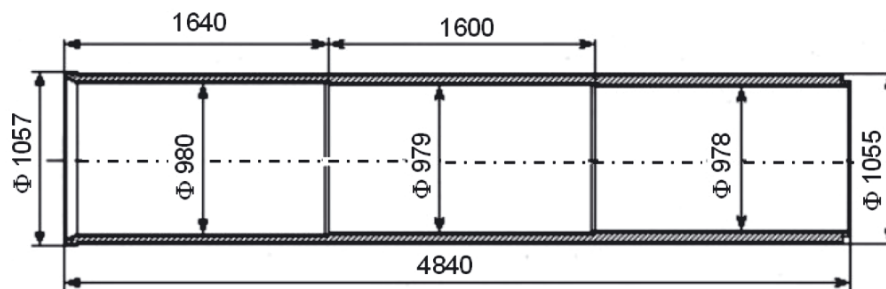
Fig. 2. The form and dimensions of the new bearing sleeve intended to be assembled on the shaft by using EPY compound

DESIGN PROJECT OF ASSEMBLING THE SLEEVE ON THE SHAFT

The design project of assembling the bearing sleeve on the ship propulsion shaft by using the EPY resin compound is shown in Fig. 3. The shaft is hollow and its outer diameter in the place of sleeve's assembling is a little differentiated alongside and has the values of 968, 967 and 966 mm over the shaft sections of 1640, 1600 and 1600 mm in length, respectively. Inside diameters of the sleeve are differentiated similarly (Fig. 2); they have respective values of 980, 979 and 978 mm. The difference of shaft and sleeve diameters over particular sections is constant and equal to 12 mm. It gives the compound pouring gap of 6 mm in height over the whole length of the connection. This is a relatively small height of pouring gap (as compared with the large remaining dimensions) that is associated with many problems which have not been recognized so far. They deal with suitable filling the pouring space and getting a good casting of a small thickness and very large remaining dimensions. As results from the practical experience has been gained so far to obtain a good effect is difficult and associated with rather great risk in such a case. Worth mentioning that in the case of assembling stern tube in ship hull hub, of comparable or even much smaller dimensions, the applied height of pouring gap usually amounts to $15 \div 20$ mm, that is an important, but not the only, difference as compared with the solution applied in the project in question.

The full length of the bearing sleeve (Fig. 2) amounts to 4840 mm, and its outer diameter is constant and equal to 1055 mm. As internal diameters of the sleeve are somewhat different its wall thickness changes stepwise and has only a little differentiated values: 37.5, 38.0 and 38.5 mm.

Because of manufacturing and assembling difficulties, three separate sleeves were prepared instead one, which - after shifting them onto the shaft – were next appropriately lap - joined together (Fig. 3, D - detail), and they fulfilled their tasks, in this case, as properly as an integral sleeve. In order to ensure sleeve - shaft coaxiality as well as constant height of pouring gap 24 spacing elements of 6 mm in height were welded in suitable places of the shaft's surface (Fig. 3, B - detail). The elements welded on the shaft are seen also in Fig. 5.

On the upper generatrix of the bearing sleeve (before assembling) 5 openings (M30) for fixing ingate and flow-off pipes (Fig. 3, see C and D details), were drilled and threaded. Seals are provided in both ends of the sleeve (Fig. 3, see a and E details): internal one made of polyurethane foam (to stop resin compound outflow) and external permanent one to secure the joints against exposure to sea water. The special expoxide paste (Phillybond Orange Sealant Resin, ITW Philadelphia Resins) was used to form the seals. In the seals four venting openings were made (at the bottom, midheight and top), which were appropriately sealed after the liquid compound has been observed in them during pouring. The lap-joints of the particular parts of the sleeve were circumferentially sealed by using an adhesive tape. Also, in the top points of these seals control venting holes were provided, which were sealed during pouring process when the resin compound has been observed in them.

Cured resin compound which fills pouring space is intended to ensure not only integrity of the connection but also safe transmission of torque applied to bearing sleeve. It was assumed that circumferential forces acting on the connection have to be fully transferred by resin compound splines located in longitudinal splineways made on the internal surface of the sleeve and the external surface of the shaft. For this reason were designed 8 longitudinal splineways placed in the angular distance of 45° to each other. Their form and dimensions are shown in Fig. 3, F and G details. After complete filling by the poured resin compound and its curing they form a correctly fitted multi-spline resin-compound connection between the shaft and bearing sleeve. The resin compound splines placed in splineways are exposed mainly to shear and surface compression. With a view of that appropriate control calculations were performed. The following input data were assumed:

- maximum propulsion shaft power $P = 15\,400$ kW
- rotational speed of shaft $n_w = 2$ s^{-1}
- radius of application of circumferential force on contact surface between shaft and resin compound $R = 483$ mm
- total length of spline (splineway) $L = 4840$ mm
- spline breadth $B = 10$ mm
- spline (splineway) depth in shaft $H_w = 3$ mm
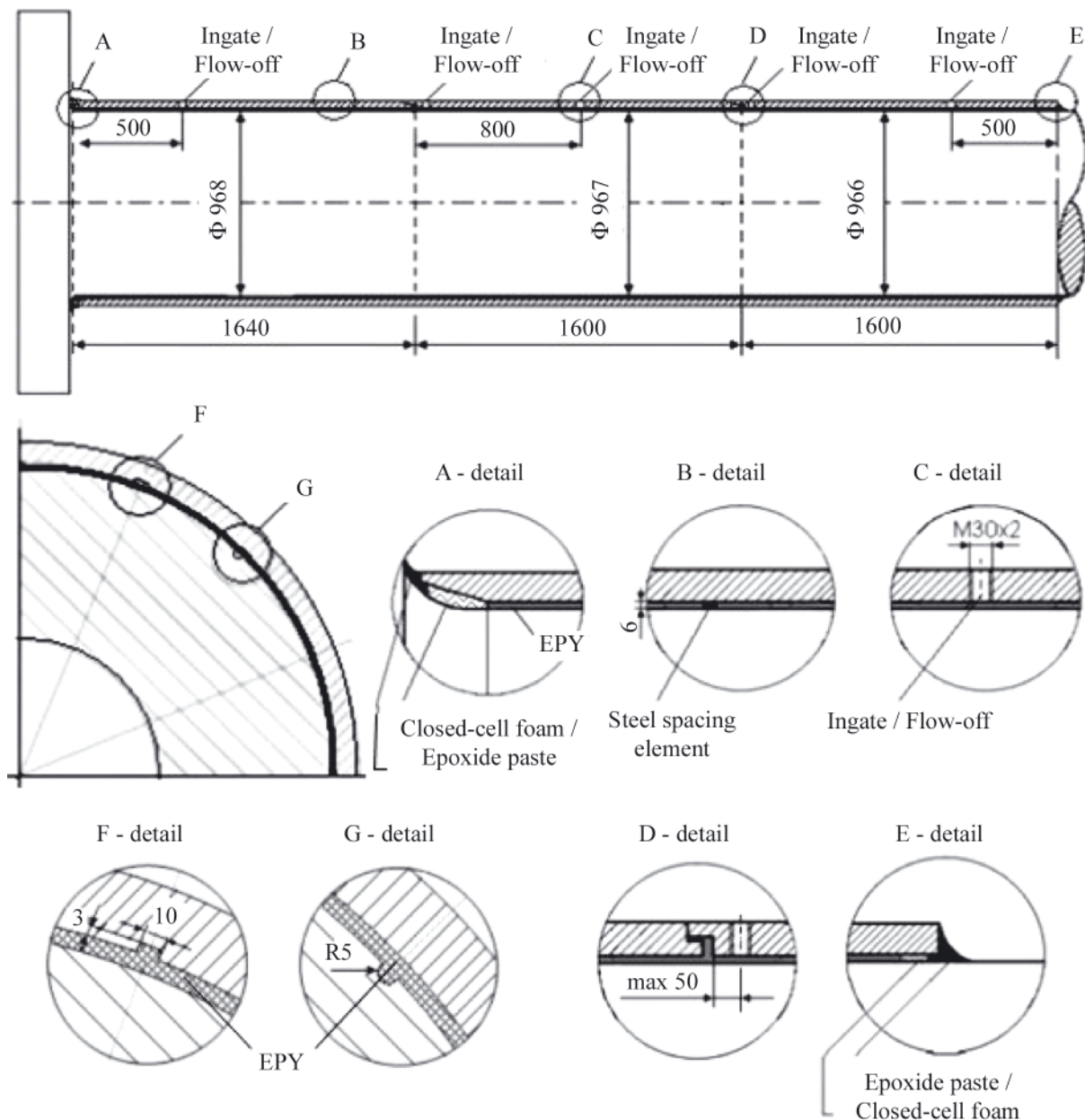
Fig. 3. *Design project of assembling the bearing sleeve on the ship propulsion shaft by using the resin compound*

- number of splines (splineways)
  over circumference $\qquad$ $n_r = 8$
- resin compound shear strength $\qquad$ $R_t = 59{,}1$ MPa
- resin compound compression strength $\qquad$ $R_c = 169$ MPa

Propulsion shaft torque:

$$M_o = 9550 \cdot 10^3 \, \frac{P}{n_w} = 1225583 \text{ Nm}$$

Total circumferential force on contact surface
between shaft and resin compound:

$$F_T = \frac{M_o}{R} = 2537438 \text{ N}$$

Shear stresses:

$$\tau = \frac{F_T}{n_r B L_T} = \frac{2537438}{8 \cdot 10 \cdot 4840} = 6.55 \text{ MPa}$$

Surface compression:

$$p = \frac{F_T}{A_p} = \cdot \frac{2537438}{8 \cdot 3 \cdot 4840} . = 21.84 \text{ MPa}$$

Shear safety factor:

$$n_\tau = R_t \, / \, \tau = 8.95$$

Compression safety factor:

$$n_p = R_c \, / \, p = 7.74$$

As results from the control calculations the values of shear and compression safety factors in conditions of extreme loading applied to the bearing sleeve by total shaft torque, are sufficiently large. Worth mentioning, that in the calculations extremely unfavourable conditions were assumed. As neither adhesion forces nor friction forces of resin compound on contact surfaces between shaft and sleeve were taken into account that really occurs and increases safety of such connection. In the calculations the maximum possible value of torque resulting from engine output was assumed to act onto the resin compound connection between shaft and sleeve. In usual service conditions of ship its shaft transmits torque from engine to screw propeller and only a small part of it is lost to overcome friction torque in bearings. In reality only this small part of torque is exerted to the made multi-spline resin-compound connection between shaft and bearing sleeve. As results from that, the real safety
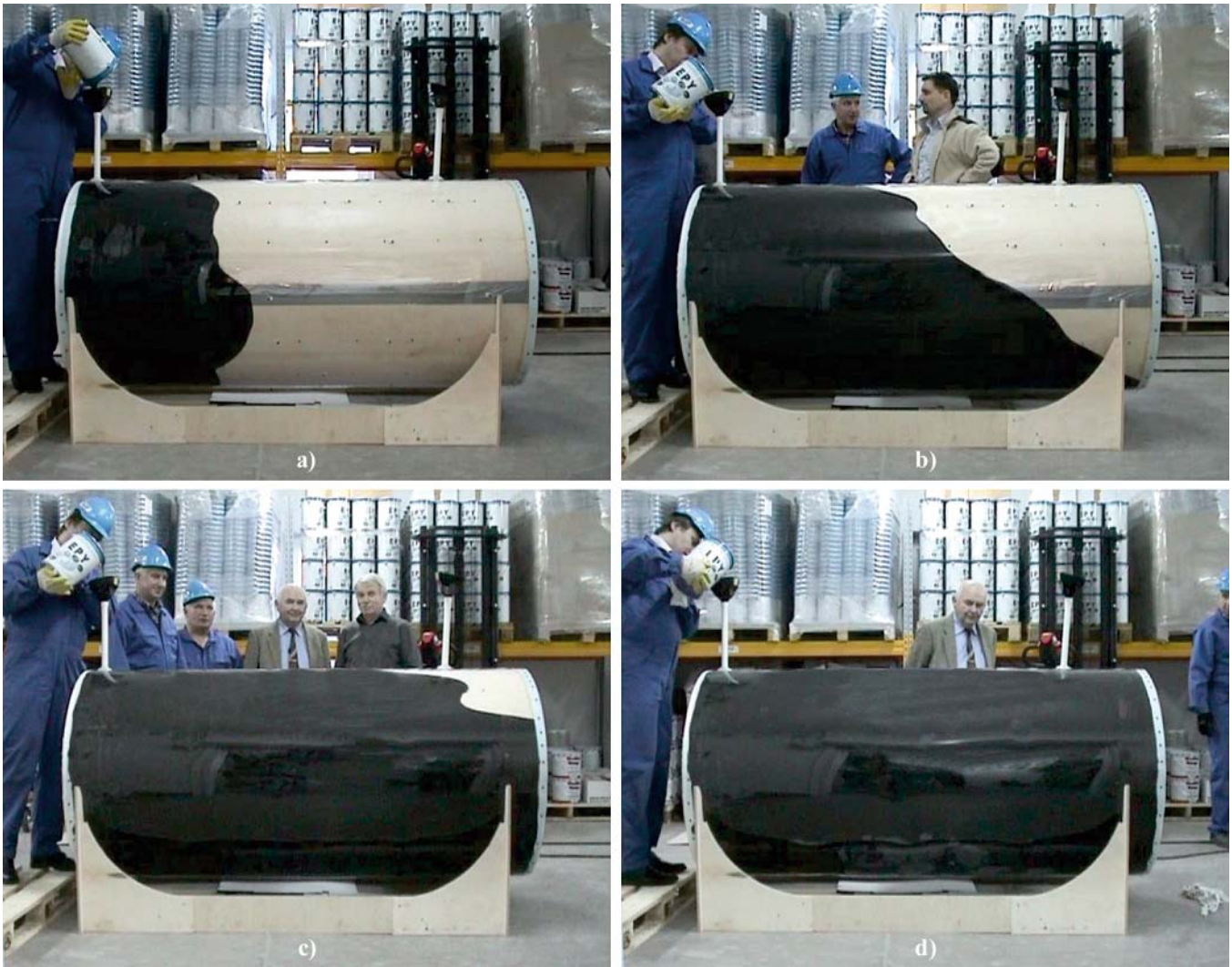
Fig. 4. *Model tests of a manner and time of filling the pouring gap between shaft and sleeve with liquid EPY resin compound*

factor values against shear and surface compression for the resin compound in regular ship operation conditions will be multifold greater than the above given ones calculated de facto for the situation of bearing failure when shaft rotation against bearing would be completely blocked. Such situations are completely unknown in practice.

Therefore it can be stated that from the strength point of view the designed connection between the sleeve and the shaft by using the EPY resin compound satisfies safety conditions with a very large margin.

MODEL TESTS

In spite of over thirty-year experience in seating ship machines and devices with the use of resin compound it was deemed necessary to conduct in advance appropriate model tests – because of definite specificity and great responsibility associated with the undertaking in question. The tests were aimed at practical checking if realization of the proposed solution is possible, and working out many details dealing with its manufacturing technology. The tested model of assembling the sleeve on the shaft with the use of EPY resin compound is shown in Fig. 4. Its diameter amounted to 1000 mm, and its length to 2000 mm. The gap height amounted to 4 mm that was ensured by appropriately arranged spacing elements. Conditions assumed for the model were less favourable than those for the real object. It concerned first of all the pouring gap height which was by 2 mm lower than that applied to the real system.

The shaft model was made of wood (model plywood wrapped around circular discs and stiffened appropriately by ribs) The outer sleeve was made of Plexiglas to make it possible to directly observe process of filling the pouring space with liquid resin compound. At the outer generatrix of the plexiglass sleeve two holes were made in which pipes ended with funnels, were fixed. They constituted ingate and flow-off for liquid resin compound, respectively. The distance between the ingate and flow-off holes to each other and from the sleeve ends were the same as in the real system. The 500 mm length of the pipes had to ensure an appropriate amount of the compound necessary for supplementing void cavities in the pouring space, until the instant of curing the compound. In the experiment it was important to practically test the pouring process performed through one hole, manner and rate of spreading the compound and possibility of correct filling the entire pouring space before starting gelation process. It was also important to determine real duration time necessary for realization of the operation in given temperature conditions.

Sealing the pouring space at its edges was made with the use of polyurethane foam of open cells. It made additional venting the space during filling, possible. An important thing in the experiment was the testing of a manner of spreading the compound within the pouring space as well as quality of the formed casting after its curing in ambient conditions.

Results of the experiment have been very useful in working out many details of assembling technology of real sleeves onto ship propulsion shaft. In assembling technology of structural

Fig. 5. *Sections of the bearing sleeve and the shaft with cut splineways and welded spacing elements*

elements with the use of resin compound there are many important details which may decide either on reaching success or suffering defeat in practical realization of such solutions.

PREPARATION OF ELEMENTS AND RUN OF THEIR ASSEMBLING

The sleeve sections to be assembled onto the shaft fragment, and the shaft itself, suitably prepared according to the design shown in Fig. 3, are presented in Fig. 5. Eight longitudinal splineways of the form and dimensions shown in Fig. 3 (F and G details) were cut both on the internal surface of the sleeve and the external surface of the shaft. On the shaft surface 24 spacing elements of 6 mm in height, were welded. They were aimed at ensuring a suitable arrangement of the sleeve against the shaft and a uniform pouring gap height. The spacing elements were appropriately beveled (Fig. 5d) to facilitate the process of shifting the sleeve onto the shaft and displacing it along the shaft. The inner surfaces of the sleeve were machined to the proper dimension by using a boring machine. The shaft surface was exactly cleaned by using sandpaper. Just before assembling the sleeve on the shaft their surfaces were exactly degreased by using acetone.

An overall view of the shaft and the first section of the bearing sleeve to be assembled (hanging on a girder crane) is shown in Fig. 6a. The sleeve is shifted onto the free (thinner) end of the shaft which is then placed on a roller support, at

a distance from the end of the shaft (Fig. 6b). Next, after the appropriate fixing of the free end of the shaft and drawing aside the rollers of the support (Fig. 6b), the sleeve was shifted along the shaft axis up to the extreme location in the neighbourhood of the shaft's flange, by using the girder crane. In the same way were put onto the shaft and shifted along it two other sections of the bearing sleeve which were then lap-joined to each other. The assembling of the third section of the sleeve is shown in Fig. 6c.

The appropriate centering of the sleeve as well as pouring gap height were ensured by the spacing elements welded to the shaft (Fig. 5d). A minimum clearance which made shifting the sleeve possible was maintained. A small surplus of the outer diameter of the sleeve for its finishing after completing its assembling was provided.

After appropriate joining the particular sections of the sleeve to each other, the steel ingate and flow-off pipes with funnels welded to their upper ends, were screwed into them. The ends of the pouring space, and the sleeve joints were sealed in compliance with the above presented design project (Fig. 3). The sleeve-shaft system prepared for filling with the resin compound is shown in Fig. 7. The length of ingate and flow-off pipes equal to about 650 mm, including funnels, was so chosen as to generate and maintain appropriate hydrostatic pressure necessary for correct filling the entire pouring space. Also, it is important to maintain some volume of resin compound within the flow-in and flow-off system after complete filling

Fig. 6. Run of putting the particular sections of the bearing sleeve onto the shaft

the pouring space. This is necessary for supplementing void cavities resulting from a sealing foam elasticity, resin shrinkage during curing process, and other causes.

During the assembling work the ambient temperature in the workshop was 20 ÷ 24°C. Before filling the system by the resin compound it was decided to heat it up to about 30°C, that had to bring better and faster filling the pouring space. The system (Fig. 7a) was covered with a tarpaulin and heated up by blowing warm air for about 24 hours. To this end three small electric heaters were applied. At the instant of starting the pouring process the measured temperature of the sleeve was equal to 27°C, and that of the poured resin compound to 30°C. The resin compound was simultaneously poured through three holes: two extreme and one intermediate (Fig. 7a). The manner of pouring the resin compound is shown in Fig. 7b. The pouring proceeded continuously and uniformly.

The necessary amount of the resin compound was precisely calculated in advance. During pouring, were observed control points at the end seals and the joints of the sleeve, which served as additional venting. When the resin compound has been

seen in the holes they were suitably sealed. The total time of pouring lasted 3 hours. After complete filling the pouring space the ingate and flow-off elements were monitored for next two hours and the resin compound was added to supplement void cavities and maintain an appropriate hydrostatic pressure. The total amount of the poured resin compound was 98.6 liters. After two hours the process of lowering the resin compound level in the ingate and flow-off elements, ceased. After next twelve hours the ingate and flow-off pipes as well as the adhesive tape seals on the joints of the sleeve, were removed. The holes in the bearing sleeve, left from the pouring pipes, were blanked off with threaded stoppers made of the same bronze material as that used for the sleeve itself. During the resin compound pouring and curing process no increase of the sleeve temperature was observed. The curing proceeded in the ambient temperature of 20 ÷ 24°C and lasted 36 hours. The resin compound hardness measured on especially cast specimens amounted to 42 ÷ 46°B. The checking if the pouring space is fully filled was done by a simple „knocking" method, and control holes were drilled in dubious places indicated by a surveyor. No resin compound lacking zones

Fig. 7. a) the sleeve-shaft system prepared for pouring with resin compound, *b)* manner of pouring

were revealed. After ending the assembling work the sleeve surface were subjected to after-machining to remove the small surplus left.

FINAL COMMENTS AND CONCLUSIONS

- The presented novel design project of assembling the large bearing sleeve on the propulsion shaft of sea-going ship by using the special EPY epoxide resin compound, as well as the elaborated and applied technology of its realization, were successfully put in practice. The used solution passed an exam in practice. After over - a - year period of operation of the repaired ship a written confirmation stating correct performance of the sleeve assembled on the shaft, and the stern bearing, was received from the ship's operator. Until now, i.e. for three-year period of operation of the ship in question, no claim concerning this matter has been reported.
- The results of the work show one of many other possible in practice applications of the elaborated EPY resin compound to solving difficult and sophisticated assembling problems which happen in building and repairing processes of sea-going ships.
- Owing to elaboration and application of special polymer resin compounds, many difficult and complex problems dealing with design and technology of assembling as well as repair of many machines and devices, which earlier have produced many troubles for designers, manufacturers and users of such objects, have been solved successfully. In some cases such solutions as that discussed in this paper, are the only practically feasible in a given situation.
- Many advantages of the advanced assembling technology of machines and devices by using the resin compound resulted in that it has appeared widely applicable not only in building and repair of sea-going ships (where it has found its beginnings and became standard one), but also more and more often to assembling many different land-based

objects. There are still many possible practical applications of resin compounds for achieving these way great technical, economical and operational profits both in shipbuilding and civil engineering. These authors have systematically conducted for many years R&D work in the area in question in tightly connection with practical activity.

BIBLIOGRAPHY

1. Grudziński K., Jaroszewicz W.: *Seating of machines and devices on foundation chocks cast of EPY resin compound.* Published by ZAPOL – Dmochowski & Sobczyk Registered Partnership, Szczecin, 2002 (in Polish), 2004 (in English), 2006 (in Russian)
2. Piaseczny L.: *Polymer technology in ship repair* (in Polish). Gdańskie Towarzystwo Naukowe (Gdańsk Scientific Society), Gdańsk, 2002

CONTACT WITH THE AUTHORS

Karol Grudziński, Prof.
Paweł Grudziński, Ph. D.
West Pomeranian University of Technology, Szczecin
Faculty of Mechanical Engineering and Mechatronics
Al. Piastów 19
70-310 Szczecin, POLAND
e-mail: Karol.Grudzinski@zut.edu.pl

Wiesław Jaroszewicz, Ph. D.
Jędrzej Ratajczak, Ph. D.
Marine Service Jaroszewicz S.C., Szczecin

The Ship Handling Research and Training Centre at Ilawa is owned by the Foundation for Safety of Navigation and Environment Protection, which is a joint venture between the Gdynia Maritime University, the Gdansk University of Technology and the City of Ilawa.

Two main fields of activity of the Foundation are:

➲ Training on ship handling. Since 1980 more than 2500 ship masters and pilots from 35 countries were trained at Iława Centre. The Foundation for Safety of Navigation and Environment Protection, being non-profit organisation is reinvesting all spare funds in new facilities and each year to the existing facilities new models and new training areas were added. Existing training models each year are also modernised, that's why at present the Centre represents a modern facility perfectly capable to perform training on ship handling of shipmasters, pilots and tug masters.

➲ Research on ship's manoeuvrability. Many experimental and theoretical research programmes covering different problems of manoeuvrability (including human effect, harbour and waterway design) are successfully realised at the Centre.

The Foundation possesses ISO 9001 quality certificate.

Why training on ship handling?

The safe handling of ships depends on many factors - on ship's manoeuvring characteristics, human factor (operator experience and skill, his behaviour in stressed situation, etc.), actual environmental conditions, and degree of water area restriction.

Results of analysis of CRG (collisions, rammings and groundings) casualties show that in one third of all the human error is involved, and the same amount of CRG casualties is attributed to the poor controllability of ships. Training on ship handling is largely recommended by IMO as one of the most effective method for improving the safety at sea. The goal of the above training is to gain theoretical and practical knowledge on ship handling in a wide number of different situations met in practice at sea.

For further information please contact:
The Foundation for Safety of Navigation and Environment Protection

Head office:
36, Chrzanowskiego Street
80-278 GDAŃSK, POLAND
tel./fax: +48 (0) 58 341 59 19

Ship Handling Centre:
14-200 IŁAWA-KAMIONKA, POLAND
tel./fax: +48 (0) 89 648 74 90
e-mail: office@ilawashiphandling.com.pl
e-mail: office@portilawa.com